DEVELOPMENT OF MULTILAYER VASCULAR GRAFTS BASED ON COLLAGEN-MIMETIC HYDROGELS

A Dissertation

by

MARY BETH BROWNING

Submitted to the Office of Graduate Studies of
Texas A&M University
in partial fulfillment of the requirements for the degree of

DOCTOR OF PHILOSOPHY

Chair of Committee,	Elizabeth Cosgriff-Hernàndez
Committee Members,	Mariah Hahn
	Duncan Maitland
	Fred Clubb
Head of Department,	Gerard Coté

August 2013

Major Subject: Biomedical Engineering

ABSTRACT

Current synthetic vascular grafts have high failure rates in small-diameter (<6 mm) applications due to inadequate cell-material interactions and poor matching of arterial biomechanical properties. To address this, we have developed a multilayer vascular graft design with a non-thrombogenic inner layer that promotes endothelial cell (EC) interactions and a reinforcing layer with tunable biomechanical properties.

The blood-contacting layer of the graft is based on a Streptococcal collagen-like protein (Scl2-1). Scl2-1 has the triple helical structure of collagen, but it is a non-thrombogenic protein that can be modified to have selective cell adhesion. For this application, Scl2-2 has been modified from Scl2-1 to contain integrin binding sites that promote EC adhesion. We have developed the methodology to incorporate Scl2 proteins into a poly(ethylene glycol) (PEG) hydrogel matrix. PEG-Scl2 hydrogels facilitate optimization of both bioactivity and substrate modulus to offer unique control over graft endothelialization. However, scaffold properties that promote endothelialization may not be consistent with the mechanical properties necessary to withstand physiological loading. To address this issue, we have reinforced PEG-Scl2-2 hydrogels with an electrospun polyurethane mesh. This multilayer vascular graft design decouples requisite mechanical properties from endothelialization processes and permits optimization of both design goals.

We have confirmed the thromboresistance of PEG-Scl2-2 hydrogels in a series of whole blood tests *in vitro* as well as in a porcine carotid artery model. Additionally, we

have shown that the electrospun mesh biomechanical properties can be tuned over a wide range to achieve comparable properties to current autologous grafts. Traditional acrylate-derivatized PEG (PEGDA) hydrogels were replaced with PEG diacrylamide hydrogels with similar properties to increase biostability for long-term implantation. These findings indicate that this multilayer design shows promise for vascular graft applications.

As vascular graft endothelialization can significantly improve success rates, the ability to alter cell-material interactions through manipulations in PEG-Scl2-2 hydrogel properties was studied extensively. By reducing Scl2-2 functionalization density and utilizing a biostable PEG functionalization linker, Acrylamide-PEG-I, significantly improved initial EC adhesion was achieved that was maintained over 6 weeks of swelling in vitro. Additionally, increases in Scl2-2 concentration and in hydrogel modulus provided increased EC interactions. It was found that PEG-Scl2-2 hydrogels promoted enhanced EC proliferation over 1 week compared to PEG-collagen gels.

In summary, we have developed a vascular graft with a biostable, non-thrombogenic intimal layer that promotes EC adhesion and migration while providing biomechanical properties comparable to current autologous grafts. This design demonstrates great potential as an off-the-shelf graft for small diameter arterial prostheses that improves upon current clinically available options.

DEDICATION

To my family, who have always told me that I was wonderful and capable of doing anything while providing whatever resources that they could to help me achieve my dreams.

ACKNOWLEDGEMENTS

In looking back on the journey that brought me to where I am today, I could not have made it here without the incredible amount of love, encouragement, mentorship, and support that I have consistently been given throughout my life. I would like to begin by acknowledging my advisor, Dr. Elizabeth Cosgriff-Hernandez. From my first meeting with her, I was blown away by her passion for research and service, and it has been a contagious force throughout my past four years. In creating opportunities for me to give back through outreach, she kept me grounded; in setting what sometimes seemed like ridiculously high expectations for me in my research, she forced me to leap out of my comfort zone and develop into a better researcher than I could have ever imagined I could be. The majority of my achievements over the past four years would not have been feasible without her advocacy, and I will be grateful to her throughout my entire career.

I would also like to thank my committee members, Dr. Mariah Hahn, Dr. Duncan Maitland, and Dr. Fred Clubb. Their diverse expertise has pushed me to grow, and their input has improved the quality of my work. I am especially thankful for the support given to me by Dr. Mariah Hahn from my very first month of graduate school onward.

Dr. Magnus Höök and Dr. Brooke Russell not only provided me with an amazing protein to base my research upon, but also encouraged me in my work, provided feedback and a different perspective, and created extra opportunities from which I was able to learn and grow. Dr. Melissa Grunlan has continually been willing to share

resources with me to help me move forward, whether it was unlimited use of her infrared spectrometer or tips on how to be an effective teacher to an “audience” of 90.

This work has been a multidisciplinary effort, with many different perspectives that helped to make it what it has become. Specifically, I would like to thank Dr. Jose Rivera for making Scl2-2; Roya Nezarati and David Dempsey, my wonderful electrospinners; Dr. Dany Munoz-Pinto, Viviana Guiza, and Silvia Becerra, for their assistance with cell studies and thrombosis testing; Drs. Matthew Miller, Egemen Tuzun, and Theresa Fossum for their expertise and work on our pig implants; Dr. Fred Clubb, for his pathology reports; Pauline Luong and Andrea Taylor for assistance on rat implants; and Dr. Jing-Fei Dong and Angela Bergeron for their work on the platelet activation studies.

Having co-workers who make me laugh and teach me lessons in and out of the lab has been invaluable to me throughout graduate school. I would like to give a very special thanks to Jenny Robinson and Roya Nezarati, who saved me from being the only girl in the lab and have become two of my closest friends. In addition, many thanks to Bobby Moglia, Nick Sears, Dave Dempsey, and Pauline Luong. I would also like to thank all of the talented undergraduates that I have worked with: Thomas Wilems, Tyler Touchet, Scott Bixler, Keegan Smith, and Stacy Cereceres.

I am so blessed to have incredible friends and family that have helped to get me through graduate school. James Monroe has been my rock, always bringing me back to earth and helping me to keep a healthy perspective. Elizabeth Terry, Kristi Patterson, and Lacy Patterson have been steadfast friends who helped me remember that there is

life outside of graduate school. Katie Moody, Brennan Bailey, and Carrie Green kept me fed with wonderful food, physically and spiritually. My parents, Catherine Dolen, Bill Browning, Joe Dolen, and Jodi Browning, and grandparents, Buddy and Mary Ann McGehee, have encouraged me to become a lifelong learner and most importantly, to pursue what makes me happy. Finally, Amy Fisher, the best sister in the world, has never failed to share her endless wisdom and love with me.

NOMENCLATURE

4-arm PEG-Acr	4-arm poly(ethylene glycol) acrylate
Aam-PEG-I	Acrylamide-poly(ethylene glycol)-isocyanate
Acr-PEG-NHS	Acrylate-poly(ethylene glycol)-N-hydroxysuccinimide
ADP	Adenosine diphosphate
BAOEC	Bovine aortic endothelial cell
CAD	Coronary artery disease
CBQCA	3-(4-carboxy-benzoyl)-2-quinoline-carboxaldehyde
CVD	Cardiovascular disease
DCM	Dichloromethane
DMAC	Dimethylacetamide
DMEM	Dulbecco's Modified Eagle Medium
DMSO	Dimethylsulfoxide
EC	Endothelial cell
ECM	Extracellular matrix
EPC	Endothelial progenitor cell
ePTFE	Expanded poly(ethylene tetrafuron)
FBGC	Foreign body giant cell
FBS	Fetal bovine serum
FTIR	Fourier transform infrared
LDH	Lactate dehydrogenase

MFI	Mean fluorescence intensity
MSC	Mesenchymal stem cell
NHS	N-hydroxysuccinimide
NMR	Nuclear magnetic resonance
NO	Nitrous oxide
PAD	Peripheral artery disease
PBS	Phosphate buffered saline
PEG	Poly(ethylene glycol)
PEGDA	Poly(ethylene glycol) diacrylate
PEGDAA	Poly(ethylene glycol) diacrylamide
PEGDI	Poly(ethylene glycol) diisocyanate
PET	Poly(ethylene terephthalate)
PGA	Poly(glycolic acid)
RO	Reverse osmosis
Scl2	Streptococcal collagen-like protein
SEM	Scanning electron microscopy
SIS	Small intestinal submucosa
SMC	Smooth muscle cell
SPU	Segmented polyurethane
TCPS	Tissue culture polystyrene
TEA	Triethylamine
TEGDA	Tri(ethylene glycol) diacrylate

TABLE OF CONTENTS

Page

Page

LIST OF FIGURES

FIGURE Page

FIGURE Page

LIST OF TABLES

CHAPTER I

INTRODUCTION

1.1 Clinical Need: Cardiovascular Disease

For over a century, cardiovascular disease (CVD) has been the leading cause of death in the United States each year. One-third of American adults are affected by CVD with approximatly 25 million coronary artery and peripheral artery disease (CAD, PAD) cases annually. [1] Both CAD and PAD are characterized by atherosclerosis that arises from smooth muscle cell hyperproliferation and thrombus formation. [2] Atherosclerosis is a progressive narrowing and occlusion of arteries that eventually results in a loss of blood flow to specific areas of the body. The coronary, iliac, and carotid arteries, abdominal aorta, and vascular bifurcations are especially susceptible to atherosclerosis, and occlusion of these vessels can have serious clinical consequences such as heart attack or stroke. [3] Ideally, CAD and PAD are treated with lifestyle changes or medications. Failing this, non-invasive options, such as angioplasty and stenting, are available to physically open the lumen of the occluded vessel. In the most severe cases, bypass procedures are required in which blood flow is rerouted around the occluded vessels. Currently, over 500,000 bypass surguries are performed each year in the U.S. [1]

1.2 Native Vasculature Structure

1.2.1 The Intima While native vasculature was initially considered to be a relatively simple tissue, it has proven very difficult to replicate the structure and function

of blood vessels in the design of viable vascular grafts. Veins and arteries are comprised of three distinct layers, each of which have a specific role in maintaining healthy vasculature. The innermost intimal layer is an endothelial cell (EC) lining. Vascular ECs actively promote vessel thromboresistance, and it has been shown that a quiescent, luminal endothelial layer inhibits both platelet aggregation and smooth muscle cell proliferation. [4-5] Thus, generation of a stable endothelium can greatly improve vascular graft success. However, the vascular endothelium is one of the few areas of the body that can survive the continual application of high pressures, which makes it difficult to produce a pre-endothelialized graft that remains stable following implantation. [6] Injury of the intimal layer causes EC activation, during which cytokines are released and proteins are expressed that promote inflammatory reactions and thrombosis. In a healthy system, this results in regeneration of a healthy, non-thrombogenic lumen, but CVD can affect this remodeling process. [7] The basement membrane, an extracellular matrix (ECM) composed primarily of type IV collagen, laminin, and heparan sulphate proteoglycans, surrounds the endothelium and bridges the intimal and medial layers. [8]

1.2.2 The Media The media is made up of vascular smooth muscle cells (SMCs) surrounded by an interstitial matrix of collagen, elastin, and fibronectin. [9] SMCs are responsible for contraction and distention of blood vessels in response to the variable pressures of blood flow. [6] The collagen in this layer provides the outer limit of distensibility of vessels and contributes to the stiffness and high burst pressure of vasculature. The elastin imparts vessel compliance and elasticity. [6] This interstitial matrix is responsible for the incredible biomechanical properties of arteries which are

very difficult to replicate. In addition to its mechanical roles, the media also plays a part in maintaining patent vessels in healthy vasculature. Medial SMCs of adult arteries exhibit very low rates of proliferation or death; however, they retain the ability to migrate and divide rapidly in response to problems such as hypertension, vascular injury, and atherosclerosis. [9-10] This is accompanied by a shift in the production of ECM molecules, wherein basement membrane proteins are downregulated and interstitial matrix components increase. [11] This provides a matrix wherein SMCs can proliferate and ultimately results in intimal thickening and vessel occlusion. [9]

1.2.3 The Adventitia The outermost adventitial layer of vasculature is comprised of fibroblasts in a loose connective tissue that contains blood vessels and fat. [9] The adventitia is important for preventing vessel dilation and rupture. Additionally, it is responsible for defining a vessel's territory and in providing boundaries to maintain vessel seperation and prevent arteriovenous fistula formation. [6] Together, the intimal, medial, and adventitial layers make up the highly organized veins and arteries that do much more than simply sustain blood flow through the body. These unique properties have proven to be very difficult to replicate in the development of small-diameter vascular grafts, but researchers have made significant progress in providing improved designs over current graft options.

1.3 Current Vascular Graft Options

1.3.1 Autologous Vessels Due to their relatively high patency rates and reduced chances of infection, the current "gold standard" for bypass grafts is to use autologous

vessels from the patients' own body. This procedure involves removal of a vessel, such as the saphenous vein or mammary artery, and implanting it into the bypass location. [12] The matched structural and biomechanical properties of autologous bypass grafts to native arteries in the bypass location results in significantly improved patency over other graft options. [13] However, due to disease, trauma, and anatomic abnormalities, autologous vessels are unavailable in up to 20% of bypass patients. [14-15] In these cases, synthetic vascular grafts are required.

1.3.2 Synthetic Grafts Current options for synthetic grafts include Dacron® (poly(ethylene terephthalate), PET) and GORE-TEX® (expanded poly(tetrafluroethylene), ePTFE). Synthetic grafts are not limited by availability and have relatively high patency rates in large diameter applications (> 6mm). However, thrombosis and low compliance cause occlusion in smaller vessels.[16-17] Even in large diameter applications, grafts made of PET and ePTFE must be accompanied by anticoagulant medications such as heparin that help to reduce the risk of thrombosis and intimal hyperplasia.[18] Thus, there is a growing clinical need for a synthetic, small-diameter vascular graft that improves on current options.

1.4 In Vivo Characterization of Vascular Grafts

1.4.1 Basic Host Response to Biomaterial Implants Acute inflammation is part of the body's innate immune response and is the immediate response to tissue injury, such as that which occurs upon implantation of a synthetic biomaterial. The effects of acute inflammation are limited to the first hours to days of injury and can therefore be

distinguished from chronic inflammation that persists over weeks to months. Briefly, following injury, nearby blood vessels dilate, resulting in redness and heating. Nearby capillaries experience an increase in permeability to allow leakage of fluid into the surrounding space. This fluid contains blood proteins, such as fibrinogen, that encourage clotting in order to create a barrier to invading organisms. Other soluble factors in the fluid attract granulocytes and monocytes that release degradative agents and phagocytose foreign oranisms that are visible microscopically, **Figure 1.1**.[19-22]

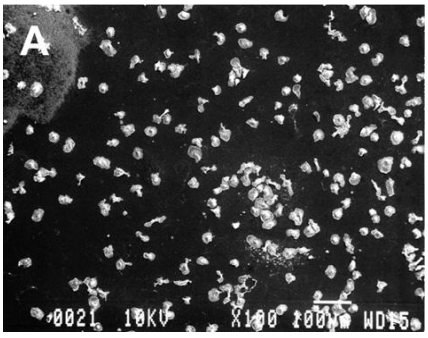

Figure 1.1. Acute host response. Scanning electron micrograph of attached monocytes on an implanted polyurethane surface at 0 days as part of the acute host response. [taken from Ref. 22]

In the case of a biostable implant, acute inflammation would ideally end with fibrous encapsulation, which begins with the formation of granulation tissue. Approximately 24 hours after implantation, macrophages and other inflammatory cells release chemoattractive signals that promote fibroblast and vascular EC migration into the area. Granulation tissue can be viewed microscopically within three to five days. Histologically, it is characterized by a pebbly, granular appearance that is a result of vascular bud formation that occurs in angiogenesis, **Figure 1.2A**.[23] Additionally,

granulation tissue is rich in fibroblasts, which serve to create an ECM of collagen and proteoglycans. Some fibroblasts in wound healing differentiate into smooth muscle cell-like myofibroblasts that are responsible for wound contraction to reduce defect size and promote healing. After appoximately four weeks, the granulation tissue matures to form a fibrous capsule. Maturation involves formation of larger blood vessels and alignment of collagen fibers as they respond to local mechanical stimuli, **Figure 1.2B**. [19,22,24-25]

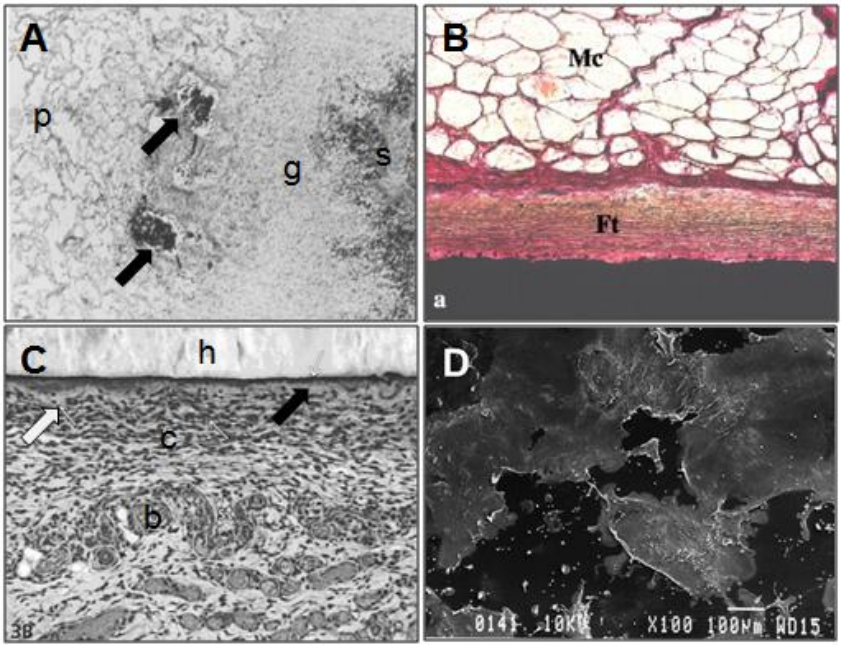

Figure 1.2. Biomaterial host response. (A) Hematoxylin and eosin stained biomaterial at 14 days post-implantation demonstrating granulation tissue (g) separating the polymeric implant (p) from the spleen (s). Arrows point to blood vessel-like areas at the leading edge of the granulation tissue. [taken from Ref. 23] (B) Safranin O/von Kossa stained polymer explant 12 weeks post-implantation demonstrating fibrous encapsulation (Ft). Aligned collagen fibrils can be seen between the polymer sample and surrounding muscle tissue (Mc). [taken from Ref. 24] (C) Toluidine blue stained dextran hydrogel (h) 5 days post-implantation demonstrating chronic inflammation. Macrophages (black arrow) are attached to surface and surrounded by lymphocytes (white arrow). [taken from Ref. 26] (D) Scanning electron micrograph of foreign body giant cells attached to polyurethane surface 14 days post-implantation, demonstrating chronic inflammation. [taken from Ref. 22]

Chronic inflammation is similar to actute inflammation except that it persists for weeks and months, rather than hours to days and it is less uniform histologically. It is characterized by the presence of mononuclear cells, such as lyphocytes and plasma cells, **Figure 1.2C**.[26] Chronic inflammation can also include granulomas, which are made up of a layer of foreign body giant cells (FBGCs) surrounding a particle that cannot be phagocytosed. FBGCs are contained within a group of epitheloid cells, which are derived from macrophages. The epitheliod cells are surrounded by lymphocytes, **Figure 1.2D**.[19,22,25]

1.4.2 Thrombosis and Intimal Hyperplasia Thrombosis is the process of blood coagulation that occurs within injured vessels. Thrombosis is mediated by platelets, non-nucleated fragments of megakaryocytes. Platelets serve to reduce bleeding after injury through the creation of a platelet plug and subsequent activation of the blood coagulation cascade to stabilize the plug. Collagen and von Willebrand factor are platelet activators that commonly adsorb to synthetic biomaterial surfaces and cause thrombosis.[27] Graft patency (% closure), platelet deposition, and thrombus coverage are common indicators utilized to measure *in vivo* thrombogencity. Patency is typically measured with Doppler ultrasonography or angiography to visualize blood flow through the graft, or it can be measured post-implantation with histology or scanning electron microscopy (SEM).[28-29] One method for quantifying platelet attachment *in vivo* involves injection of radiolabelled platelets. Detectors can be utilized outside of the body to measure radioactivity inside of grafts relative to healthy vessels.[28,30-31] Qualitative assessment of platelet deposition and thrombus coverage can be made using SEM on explanted

specimens, **Figure 1.3A**.[28] Current synthetic graft materials (PET and ePTFE) support adsorption of platelet activators and successive platelet adhesion and activation and thus have high failure rates due, in part, to thrombosis.[32-33] Thrombosis can be prevented in vascular grafts through the use of materials that do not promote platelet interactions and/or through the formation of a stable, quiescent EC layer.

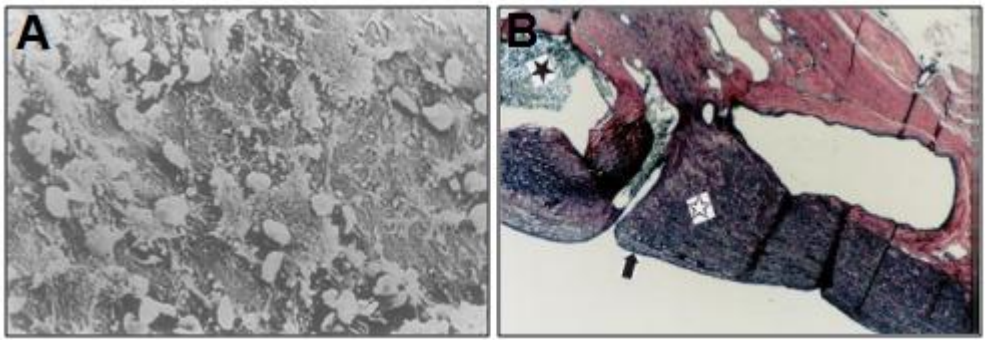

Figure 1.3. Thrombosis and intimal hyperplasia. (A) Scanning electron micrograph demonstrating platelet, erythrocyte, and leukocyte deposition to the inner layer of a Dacron® vascular graft 12 weeks post-implantation in a dog model. [taken from Ref. 28] (B) Longitudinal histological section (7.5X) of a distal anastomosis of a GORE-TEX® vascular graft after 12 weeks in a dog model. [White star denotes native artery; black star denotes synthetic graft; arrows identify regions of neointimal hyperplasia. Flow is from left to right] [taken from Ref. 38]

Intimal hyperplasia is characterized as a chronic structural change that occurs at vascular graft distal anastomoses wherein a thickened fibrocellular layer forms between the endothelium and the inner elastic lamina. This causes narrowing of the lumen and reduced blood flow, and it has been reported to happen to some extent in all vascular bypass grafts.[12,34-35] The development of intimal hyperplasia at vascular graft anastomoses is directly related to the alterations in wall shear stresses that occur due to a

compliance mismatch with native vasculature.[13,36] Namely, the transition of blood flow into a stiffer tube results in a flow stagnation point and creates a region of low and oscillating shear forces on the vascular walls.[36] These alterations in shear forces have a large effect on the underlying endothelium. ECs in these regions increase their uptake of lipoproteins, produce leukocyte adhesion molecules on their surfaces, and secrete chemotactic factors that promote proliferation of nearby monocytes/macrophages (MCP-1, VCAM-1) and underlying SMCs (Angiotensin II, PDGF, Endothelin-I).[37] This process ultimately results in atherosclerosis, characterized by accumulation of lipids and fibrous plaques and hyperproliferation of medial smooth muscle cells into the intimal layer. Where thrombosis is an acute response that results in rapid graft failure, athersoclerosis is associated with late graft failure.[34,38] These changes can be observed histologically in the graft anastomoses post-explantation as substantially thickened intimal layers dominated by SMCs and reduced medial layers, **Figure 1.3B**.[38] A direct relationship exists between vascular graft patency and compliance; thus, improved compliance matching is an important factor in improving synthetic vascular grafts to prevent intimal hyperplasia.[13]

1.4.3 Endothelialization Due to the role of ECs in providing thromboresistance and reducing intimal hyperplasia, endothelialization of vascular grafts has been identified as a key goal in improving their performance. This process can occur via EC migration from connecting native vasculature or through recruitment of circulating endothelial progenitor cells (EPCs).[39-40] The extent to which either of these events occur *in vivo* can be determined post-explantation using histology or SEM.[39-40] ECs that have

migrated from graft anastamoses are limited to the graft edges, whereas recruited cells from circulation are dispersed throughout the graft surface. Confluent and quiescent endothelial layers feature ECs in contact with each other and aligned in the direction of blood flow, **Figure 1.4A**.[40] Current synthetic vascular graft endothelialization is limited to ECs that migrate from surrounding vasculature onto the outer graft edges, as these materials do not promote significant EC adhesion or migration, **Figure 1.4 B and C**.[41]

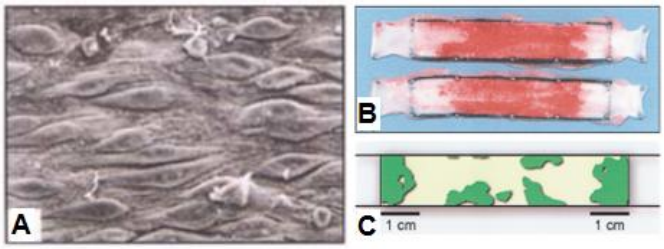

Figure 1.4. Vascular graft endothelialization. (A) Scanning electron micrograph of endothelial cells on PET grafts with granulate-colony stimulating growth factor that have been recruited from circulating blood after 4 weeks in a dog model. [taken from ref 40] (B) Gross specimen and (C) map of endothelial cell-like coverage distribution in Dacron vascular graft at 4 weeks in a dog model. [taken from ref 41]

1.5. Vascular Graft Design Advances

1.5.1 Cadaveric Allografts

1.5.1.1 Direct Allografts Cadaveric allografts were initially considered as a replacement solution for the cases in which autologous vessels are unavailable and synthetic grafts fail. Unfortunately, these grafts have had very limited success. Heterografts from the bovine carotid artery and homografts from the human umbilical cord vein have been shown to fail in the long-term due to degradation, dilation, and aneurysm formation.[42] Antigenicity of saphenous vein allografts results in immunologic

rejection and correspondingly low patency rates.[42-43] Early work by Weber et al. indicated that cryopreservation of venous allografts in dimethylsulfoxide (DMSO) served to maintain graft viability and resulted in long-term patency in dogs that was comparable to autografts.[44] However, Axthelm et al. showed that cryopreservation does not reduce the immunologic concerns of venous allografts in rats.[43] A T cell-mediated response to cyropreserved saphenous vein allografts in humans has since been confirmed, and these grafts have shown high failure rates even when used in conjunction with immunosuppressants.[45-46] This is possibly due to graft imbrittlement that occurs during the cryopreservation process and can cause early rupture in humans.[47]

1.5.1.2 Decellularized Allografts In efforts to reduce immunological concerns of venous allografts, researchers have turned towards decellularization techniques. This process removes cells and cellular debris while maintaining the structural ECM proteins of native vasculature. Although enzymatic digestion of the cellular components of allografts is successful in reducing antigenicitiy, it also results in thinner vessel walls and increased difficulty in handling.[48] New decellularization techniques have focused on improving the maintenance of structural integrity and biomechanical properties.[49-50] While these grafts are promising alternatives and show positive results in short-term *in vivo* studies, it has been found that their luminal layer is thrombogenic and that *in vivo* endothelialization is minimal.[49,51-53] Due to the important role that vascular ECs play in preventing thrombosis and intimal hyperplasia, endothelialization of the graft inner layer is required to maintain long-term patency.[4-5] To address this issue, researchers have pre-endothelialized decellularized grafts with patient cells. This results in significantly

improved graft patency in humans. However, approximately 3 weeks are required to prepare the grafts for implantation, which increases the cost of the graft and the risk of graft infection. Additionally, in some cases, the endothelial layer destabilizes under the application of vascular flow and pressures, and there are some concerns about side effects from use of the required *in vitro* growth factors used to promote endothelialization.[54-55]

1.5.1.3 Small Intestine Submucosa Allografts An alternative allograft material that has been studied is the small intestine submucosa (SIS). These scaffolds are prepared by mechanically removing the mucosa and muscle from the small intestine and lysing native cells to obtain an acellular collagen matrix with retained angiogenic growth factors, such as basic fibroblast growth factor and vascular endothelial growth factor.[56-57] Roeder et al. measured mechanical properties of small-diameter SIS grafts and determined that they have compliance and burst pressure values that are suitably high for implantation.[58] Badylak et al. provided one of the first reports of the use of SIS as a vascular graft in large diameter applications in dogs.[59] These studies laid the groundwork for a novel vascular graft material, and the grafts remained patent for up to one year. However, there was no evidence of *in vivo* endothelialization, and this study utilized autogenous tissue in large diameter vessels. Lantz et al. implanted small diameter arterial SIS autografts in dogs.[60] They observed an overall graft patency rate of 75% after up to 82 weeks, but no surface EC growth occurred. Sandusky et al. implanted small-diameter, xenogenic (porcine) SIS grafts into dogs and compared them to autologous savenous vein grafts. They found similar patency for the two graft types and no cases of aneurysm,

infection, or rupture occurred. Additionally, both SIS and saphenous vein grafts had smooth muscle medial layers and endothelial intimal layers at 90 and 180 days post-implantation. Similar patency rates and remodeling were seen in a study comparing xenogenic SIS grafts to ePTFE grafts in dogs, wherein the ePTFE grafts demonstrated a 75% occlusion rate.[61] However, it has since been shown that canine animal models will spontaneously endothelialize natural vascular graft materials whereas humans do not.[62] Robotin-Johnson et al. evaluated autogenic SIS grafts with bound heparin as growing vascular grafts in piglets over 90 days.[63] The grafts showed to be non-thrombogenic and were patent with evidence of endothelialization and remodeling. Additionally, the graft dimensions increased throughout the implant time as the piglets grew. Some concerns have arisen concerning the risks associated with remnant porcine DNA in SIS scaffolds. To address this, SIS could be obtained as an autograft from the patient to circumvent these issues; however, this would require a second surgical site that increases patient risk, and autologous tissue is limited in availability.[64-65]

1.5.2 Synthetic Graft Modification

1.5.2.1 Surgical Approach Due to the decreased cost and time of getting a new graft material to the market, many researchers have attempted to modify existing synthetic vascular grafts to improve their patency in small diameter applications.[66] The most simple of these techniques is to alter the surgical approach, which has been utilized to reduce the compliance mismatch between the synthetic graft and native vasculature. These include the use of vein cuffs, vein patches, vein boots, and arteriovenous fistulas at the distal anastomosis.[67-71] While some of these techniques have shown significant

improvements compared to unmodified grafts, these have been limited to large diameter (6 mm) grafts, and overall patency rates remain below 71%.[68,70-71]

1.5.2.2 Thromboresistant Coatings An alternate approach is to apply coatings to smaller diameter ePTFE and PET grafts to reduce thrombosis. Poly(propylene sulfide)-poly(ethylene glycol) coatings on ePTFE grafts showed decreased thrombogenicity following nine minutes of perfusion in an extracorporeal porcine arteriovenous graft when used with heparin.[72] In an alternate approach, an acrylate phosopholipid was utilized as a membrane-mimetic film on the luminal surface of a 4 mm ePTFE grafts. These grafts demonstrated thromboresistance following one hour in a baboon arteriovenous shunt model.[73] Similarly, hydrophilic acrylic coatings on PET grafts that release salicylic acid showed decreased thrombogenicity in an *ex vivo* canine circuit.[74] While these techniques show some potential for improving synthetic graft thromboresistance, there is little data indicating their long-term effectiveness.

Drug coatings have also been investigated as a potential method for improving synthetic grafts. Poly(ethylene glycol) (PEG) was used as a delivery system for hirudin, an anticoagulant, and iloprost, a vasodilation promoter, in 4 mm ePTFE grafts. This resulted in 100% patency in a porcine model with reduced intimal hyperplasia compared to the ePTFE control after 6 weeks.[75] While this is promising data, the long-term effectivness of this delivery method is yet to be established. Greisler et al. pretreated ePTFE grafts with a mixture of fibroblast growth factor-1, fibrin glue, and heparin to induce endothelialization through capillary ingrowth.[76] Although this resulted in

improved endothelialization in a canine model after 28 days, no discussion of thrombosis or intimal hyperplasia was included.

1.5.2.3 Pre-endothelialization Due to the importance of a stable endothelium in reducing thrombosis and intimal hyperplasia, researchers have attempted to improve synthetic graft patency by seeding them with ECs prior to implantation. Laube et al. cultured patient ECs and seeded them onto 4 mm ePTFE grafts for coronary artery bypass procedures.[77] This resulted in a 91% patency rate after 28 months. Similar studies have been conducted with EPCs isolated from patient peripheral blood or bone marrow with improved patency seen in animal models.[78-79] While these results are promising, culture of patient cells introduces a delay prior to implantation and is associated with the same concerns that are dicsussed above with pre-endothelialized allografts.[54] To address this, Rotmans et al. coated ePTFE grafts with anti-CD43 antibodies to recruit EPCs *in vivo*. This enhanced graft endothelialization in a porcine model at 72 hours.[80] However, the technique did not reduce intimal hyperplasia in the distal anastomosis, and there is still some controversy as to whether EPCs function as true endogenous ECs following seeding and implantation.

1.5.2.4 Nitric Oxide The incorporation of nitric oxide (NO) is another method that has been employed to improve synthetic graft patency. NO is produced by quiescent ECs and has been found to play a role in regulating vascular tone, preventing platelet aggregation, and inhibiting vascular smooth muscle cell migration and proliferation.[81] The presence of NO helps to maintian healthy vasculature and prevent neointimal hyperplasia following vascular injury. The majority of NO modifications utilize one of

two classes of NO donors: diazeniumdiolates and S-nitrosothiols. Diazeniumdiolates are stable solids that can be altered to provide tunable NO release rates in aqueous environments.[82] Initial attempts to use NO-releasing diazeniumdiolates to reduce thrombosis and intimal hyperplasia were promising, but it was found that some diazeniumdiolate polymers can leach out of polymer matrixes and form nitrosamines, which are carcinogenic.[83-85] To avoid this problem, Batchelor et al. developed a more lipophilic, discrete diazeniumdiolate species that is resistant to leaching and used it to coat 5 mm diameter commercially available polyurethane vascular grafts. These grafts were patent after 21 days in a sheep arteriovenous shunt, at which point all control grafts had occluded.[86] An alternate approach to prevent leaching of undesired byproducts is to covalently bind diaseniumdiolates to a polyurethane backbone.[87-88] *In vitro* studies with these polyurethane films have shown initial hemocompatibility, suitable mechanical properties, and sustained NO production for 2 months.

S-nitrosothiols are a biological NO transporter that are present in circulating blood.[89] Bohl and West developed NO-releasing PEG-based hydrogels through covalently linking S-nitrosothiols within the hydrogel network.[90] This resulted in reduced SMC proliferation and platelet adhesion *in vitro*, and these gels could be used to coat synthetic vascular grafts to provide controlled and localized NO delivery. While these methods are promising, the delivery of NO from these materials is limited to relatively short time frames. To address this, new materials are being developed that utilize the nitrosothiols and nitrates that are already present in circulating blood. Gappa-Fahlenkamp et al. immobilized L-cysteine on Dacron and polyurethane surfaces to

provide a free thiol group that can undergo NO exchange reactions to release NO. This resulted in improved hemocompatibility *in vitro* and has the potential to provide localized NO release throughout the lifetime of the graft.[91]

While these methods have shown some preliminary effectiveness at decreasing synthetic graft thrombogenicity, they do not reduce the compliance mismatch with the native vasculature, which is a primary cause of intimal hyperplasia in ePTFE and PET grafts. Thus, there is a need for new graft materials that improve on both biomechanical properties and hemocompatibility.

1.5.3 Protein-Based Vascular Grafts

1.5.3.1 Collagen To provide a more functional vascular graft, many researchers have incorporated native ECM proteins into graft designs. The use of biological scaffolding provides the potential for cell-mediated remodeling and functional vasoactivity over time.[92] Collagen has been extensively studied as a vascular graft material due to its inherent binding sites for ECs and its presence in native vasculature.[93-94] Weinberg and Bell developed one of the first collagen-based vascular grafts by embedding vascular cells into tubular collagen gels. However, these grafts had very poor mechanical properties (burst pressure <10 mmHg) and required incorporation with PET vascular graft sleeves to support the physiological pressures of vasculature.[94] Researchers have attempted to improve upon these properties by culturing constructs with inner mandrels to promote gel contraction, varying collagen concentration, using magnetic prealignment of the collagen fibers during fibrillogenesis, and fabricating electrospun collagen scaffolds.[95-98] While these methods have improved the mechanical

properties of collagen-based scaffolds, they fail to provide sufficeint strength for use as vascular grafts without the use of an outer stabilizing layer. Additionally, native collagen is thrombogenic, and collagen-based grafts must be pre-endothelialized to prevent *in vivo* occlusion.[99] Small-diameter vascular grafts with pre-cultured and pre-endothelialized collagen scaffolds that demonstrate adequate mechanical properties and hemocompatibility have been developed, but these techniques require increased preparation time and cost, and more work has turned to the development of bioactive grafts based on alternate ECM proteins.[100-101]

1.5.3.2 Elastin It has been proposed that the shortcomings in the biomechanical properties of collagen-based scaffolds could be due to the lack of elastin in the scaffolds.[102] Elastin is the ECM protein that contributes to the compliance of native vessels and has been investigated as a tool to provide bioactive vascular grafts with mechanical properties that more closely match those of the surrounding vasculature.[103] Additionally, studies have suggested that intact collagen and elastin networks in vasculature play a role in inhibiting SMC hyperproliferation.[104-105] Many researchers have attempted to harness these properties through fabrication of collagen-elastin-based vascular grafts. Electrospinning in particular has emerged as a fabrication technique for these protein scaffolds.[106] Boland et al. electrospun a collagen/elastin blend onto a rotating mandrel to create tubular constructs that were then crosslinked with glutaraldehyde.[107] Following culture of ECs and SMCs in a bioreactor, three-layer grafts that mimic the architecture of native vasculature were produced. Similarly, Buttafoco et al. co-electrospun collagen and elastin, but utilized a non-organic solvent (10 mM

hydrochloric acid) and a crosslinker with improved biocompatibility over glutaraldehyde (N-(3-dimethylaminopropyl)-N0-ethylcarbodiimide hydrochloride (EDC), in the presence of N-hydroxysuccinimide (NHS)).[108] While most of the presented data was proof-of-concept, this fabrication technique has the potential to provide improved scaffolds for vascular tissue engineering. Researchers have also investigated the potential of synthetic-natural polymer blends. Stitzel et al. fabricated electrospun vascular grafts with a blend of collagen type I, elastin, and poly(D,L-lactide-co-glycolide).[109] These grafts had high compliance and burst pressure, promoted SMC and EC growth *in vitro*, and induced a minimal inflammatory response when implanted subcutaneously into mice. However, thromboresistance was not reported, and these grafts would likely require *in vitro* endothelialization prior to implantation to prevent thrombus formation. Wise et al. was the first group to develop a vascular graft with recombinant human elastin.[110] The authors incorporated elastin into a synthetic poly(caprolactone) electrospun mesh to provide thromboresistant vascular grafts with tunable biomechanical properties that support EC adhesion. These grafts were well-tolerated in a rabbit carotid animal model for 1 month, but *in vivo* endothelialization and thrombosis were not assessed. In general, elastin-based scaffolds show potential in the development of small-diameter vascular grafts. However, this is a relatively new approach, and much of the research in the use of elastin in small diameter grafts is still in the developmental phase.

1.5.3.3 Fibrin Fibrin, a protein involved in blood clotting, has been investigated as an alternative vascular graft material. Although it is not a main ECM component of

native vasculature, its role in wound healing can be harnessed to stimulate regeneration and remodeling in a variety of cell types.[111] Autologous fibrinogen can be isolated from patient blood and mixed with thrombin to yield insoluble fibrin fibers.[112-114] SMCs and fibroblasts cultured in fibrin gels have shown to produce greater amounts of collagen than those in collagen gels, and fibrin gels supported *in vivo* remodeling of collagen and elastin when implanted into sheep for 15 weeks following *in vitro* culture with SMCs and ECs.[112,114-115] Fibrin and collagen have been co-polymerized to produce bioactive gels with improved mechanical properties compared to those of the pure components. These gels also allow manipulation of scaffold properties by varying the ratios of the protein components and the mechanical stimulation of the resulting gels.[116-117]

Many of the ECM protein-based approaches to small diameter vascular grafts represent progress in this difficult area. However, native ECM proteins demonstrate significant batch-to-batch variability that makes it difficult to acheive reproducible mechanical properties without the use of a significant amount of pre-culture with SMCs, fibroblasts, and/or ECs to synthesize a network of ECM proteins prior to *in vivo* use.[96,98,101,109,112,114-125] Additionally, most of these designs rely on *in vitro* endothelialization to prevent thrombosis and intimal hyperplasia following implantation.[95,100-101,109,114,118,120,125] This not only presents a significant increase in treatment cost and time, but there is little evidence that pre-endothelialized grafts retain a quiescent endothelium under the flow conditions of native vasculature.[120,126-127]

1.5.4 In Vitro Cultured Biological Vascular Grafts L'Heureux et al. initiated a new approach to vascular tissue engineering with the introduction of cell sheet-based

tissue engineering in which scaffolds are synthesized by cultured human cells without the use of an additional scaffold.[97,128] Cells are cultured *in vitro* under conditions that induce deposition of ECM to produce a solid sheet. In this first approach, a fibroblast sheet was wrapped around a cylindrical support tube, matured, and dehydrated to provide an acellular scaffold for EC seeding. An SMC sheet was wrapped around this layer to provide the medial layer, and these layers were matured in a bioreactor. The adventitial layer was comprised of a second fibroblast sheet, and the grafts were matured and endothelialized following addition of this third layer. Through increasing the culture period of the adventitial layer to 5 weeks, burst pressures of greater than 2000 mmHg were acheived, which are comparable to or greater than those of human saphenous veins (~1700 mmHg). Additionally, the EC layer provided increased *in vitro* thromboresistance.[128] These grafts were implanted into rats for long-term (8 months) *in vivo* characterization and into primates for 8 weeks to provide a more physiologically relevant model.[129] In the rat model, the grafts had an 85% patency rate with no evidence of a chronic inflammatory response and remodeling into a more physiological tissue. The grafts in the primate study were 100% patent at explantation and showed signs of remodeling as well.

Niklason et al. developed an alternative approach to biological vascular grafts by seeding SMCs onto tubular biodegradable polyglycolic acid (PGA) scaffolds in a bioreactor.[130] The PGA scaffold degrades to less than 15% of its initial mass within 5 weeks of culture. After 8 weeks of culture, the grafts were seeded with ECs and cultured for an additional 3 days. This resulted in scaffolds with burst pressures of greater than

2000 mmHg that remained patent in a porcine saphenous vein model for 4 weeks. Solan et al. utilized this same approach and investigated the effect of pulse rate during the culture period on collagen depostion by the SMCs.[131] It was found that grafts grown with higher pulse rates had significantly higher levels of collagen than those grown under static conditions. This provided a tool to enhance the graft physical and mechanical properties and to possibly decrease culture time. Unfortunately, translation of the approach from swine to adult human cells failed due to the limited proliferative capacity of terminally differentiated SMCs.[132] To address this issue, human telomerase (hTERT) was introduced into SMCs. This resulted in cells with significantly extended proliferation and mechanically robust human grafts which burst pressures up to 600 mmHg.[133-134] While this was promising, these grafts still lacked the strength necessary for use in vascular grafts, and there are some concerns about long-term oncogenicity of hTERT-infected SMCs. Thus, current work is focused on the use of human bone marrow-derived mesenchymal stem cells (MSCs) rather than SMCs.[135] Gong and Niklason able to optimize culture conditions to drive MSC differentiation and matrix production to provide grafts that were histologically and molecularly similar to native vessels.

While these approaches shows potential, they required a total culture time of 2-3 months to produce viable vascular grafts. This prevents this technology from being applied to urgent clinical use and significantly increases the cost of the graft.[92,129] However, individuals who have a disease with a well-defined progession and who lack healthy autologous vessels for use in bypass surgery can be identified during the pre-

operative waiting periods. In these cases, these vascular grafts could provide useful alternatives to current synthetic options.[136] Additionally, it has been proposed that the graft maturation period could be accelerated by providing the cells with mechanical stimulation in a dynamic culture environment.[92] This could reduce the time frame for obtaining suitable grafts, but could also increase the total cost of the constructs.

1.5.5 Synthetic ECM Analogs

1.5.5.1 Peptide-Based Scaffolds An alternative approach to developing bioactive grafts is the incorporation of ECM peptides into synthetic polymer scaffolds. While many researchers are interested in harnessing the control that synthetic polymers provide over material properties, non-specific protein adsoprtion and cell adhesion to synthetic materials *in vivo* can have detrimental effects on synthetic vascular graft success.[137] To overcome this, a synthetic material that is highly resistant to protein adsoprtion, such as PEG, is used as a base for covalently attaching bioactive moities to provide synthetic scaffolds with controlled cell-material interactions. Arg-Gly-Asp (RGD), a cell-binding peptide sequence found in fibronection, fibrinogen, and vonWillebrand factor, is one of the most extensively used peptide sequence bases.

RGD has been incorporated into polyurethanes to enhance EC adhesion and proliferation for use in vascular grafts, and alterations in RGD concentration can be used to easily control levels of cell adhesion.[138-139] Additionally, RGD has been immobilized in electrospun fibers to provide bioactive scaffolds with mechanical properties and structures that could be tuned to approach those of native vasculature.[140-141] While RGD-based scaffolds provide tunability and a means for endothelialization, RGD sequences

can be recognized by platelet integrin receptors, which could result in thrombosis in vascular grafts.[137,142] Thus, signalling peptides that specifically interact with ECs have been sought out. Specifically, Tyr-Ile-Gly-Ser-Arg (YIGSR) and Arg-Glu-Asp-Val (REDV) have been used to provide enhanced EC adhesion while preventing platelet adhesion and aggregation.[137,143] In a different approach to create vascular grafts, Gobin and West incorporated the elastin-derived peptide Val-Ala-Pro-Gly (VAPG) into PEG hydrogels to promote SMC-specific adhesion while preventing adhesion of fibroblasts, ECs, and platelets.[144] This could be used to create an SMC-rich medial layer of a vascular graft that mimics the architecture of native arteries. While these results are promising, the high cost and purity concerns associated with large scale solid-phase peptide synthesis limits the utility of this approach.[145-146] Additionally, short peptide sequences lack the triple helical conformation of native ECM proteins, which has been shown to affect EC adhesion strength and endothelium remodeling processes.[147-150]

1.5.5.2 Multilayer Vascular Grafts

Many of the synthetic polymer-based approaches utilize either hydrogel scaffolds, which lack the mechanical properties to sustain the pressures of native vasculature, or stiff polymer scaffolds, which may not provide the optimal substrate for EC adhesion and growth.[151-152] The ability to decouple cell-material interactions from biomechanical properties would be valuable in the development of synthetic vascular grafts. Many groups have created multilayer vascular grafts with electrospun polyurethanes supporting gelatin or collagen hydrogels to attempt this.[153-154] Similarly, PEG-fibrin gels were added as an inner layer to electrospun polyurethane to provide

vascular grafts with suitable substrates for endothelialization and adequate mechanical properties.[155] While these are promising approaches, they currently require pre-endothelialization to reduce thrombogenicity of the luminal layer, which is associated with previously mentioned concerns.

1.6 Summary

Vascular grafts that combine the cell-material interactions of native polymers with the thromboresistance and tunability of synthetic polymers have the potential to improve upon current small diameter graft options. While endothelialization has proven to be very important in vascular graft success, thus far, luminal EC layers have typically been been obtained through *in vitro* cell culture and seeding. An "of-the-shelf" vascular graft that does not require pre-culture with ECs would represent a significant advantage in terms of treatment time and cost. Thus, gaining a better understanding of how *in vivo* endothelialization can be obtained through rational design of scaffolds to promote desirable EC interactions is an important step forward in developing a successful off-the-shelf, small diameter vascular graft.

CHAPTER II

DEVELOPMENT AND CHARACTERIZATION OF MULTILAYER VASCULAR GRAFTS*

2.1 Introduction

Due to the low availability of autologous vessels and the high failure rates of synthetic vascular grafts, an urgent clinical need for off-the-shelf, small diameter vascular prostheses has prompted investigation of biomimetic grafts with properties that more closely match those of native blood vessels.[130-131,156-157] For a graft to be effective as an off-the-shelf arterial prosthesis, it must avoid cell harvesting and construct pre-culture, which delay treatment and increase cost.[94,128,158-159] Thus, generation of the luminal endothelial cell (EC) layer critical to inhibiting platelet aggregation and smooth muscle cell hyperproliferation must occur following implantation, and rapid endothelialization has been identified as a critical element in the development of off-the-shelf vascular prostheses to prevent small-caliber graft reocclusion.[4,158]

A vascular graft that incorporates the potential for endothelialization of native collagen while circumventing thrombogenicity concerns and providing appropriate mechanical properties would represent a significant advance in off-the-shelf graft design. To this end, we have developed a novel biomaterial platform based on a collagen-

*Reprinted with permission from "Multilayer Vascular Grafts Based on Collagen-Mimetic Proteins," by MB Browning, D Dempsey, V. Guiza, S. Becerrea, J. Rivera, B. Russell, M. Höök, F. Clubb, M. Miller, T. Fossum, J-F Dong, A.L. Bergeron, M. Hahn, and E. Cosgriff-Hernandez, Acta Biomaterialia 2012, 8 (3), 1010-1021. Copyright (2012) Elsevier.

mimetic protein derived from group A Streptococcus, Scl2.28 (Scl2-1). Scl2-1 has several properties that make it desirable for cardiovascular applications. It contains the Gly-Xaa-Yaa (GXY) motifs that form collagen's characteristic triple-helix but lacks hydroxyproline, which eliminates the need for costly post-translational modifications.[160-161] This enables facile recombinant expression in *E. coli* and eliminates the batch variability concerns associated with native collagen as well as the need for expensive solid-phase synthesis of ECM peptides.[161-162] Perhaps the most novel aspect of these proteins is that they can be designed to induce selective cell adhesion and function. Scl2-1 acts as a biological blank slate in that it resists cell adhesion even in the presence of serum and displays low platelet aggregation. However, specific receptor binding motifs can be readily inserted into the Scl2-1 sequence by site-directed mutagenesis.[162]

In native vessels, collagen-based $\alpha_1\beta_1$ and $\alpha_2\beta_1$ integrin binding motifs have been shown to modulate EC adhesion and phenotype.[163] We therefore inserted the GFPGER motif into the Scl2-1 sequence, since it has previously shown to mediate binding by $\alpha_1\beta_1$ and $\alpha_2\beta_1$ integrins.[3,149] This modified Scl2-1 (Scl2-2) maintains the triple helical structure and low platelet aggregation of Scl2-1 while promoting EC adhesion and spreading.[164] Until recently, the use of Scl2 proteins was limited to coatings due to their inability to self-assemble into stable 3D structures. To address this limitation, we have developed a synthetic methodology to incorporate Scl2 proteins into poly(ethylene glycol) (PEG) based hydrogels.[164] PEG hydrogels were selected for this application due to their resistance to protein adsorption, which underlies their thromboresistance and isolates cell-material interactions of PEG-Scl2 hydrogels to the adhesion sites introduced

by the Scl2 proteins.[165] In addition, the modulus of PEG hydrogels can be broadly tuned by altering PEG molecular weight, concentration, or functionality.[166] Pelham, et al. found that cells on flexible substrates exhibited reduced spreading and increased motility compared to cells on rigid substrates.[167] Thus, the ability to control substrate modulus allows for further manipulation of cell adhesion, phenotype, and migration.[151-152,168]

The tunability of both bioactivity and mechanical properties of PEG-Scl2 hydrogels offers unique control over the endothelialization of the graft; however, properties that promote endothelialization may not be consistent with those that are sufficient to withstand physiological loading.[151-152,167-168] To address this issue, we have developed a multilayered graft comprised of a luminal PEG-Scl2-2 hydrogel layer designed to induce rapid endothelialization and a reinforcing mesh sleeve designed to provide bulk strength, compliance matching, and suture retention. Thus, each component can be individually tuned to achieve improved outcomes without detriment to other design goals and then bonded together into composite grafts. In generating the reinforcing mesh sleeve, segmented polyurethanes (SPUs) were selected due to their established biocompatibility, durability, and fatigue resistance.[169] Electrospinning was chosen for fabricating the SPU mesh sleeve, since this process produces fibrous, porous scaffolds with mechanical properties which can be broadly tailored via modification of electrospinning parameters.[170] Despite having high burst pressures and suture retention strengths, current synthetic vascular grafts have low 2 year patency rates (40-50%) due to their low compliance values.[13] The ability to tune the biomechanical properties of

electrospun SPUs to improve matching to those of native vasculature is important in preventing intimal hyperplasia and thrombosis-induced failure in small diameter grafts.

In these studies, multilayer grafts were fabricated and characterized to assess their potential as off-the-shelf small-caliber vascular prostheses. The maintenance of graft integrity as well as biological and mechanical properties following vacuum drying and rehydration was evaluated to obtain an initial assessment of the capacity of the fabricated grafts to undergo the processing associated with long-term storage. The stability of the interlayer bonding and graft mechanical properties following four week exposure to physiological flow was then investigated. Additionally, the capability to tune graft burst pressure, suture retention strength, and compliance by varying electrospun mesh thickness was assessed. The thromboresistance of the luminal PEG-Scl2 hydrogels was tested through a series of *in vitro*, whole blood tests and in a porcine carotid model. Cumulatively, these studies indicate that the proposed multilayer design has significant potential as an off-the-shelf vascular prosthesis.

2.2 Materials and Methods

2.2.1 Materials All chemicals were used as received and purchased from Sigma Aldrich (St. Louis, MO) unless otherwise noted.

2.2.2 Scl2 Functionalization The Scl2.28 sequence was amplified and purified as previously described.[164] Scl2-1 served as a negative control with no binding sites for $\alpha_1\beta_1$ or $\alpha_2\beta_1$. Scl2-2 is a variant of this protein containing the sequence GFPGER that was generated by site directed mutagenesis as previously described.[161] Scl2 proteins and

a rat tail collagen type I control were functionalized with photoreactive crosslink sites according to a protocol adapted from Sebra et al.[171] Scl2 proteins include ~9% lysine groups that allow for bioconjugation through the established NHS-lysine Ɛ-amino group reaction. Briefly, the proteins were reacted with acrylate-PEG-N-hydroxysuccinimide (Acr-PEG-NHS, MW 3500, Jenkem Technologies USA, Allen, TX) in 50 mM sodium bicarbonate buffer (pH 8.5). The Acr-PEG-NHS:NH_2 molar ratio was 1:1, and the reaction was allowed to proceed with stirring for 24 hours at room temperature. Basic byproducts were removed via dialysis against 0.1M hydrochloric acid for 24 hours, and further purification was carried out with dialysis against deionized water for 24 hours (MWCO = 20,000). Functionalization of the modified proteins was confirmed with Fourier transform infrared (FTIR) spectroscopy and sodium dodecyl sulfate poly-acrylamide gel electrophoresis (SDS-PAGE), as previously shown.[164]

2.2.3 Preparation of Bioactive PEG-Scl2 Hydrogels Poly(ethylene glycol) diacrylate (PEGDA) was synthesized according to a method adapted from Hahn, et al.[172] Briefly, 4 molar equivalents of acryloyl chloride were added dropwise to a solution of PEG (3.4 kDa or 6kDa; 1 molar equivalent) and triethylamine (2 molar equivalents) in anhydrous dichloromethane (DCM) under nitrogen. After the addition was complete, the reaction was stirred for 24 hours. The resulting solution was washed with 2M potassium bicarbonate (8 molar equivalents) and dried with anhydrous sodium sulfate. The product was precipitated in cold diethyl ether, filtered, and dried under vacuum. FTIR spectroscopy and proton nuclear magnetic resonance (^{1}H-NMR) spectroscopy were used to confirm functionalization of PEGDA. Control and functionalized polymers were

solution cast directly onto KBr pellets to acquire transmission FTIR spectra using a Bruker TENSOR 27 spectrometer. Successful acrylation was indicated by an ester peak at 1730 cm^{-1} and loss of the hydroxyl peak at 3300 cm^{-1} in the spectra. Proton NMR spectra of control and functionalized polymers were recorded on Mercury 300 MHz spectrometer using a TMS/solvent signal as an internal reference. All syntheses resulted in percent conversions of hydroxyl to acrylate endgroups of greater than 85%. ^{1}H-NMR ($CDCl_3$): 3.6 ppm (m, -OCH_2CH_2-), 4.3 ppm (t, -CH_2OCO-), 6.1 ppm (dd, -CH=CH_2), 5.8 and 6.4 ppm (dd, -CH=CH_2).

PEG, PEG-Scl2, and PEG-collagen hydrogels were prepared by dissolving PEGDA (10 or 20 wt%) and functionalized Scl2 or collagen (4, 6, 9, 12 or 15 mg ml^{-1}) in deionized water. A photoinitiator solution (1 mg Irgacure 2959 per 0.1 ml 70% ethanol) was added at 1 vol% of precursor solution. Solutions were pipetted into a mold and crosslinked by 6 min exposure to long wave UV light (Intelli Ray Shuttered UV Flood Light, Integrated Dispensing Solutions, Inc., 365 nm, 4 mW/cm^2).

2.2.4 SPU Electrospinning BioSpan® (DSM-Polymer Technology Group; Berkeley, CA, USA) and Carbothane® (Lubrizol; Wickliffe, Ohio, USA) were dissolved at 15 wt% in dimethylacetamide (DMAC) for electrospinning. A 4 mm diameter copper rod collector was dipped in a 5 wt% PEG solution in chloroform. After drying, it was grounded and positioned 35 cm away from the tip of a blunted 20 gauge syringe needle. The SPU solutions were dispensed at a rate of 1.0 ml per hour with a syringe pump (KDS 100, KDS Scientific) as a voltage of approximately 14 kV was applied to the needle tip using a high voltage source (Gamma High Voltage, Ormond Beach, FL, USA)

for 2 to 8 hours.[170] After the designated time period, the copper rod with the mesh was placed in water overnight to dissolve the inner PEG layer, and the mesh was removed from the rod while submerged. High resolution images of electrospun fiber mats were captured using a field emission – scanning electron microscope (JSM-7500F, JEOL) operated at 2kV to confirm fibrous morphology (average fiber diameter = 1.6 ± 0.1 µm), **Figure 2.1**.

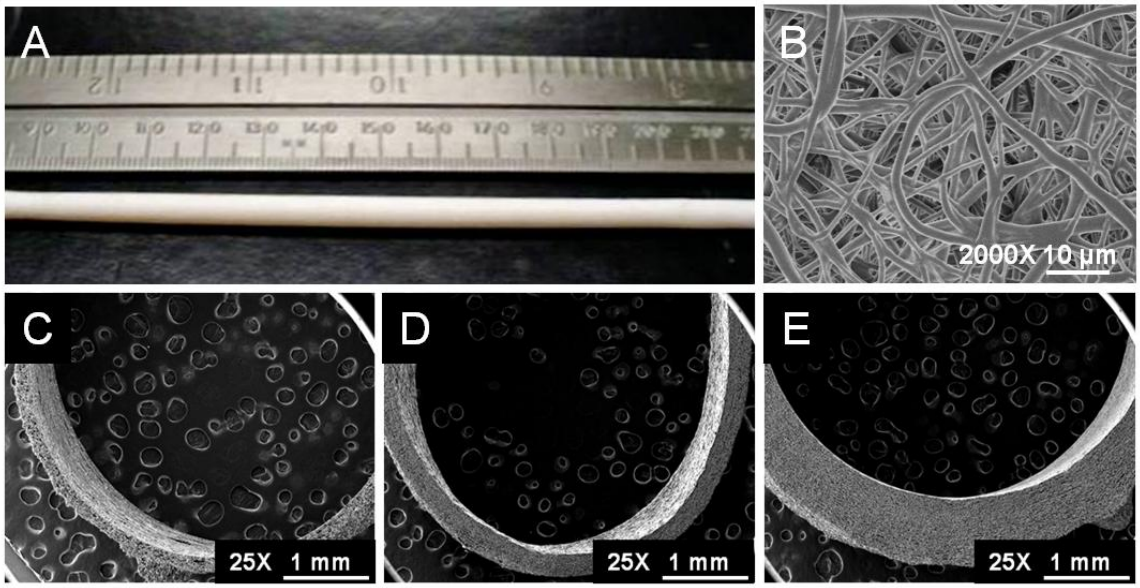

Figure 2.1. Reinforcing electrospun mesh tube. (A) Electrospun SPU mesh tube. (B) Representative SEM image of fibrous SPU mesh tube. Cross-sectional views of (C) low thickness tube (wall thickness ≈ 0.17 mm), (D) medium thickness tube (wall thickness ≈ 0.36 mm), and (E) high thickness tube (wall thickness ≈ 0.78 mm).

2.2.5 Multilayer Graft Fabrication Mesh sleeves were taken through a graded ethanol/water soak (70%, 50%, 30%, and 0%; 30 minutes each) to ensure hydration and penetration of the aqueous hydrogel precursor solutions into the mesh prior to polymerization. The pre-wetted meshes were placed in a cylindrical mold with an inner

glass mandrel (3 mm OD). Hydrogel solutions were pipetted between the mandrel and the hydrated mesh (4 mm ID) and crosslinked as described in Section 2.3, **Figure 2.2.** Given that the inner diameters of the mesh and the multilayer graft (i.e. the hydrogel layer) were held constant, the outer diameter of the multilayer graft was dependent on the thickness of the electrospun mesh. In these studies, the electrospun mesh thickness was modulated from approximately 0.2 to 1.2 mm, resulting in graft wall thickness between 0.7 and 1.7 mm and corollary graft outer diameters between 4.4 and 6.4 mm.

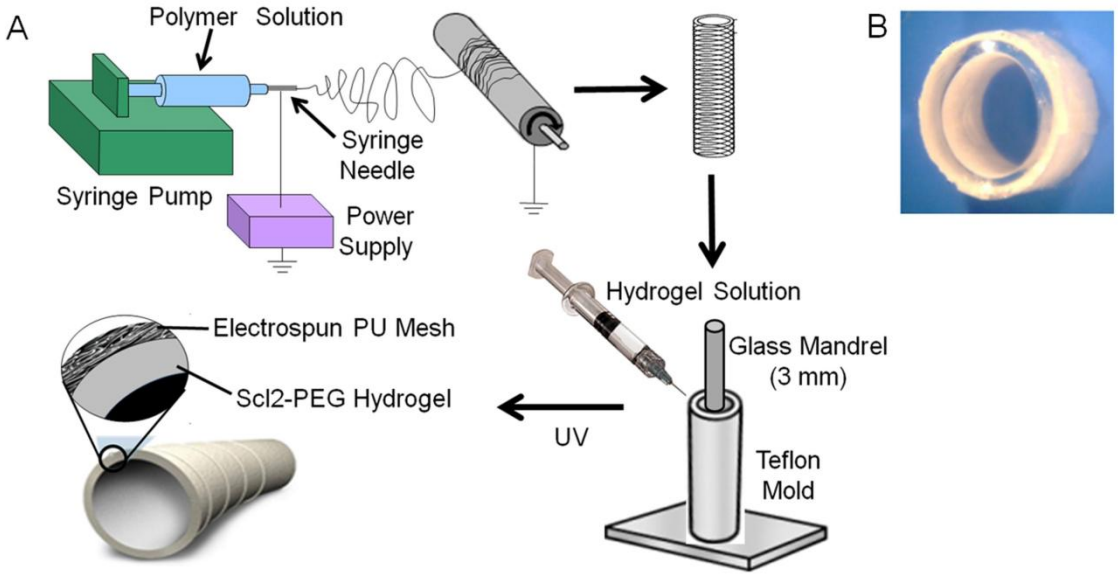

Figure 2.2. Multilayer graft fabrication. (A) Fabrication process of multilayer grafts. (B) Multilayer graft.

2.2.6 Multilayer Graft Structural Stability Following Vacuum Drying To analyze the effects of vacuum drying on graft inter-layer cohesion, Carbothane was electrospun for 4 hours, and multilayer grafts were fabricated with PEG hydrogels (10 wt% PEGDA, 3.4kDa). After crosslinking, grafts were cut in half and either dried under

vacuum or swelled in phosphate buffered saline (PBS) overnight. Vacuum-dried samples were then swollen in PBS. Cross sectional images of both the vacuum dried and rehydrated samples and the immediately-swollen controls were obtained with an optical zoom microscope (Z-Pix MM-640, Carson Microscopes, 130X) to document delamination, or macro-scale physical separation between the hydrogel and electrospun mesh. Burst pressure testing of multilayer grafts was carried out as described in Section 2.7 to determine if mechanical properties were affected by drying.

2.2.7 Retention of Hydrogel EC Adhesion Following Vacuum Drying and Sterilization The effects of vacuum drying and ethylene oxide sterilization on cell adhesion were evaluated. PEG-collagen hydrogels (10 wt% PEGDA, 3.4 kDa, 12 mg of protein ml^{-1}) and PEG hydrogels (10 wt% PEGDA, 3.4 kDa) were fabricated between 0.75 mm thick spacers. Each of the resulting gels was cut in half, and one segment was immediately submerged in PBS while the remaining half was vacuum-dried, ethylene oxide sterilized, and rehydrated in PBS. Bovine aortic endothelial cells (BAOECs, Cell Applications) were harvested and seeded onto the swollen gels at 10,000 cells cm^{-2}. Gels were cultured for 3 h at 37 °C/5% CO_2, and cell adhesion was evaluated using a Zeiss Axiovert microscope in 5 randomly selected fields of view. Cell adhesion was calculated by manually counting the cells in each field view, and cell morphology was qualitatively assessed to evaluate spreading before and after treatment.

2.2.8 Multilayer Graft Stability Following Prolonged Exposure to Physiological Flow Freshly prepared multilayer grafts were exposed to flow in a pulsatile flow bioreactor system for 4 weeks, and resulting delamination between layers

and mechanical properties were observed.[156] BioSpan meshes were electrospun for 8 hours as described in Section 2.5. Multilayer grafts were prepared with 20 wt% PEGDA hydrogels (6 kDa). A peristaltic pump (KrosFlo Research II Pump, Spectrum Laboratories, Rancho Dominguez, CA) drew fluid (250 μM Dextran T70 (Pharmacosmos, Denmark) in PBS with 1% v/v antibiotic-antimycotic solution (CellGro, Manassas, VA)) from a stock reservoir at 120 ml min^{-1} with 120 pulses min^{-1}. Fluid was pumped through six multilayer grafts that were set up in parallel and held in place with sutures on each end. After flowing through the grafts, fluid was passed back to the reservoir to complete the flow circuit. Prior to beginning the study, the pressure profile experienced in each line was monitored using a pressure transducer (Merit Medical, South Jordan, UT) in conjunction with a clinical pressure monitor (DataScope 3000A). It was verified that the pressure through each graft was consistent and that a pulsatile pressure waveform was generated with a mean pressure of ~50 mmHg and a peak-to-trough pressure differential of ~20 mmHg, as previously described.[173] Fluid was changed every 4 days during the 4 week flow period.

The macroscopic interlayer bond integrity was observed with an optical zoom microscope (Z-Pix MM-640), and tensile testing was carried out on ring specimens (2-4 mm long, n=4) before and after the flow study. Rings were mounted onto specialized stainless steel grips and strained until failure at a uniaxial strain rate of 6 mm min^{-1} using an Instron 3342. Stress and strain were calculated from the force elongation data as described in Johnson, et al.[174] The tangential modulus of elasticity was calculated from

the resulting stress-strain data at a stress representative of that *in vivo*. This physiological stress (σ) was approximated with the equation:

$$\sigma = \frac{PR}{H} \qquad [2.1]$$

where P is pressure (approximated to be 100 mmHg for physiological conditions), R is the inner radius, and H is the wall thickness. The modulus was taken to be the stress divided by the strain at this point.[174]

2.2.9 Multilayer Graft Biomechanical Properties To determine the dependence of multilayer graft suture retention strength, burst pressure and compliance on the thickness of the electrospun mesh layer, BioSpan was electrospun for 2 to 8 hours to form reinforcing meshes with varied thicknesses. Electrospun meshes were then combined with 20 wt% PEGDA (6 kDa) hydrogels for testing. Graft suture retention strength was determined in accordance with the straight across procedure described in the American National Standard Institute- Association for the Advancement of Medical Instruments VP20-1994.[175] Briefly, 18 mm long tubular samples were cut lengthwise to obtain rectangular strips (approximately 12 mm wide). A 5.0 commercial PDS II monofilament suture (Ethicon, Inc) was inserted 2 mm from the short edge of the sample, looped, and tied. The lower end of the sample and the suture loop were secured in the grips of a uniaxial load test machine (Instron 3342) and extended at a rate of 100 mm min^{-1} until the suture pulled through the sample wall. Suture retention strength was considered to be the maximum force recorded prior to sample failure.

For burst pressure and compliance assessment, a nonporous latex tube lining was inserted into multilayer grafts (35 mm long). Burst pressure was determined from a

method adapted from Sarkar et al.[176] Deionized water was pumped into the latex tubes at a rate of 140 ml min^{-1} using a syringe pump (KDScientific), and the pressure was measured using a high pressure gauge (0 to 60 psi pressure range, NoShok) connected downstream of the graft. The ends of the grafts were firmly secured and sealed to prevent leaking. The maximum pressure prior to construct failure was recorded as the burst pressure.

The static compliance of separate latex-lined grafts was measured as previously described.[177] Briefly, a syringe pump (Harvard Apparatus) was used to subject the multilayer grafts to a pressure ramp (0-150 mmHg). Intraluminal pressure was monitored using standard in-line strain gauge pressure transducers (Merit Medical, South Jordan, UT), and the outer diameter was measured with a He-Ne laser micrometer (BenchMike, Lasermike). Compliance (C) was calculated from the recorded pressure, P, and diameter, D, according to the following equation:

$$C=\frac{\Delta D}{D_0 \cdot \Delta P}=\frac{D_{120}-D_{80}}{D_{80} \cdot 40} \qquad [2.2]$$

2.2.10 Multilayer Graft Thromboresistance

2.2.10.1 Parallel Plate Flow Studies As a first step in evaluating graft thromboresistance, the adhesion of platelets exposed to the surface of PEG-Scl2 hydrogels was evaluated. Glass slides were functionalized with methacrylate groups to enable bonding between the PEG-Scl2 hydrogels and the glass.[178] In brief, glass slides were cleaned in a solution of 70% sulfuric acid and 9% hydrogen peroxide (v/v in deionized water) for 30 minutes and rinsed thoroughly. After drying, the slides were

treated with a 2% v/v solution of 3-(trimethoxysilyl) propyl methacrylate in 95% ethanol (pH 5, adjusted with acetic acid) for 5 minutes under nitrogen. They were rinsed with deionized water then dried, leaving free methacrylate groups on the glass to react with PEGDA during UV exposure. Hydrogels (0.3 mm thick) were formed between an acrylated glass slide and a non-acrylated glass slide under sterile conditions. PEG hydrogels (10 wt% PEGDA, 3.4 kDa) served as the negative control, and PEG-Scl2-1 and PEG-Scl2-2 hydrogels (10 wt% PEGDA, 3.4 kDa, 9 mg protein ml^{-1}) were tested. Tissue-culture polystyrene (TCPS) and collagen-coated TCPS served as positive controls. Rat tail collagen type I (BD Biosciences) was coated onto TCPS as per the manufacturer's instructions. Briefly, the collagen solution was diluted with 0.02 M acetic acid to 50 µg ml^{-1} and then added to a sterile 6-well TCPS plate at 5 µg cm^{-2}. After incubation at room temperature for one hour, the remaining solution was aspirated off and the coated wells were rinsed with PBS.

Mepacrine (MP Biomedicals) was added to heparinized whole blood from Yucatan miniature pigs at 10 µM to fluorescently label platelets. All studies were complete within 8 hours of obtaining blood from the animals. A parallel plate flow chamber fitted with a silicon rubber gasket (0.05 in thick; Glycotech) and syringe pump (Harvard Apparatus) were used as previously described.[179] A vacuum source was used to secure the flow chamber to each sample surface. Blood was flowed over the samples for 2 minutes with a shear rate of 2000 s^{-1}.[180] Specimens were run in a random order to reduce the effects of time on observed sample-specific platelet activity. Afterwards, the

samples were rinsed with PBS and placed into lysis buffer (0.5% v/v TritonX-100 in PBS) to lyse adherent platelets or into 2.5% v/v glutaraldehyde solution for fixation.

Following an hour long incubation at room temperature, the three specimens of each surface type that were immersed in lysis buffer were evaluated for lactate dehydrogenase (LDH) activity using an LDH assay kit (Roche). The number of platelets on each sample was quantified by comparison with the LDH readings of lysed platelet suspensions of known concentrations.[180] The three samples per surface area reserved for fixation were exposed to 2.5% glutaraldehyde for 2 hours. After gentle rinsing with PBS, the fixed specimens were imaged using fluorescent microscopy (Axiovert 200, Zeiss). Three fields of view (200X) were selected at random, and the number of adherent platelets in each field was counted.[87] Parallel brightfield microscopy images taken at each field of view were utilized to qualitatively analyze platelet aggregation.[180]

2.2.10.2 Bioreactor Flow Study As a next step in evaluating graft thromboresistance, heparinized whole blood was flowed through the lumen of multilayer grafts for extended time periods. Reinforcing Carbothane meshes were electrospun for 4 hours to form multilayer grafts as described in Section 2.5. PEG hydrogels (20 wt% PEGDA, 6 kDa) functioned as a negative control to test the thromboresistance of PEG-Scl2-1 and PEG-Scl2-2 hydrogels (20 wt% PEGDA, 6 kDa, 15 mg protein ml^{-1}). A 6 mm internal diameter GORE-TEX® vascular graft served as a clinical control (ePTFE, Gore Medical, Flagstaff, AZ). The multilayer grafts were fitted onto custom glass chambers connected to a peristaltic pump (Masterflex, Cole Parmer). Fresh, heparinized Yucatan miniature pig whole blood was incubated with mepacrine (10 μM) for 30

minutes prior to testing to fluorescently label platelets. After ensuring that all air bubbles were removed from the system, blood was flowed through the samples at a temperature of 37°C and a volumetric flow rate of 120 ml min^{-1}. As with the parallel plate flow studies, the specimens were run in random order to reduce the effects of time on observed sample-specific platelet activity. Local pressures were monitored and kept constant in all lines during flow. After 6 hours of constant flow, samples were removed, gently rinsed with PBS, and fixed in formalin (10% v/v) overnight at 4°C. After fixation, grafts were cut longitudinally and imaged (Axiovert 200, Zeiss) to qualitatively analyze platelet adhesion.

2.2.10.3 Activation of Non-Adherent Platelets Given reports that some surfaces can activate circulating platelets despite displaying relatively low platelet adhesion, activation of non-adherent platelets was investigated in addition to the aggregation/activation of surface-adherent platelets.[33,181] PEG-Scl2-2 (10 wt% PEGDA, 3.4 kDa, 12 mg protein ml^{-1}) and PEG-collagen (10 wt% PEGDA, 3.4 kDa, 4 mg protein ml^{-1}) hydrogels as well as a 10 wt% PEGDA (3.4 kDa) control were prepared directly in 24 well plates. Prior to testing, the hydrogels were vacuum dried, ethylene oxide sterilized, and swollen in sterile PBS.

The surface expression of P-selectin (CD62P) and PAC-1 binding associated with sample-exposed, non-adherent platelets were analyzed using flow cytometry, as previously described.[182] Briefly, P-selectin expression was determined using an R-phycoerythrin-conjugated anti-CD62P antibody (BD Pharmingen, San Jose, CA, USA), and integrin $\alpha_{IIb}\beta_3$ activation was assessed with a fluorescein isothiocyanate (FITC)-

conjugated PAC-1 antibody (Becton Dickinson, San Jose, CA, USA). Whole blood was drawn from five healthy human volunteers, and citrate was added at 0.38% of the final volume to prevent clotting. Baseline controls were stored in polypropylene tubes, and each hydrogel sample was simultaneously incubated with 1 ml of whole blood for 2 hours. After incubation, 5 µl of blood from each sample was diluted with 75 µl of Tyrodes buffer (139 mM NaCl, 3 mM KCl, 17 mM $NaHCO_3$, 12 mM Glucose, 3 mM $CaCl_2$, 1 mM $MgCl_2$ in deionized water) with 1% w/v bovine serum albumin (BSA, Calbiochem). For the positive activated control, 5 µl of baseline blood was added to 65 µl of Tyrodes with 1% BSA followed by the addition of 10 µl of 200 µM adenosine diphospate (ADP, Helena). Twenty microliters of antibody (anti-CD62b or PAC-1 antibody directed against integrin $\alpha_{IIb}\beta_3$) was added to each tube. After a 20 minute incubation, the mixtures were fixed with 1 ml of 1% v/v paraformaldehyde (Electron Microscopy Sciences) in PBS. Samples were vortexed and analyzed with a Coulter Epics XL MCL flow cytometer (Beckman Coulter, Miami, FL, USA). Both PAC-1 binding and P-selectin expression were expressed as log mean fluorescence intensity (MFI).

Factor X activity in sample-exposed whole blood was determined using a chromogenic assay (Actichrome FX, American Diagnostica Inc, Stamford, CT). After the 2 hour incubation, blood was removed from hydrogel laden wells and from the baseline polypropylene tube and centrifuged at 1500 X g for 15 minutes at 25°C. Platelet poor plasma was harvested for duplicate measures of Factor X activity. Fifty microliters of each sample and standards in duplicate were incubated in a 96 well microplate at 37°C for 4 minutes. Then, 50 µl each of Russell's Viper Venom (0.2 mg ml^{-1} deionized

water) and 0.1 M calcium chloride were added to each sample. Following a 2 minute incubation at 37°C, 50 microliters of 5 mM Spectrozyme FXa were added, and the plate was incubated at 37°C for 10 minutes. The reaction was stopped by adding 50 µl of 20% acetic acid to each well, and absorbance was measured at 405 nm using a microwell plate reader. Percent Factor X activation was determined for samples and the baseline control relative to the included standards

2.2.10.4 In Vivo Acute Thromboresistance All procedures were approved by the Institutional Animal Care and Use Committee. Multilayer grafts (3 cm in length, 4 mm inner diameter) were implanted in a 6 month old Yucatan miniature pig (30-40 kg) using a previously described technique.[183] Briefly, anesthesia was induced by intramuscular injection of Telazol (5 mg/kg) and buprenorphine (0.01-0.05 mg/kg) followed by intubation and administration of isoflurane (2-4% MAC) in 100% oxygen for maintenance of a surgical plane of general anesthesia. Using sterile technique, an 8-12 cm incision was made in the ventral midline of the neck. The carotid arteries were sequentially exposed and vascular clamps placed at each end of the area of interest on the artery to provide temporary vessel occlusion. An end-to-end anastomosis was performed using a continuous pattern of 7-0 prolene sutures. A multilayer graft with PEG-Scl2-2 (10% 3.4 kDa, 12 mg protein ml^{-1}) was implanted on the left side, and a PEGDA (10% 3.4 kDa) control graft was implanted on the right side. After confirming patency and hemostasis, subcutaneous tissues and skin were closed routinely. Digital subtraction and 3-D angiography were performed via the transfemoral technique with systemic anticoagulation using heparin after placement of the sheath and maintenance of

activated clotting times of 2-3x baseline in order to prevent thromboembolic complications related to the procedure itself. After removal of the catheter and sheath, the animal was maintained under anesthesia for 5 hours. The patency and anatomy of the grafts were assessed using vascular Doppler and two dimensional ultrasound imaging techniques. The study subject was then heparinized and humanely euthanized while still under general anesthesia. The carotid arteries were carefully removed for further evaluations.

2.3 Results and Discussion

2.3.1 Stability of Multilayer Graft Structure and Bioactivity Follow Vacuum Drying The stability of the multilayer grafts was evaluated after vacuum drying as a preliminary assessment of their potential for long term storage. Vacuum drying and reswelling had no visible effects on the interface between the luminal hydrogel layer and the reinforcing mesh, **Figure 2.3 A-B**. Furthermore, graft wall thicknesses were unchanged (1.96 ± 0.04 mm before drying versus 1.98 ± 0.05 mm after drying, n=6). The burst pressure of dried and rehydrated grafts did not statistically differ from fresh, swollen composites, indicating that biomechanical properties were not significantly affected by vacuum drying. In future evaluations, graft physical and biomechanical properties over time will be measured in response to varied storage conditions (i.e. temperature, drying/sterilization processes, time). In addition, BAOEC adhesion on PEG-collagen hydrogels was evaluated relative to pure PEG hydrogels after vacuum drying and ethylene oxide sterilization as a first step in determining potential effects of

the processing measures on bioactivity, **Figure 2.3 C-F**. There were no significant differences in BAOEC adhesion on either the PEG surfaces (51 ± 18 cells mm^{-2} versus 47 ± 36 cell mm^{-2}) or the PEG-collagen surfaces (122 ± 27 cells mm^{-2} versus 113 ± 23 cell mm^{-2}) before or after drying and sterilization. Additionally, qualitative analysis of BAOEC spreading revealed similar morphologies on the two surfaces before and after treatment; namely, BAOECs bound to the PEG surfaces were generally singular and rounded, while BAOECs bound to the PEG-collagen hydrogels were highly spread with extended pseudopodia. These results serve as an initial indication that the multilayer grafts could be stored dry and re-swollen immediately prior to implantation without detriment to their ability to support endothelialization. Future studies will include analysis of Scl2-2 degradation and retention in dried and swollen hydrogels over time and the corresponding effects on bioactivity and thromboresistance.

2.3.2 Multilayer Graft Stability Following Prolonged Exposure to Physiological Flow Since graft stability under physiological stresses is critical to its bioactivity, thromboresistance, and mechanical stability, multilayer grafts were subjected to pulsatile flow for a period of 4 weeks. Alterations in graft architecture and/or mechanical properties were then examined. The conditioned grafts showed no visible signs of delamination between the hydrogel and mesh layers, and measurements of graft wall thickness before and after exposure to flow were statistically similar (2.49 ± 0.06 mm and 2.45 ± 0.14 mm, respectively, n=6). These results indicate that grafts were not subject to significant degradation or erosion as a result of pulsatile flow over the selected time frame. Specifically, degradation of the luminal hydrogel layer would have resulted

in thicker walls, due to associated decreases in crosslink density that would cause increases in swelling.[184] Conversely, physical erosion of the hydrogel layer due to pulsatile flow would have decreased the overall wall thickness. The circumferential modulus of multilayer constructs at physiological stresses (~190 kPa for the construct dimensions assuming an average luminal pressure of 100 mmHg) was statistically unchanged after exposure to flow (560 ± 270 kPa before flow vs. 470 ± 110 kPa after flow, n=6). The physical and mechanical stability of these multilayer grafts under flow is an important aspect in developing a biostable vascular graft, and these results serve as a preliminary indication of the potential for long term success of this graft design in the body.

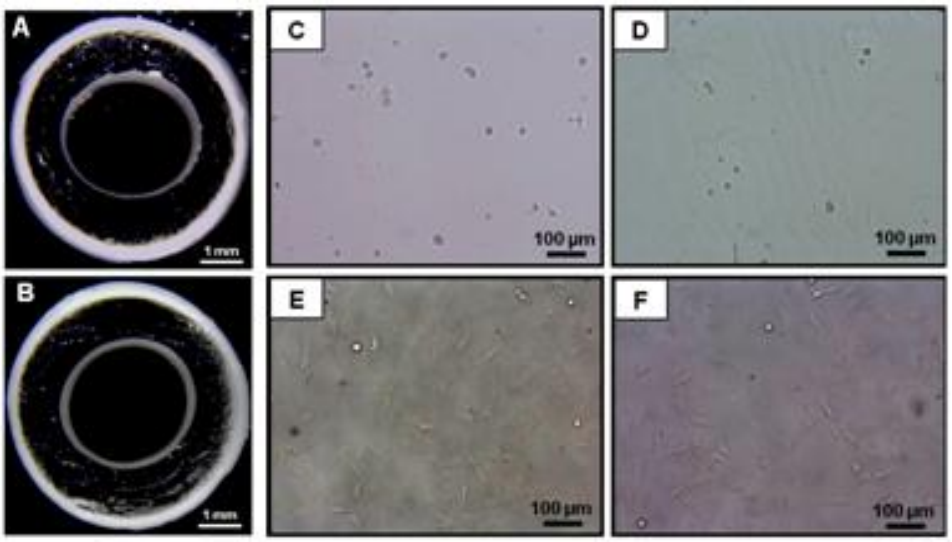

Figure 2.3. Multilayer graft integrity and maintenance of bioactivity. No visible delamination between layers was observed (A) before or (B) after vacuum drying and reswelling. Similarly low levels of BAOEC adhesion and spreading were observed on pure PEG hydrogel (C) before and (D) after sterilization. BAOEC adhesion and spreading on PEG-collagen hydrogel (F) after sterilization is increased relative to pure PEG hydrogel, similarly to (E) unprocessed gel, indicating that sterilization process does not affect bioactivity.

2.3.3 Multilayer Graft Biomechanical Properties A functional small-caliber vascular graft must have suture retention strength sufficient for immediate implantation as well as requisite long-term burst strength. In addition, graft compliance is not only important in matching the physical and bulk mechanical characteristics of native arteries; it has a large effect on preventing reocclusion of grafts. Stewart et al. found that a compliance mismatch between the graft and host tissue resulted in trapped microspheres at the wall near graft connections under pulsatile flow *in vitro*. Thus, microscopic flow separation and stagnant zones in vasculature caused by compliance mismatches may contribute to intimal hyperplasia and thrombosis seen in failed synthetic grafts.[185] Given the need for both appropriate compliance and sufficient strength, the ability to employ varied electrospinning conditions to tune graft biomechanical properties was investigated. By adjusting electrospinning times, the thickness of the reinforcing meshes can be altered over a wide range. It was observed that suture retention strength and burst pressure increased and compliance decreased as the thickness of the electrospun meshes was increased, **Table 2.1**.

Over the thickness range investigated (0.21 to 1.19 mm), burst pressure increased 163%, suture retention strength increased 327%, and compliance decreased 69%. These results are in agreement with the known dependence of these various material properties on construct dimensions. Namely, all materials have a finite stress limit (*f*, force/area) that they can sustain without failure. As mesh thickness increases, the cross sectional area of a sample that is strained during suture retention testing is increased, and the maximum force that can be sustained, or suture retention strength in this case, increases.

Mesh thickness has a similar effect on burst pressure of vascular grafts. For a thin walled tube, the stress limit (σ) of a material is defined as:

$$\sigma = \frac{PD}{2H} \qquad [2.3]$$

where D is diameter, H is wall thickness, and P is the maximum pressure that the wall can withstand, or burst pressure. Thus, as thickness increases, the burst pressure of a thin walled tube should increase. The effects of changing thickness on compliance can be determined from the definition of elastic modulus (E):

$$E = \frac{Stress}{Strain} = \frac{PD}{2H} \cdot \frac{D_0}{\Delta D} \qquad [2.4]$$

This equation can be rearranged to relate compliance measurements to elastic modulus:

$$C = \frac{\Delta D}{D_0} \cdot \Delta P = \frac{D}{E} \cdot 2H \qquad [2.5]$$

From this equation, it can be seen that increased mesh thickness causes decreases in compliance.[58]

Table 2.1. Biomechanical properties of multilayer vascular grafts. Burst pressure, suture retention strength, and compliance can be tuned over a wide range by altering electrospun mesh thickness.

Thickness (mm)	Burst Pressure (mmHg)	Suture Retention Strength (gf)	Compliance (%/mmHg X 10^{-4})
0.21 ± 0.06	534 ± 84	406 ± 124	5.9 ± 1.4
0.39 ± 0.06	665 ± 113 **(↑ 25%)**	764 ± 234 **(↑ 88%)**	3.6 ± 1.0 **(↓ 39%)**
0.72 ± 0.06	905 ± 186 **(↑ 69%)**	1390 ± 316 **(↑ 242%)**	2.7 ± 0.2 **(↓ 54%)**
1.19 ± 0.17	1404 ± 40 **(↑ 163%)**	1734 ± 33 **(↑ 327%)**	1.8 ± 0.1 **(↓ 69%)**

The lowest suture retention strengths measured (406 ± 124 gf) exceeded reported values of saphenous vein grafts (196 ± 2 gf).[136] This indicates that the multilayer grafts

are suitable for the implantation process. Maximum burst pressure of constructs made with a reinforcing BioSpan layer (1.19 ± 0.17 mm thick, n=3) was measured to be 1440 ± 40 mmHg, which approaches reported values of saphenous vein grafts (1680 ± 307 mmHg).[128] Finally, maximum graft compliance measured (mesh thickness = 0.21 ± 0.06 mm) was 5.9 ± 1.4 % radial change per mmHg X 10^{-2}. This falls within the previously reported range of compliance measured for saphenous vein grafts (4.4 ± 0.8 % per mmHg X 10^{-2}) and improves on reported compliance values of Dacron vascular grafts made from PET (1.9 ± 0.3 % per mmHg X 10^{-2}).[186] These results indicate that the reinforcing electrospun mesh can be tuned to provide biomechanical properties comparable to saphenous vein grafts and that improve on the properties of current synthetic options.

Although BioSpan meshes displayed properties comparable to saphenous vein autografts in these studies, meeting both compliance and burst pressure requirements with a single set of electrospinning parameters was not possible by varying mesh thickness alone. However, the ability to tune scaffold properties over a large range by simply changing mesh thickness is a powerful tool which should aid in fabricating improved synthetic vascular grafts. Future studies will investigate the effects of altering SPU chemistry to gain further control over biomechanical properties and achieve both desired burst pressure and compliance.

2.3.4 Thromboresistance Assessment

2.3.4.1 In Vitro Flow Studies To address the possibilities of graft occlusion at the site and downstream of the graft, both platelet adhesion and non-adherent platelet

activation were analyzed in these studies. The shear rate of blood flow can have conflicting effects on the measured blood compatibility of a surface. Increased shear rates cause flow separations that increase platelet activity, thereby increasing apparent robustness of testing; however, they can also cause dilution of activated clotting factors and prevent them from causing clots *in vitro*, resulting in falsely high blood compatibility.[187-188] The PEG-Scl2-2 surface was tested under both high shear rate flows (parallel plate flow study) and venous-like flows (bioreactor flow study). Surface platelet adhesion/aggregation was first assessed under relatively short-term flow conditions by passing heparinized whole blood over the hydrogel surfaces using a parallel plate flow setup. Quantitative values of platelets adhered per square centimeter were found using the LDH assay, **Figure 2.4A**. The levels of platelet adhesion on the PEG, PEG-Scl2-1, and PEG-Scl2-2 hydrogels were statistically similar and were each significantly lower than the values for the TCPS and collagen-coated TCPS positive controls. Manual counting of fluorescently-labeled platelets (data not shown) confirmed these trends.

These LDH measurements do not distinguish aggregated platelets from those that have simply adhered. Therefore, brightfield microscopy was utilized to qualitatively analyze platelet morphology and aggregation, **Figure 2.4B**. Platelets were generally singular and rounded on PEG, PEG-Scl2-1 and PEG-Scl2-2 hydrogels, indicating that they were unactivated or in the initial stages of activation. In contrast, TCPS and collagen-coated TCPS showed large aggregates of non-uniformly shaped platelets, and much higher numbers of platelets can be seen in each field view. The combined LDH

and microscopy results thus suggest that the positive controls induced not only greater platelet adhesion but also greater platelet activation during the two minute flow study.

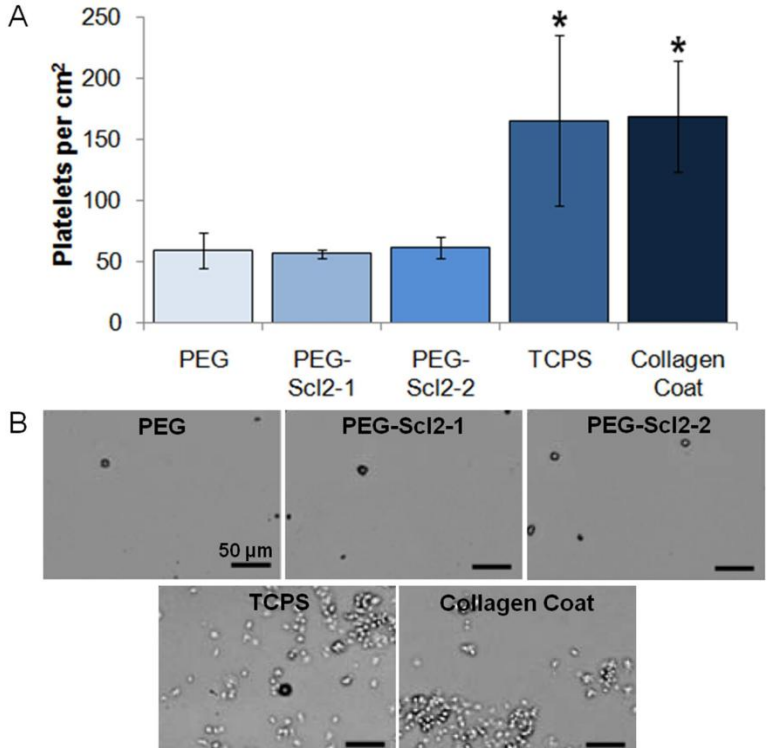

Figure 2.4. Platelet adhesion and aggregation after 2 minutes of whole blood exposure in parallel plate flow setup. (A) Platelet levels per square cm of surface determined by the LDH assay. No significant differences in platelet adhesion were seen between hydrogel samples. All hydrogels had significantly lower adhesion levels than positive controls. n=3; mean ± standard deviation displayed; *$p<0.05$ relative to PEG hydrogel control. (B) Hydrogel samples had lower levels of platelet adhesion, spreading, and aggregation relative to TCPS and collagen-coated TCPS positive controls. Attached cells were fixed with 2.5% glutaraldehyde and imaged by brightfield microscopy.

Given the short-term flow results, platelet surface adhesion and aggregation under the more complex conditions associated with the composite graft structure, physiological pressurization, and longer-term flows was assessed. Macroscopically, the

hydrogel-mesh multilayer grafts subjected to flow of heparinized whole blood in a pulsatile flow bioreactor withstood flow for the full, 6 hour time period and displayed no visible signs of clot formation. In contrast, the ePTFE (GORE-TEX®) vascular graft used as a clinical control in this study occluded within one hour due to thrombosis. These observations were confirmed microscopically, **Figure 2.5**. PEG, PEG-Scl2-1, and PEG-Scl2-2 grafts showed sparsely adhered platelets with regular rounded morphologies. These results indicate that PEG-Scl2 hydrogels did not induce significant platelet activation after longer periods of flow, further confirming the parallel plate study results. High levels of platelet spreading and aggregation were observed on the ePTFE clinical graft, suggesting significant activation of adherent platelets. This study implies that PEG-Scl2 hydrogels provide a surface with significantly improved thromboresistance over current clinical options for synthetic vascular grafts.

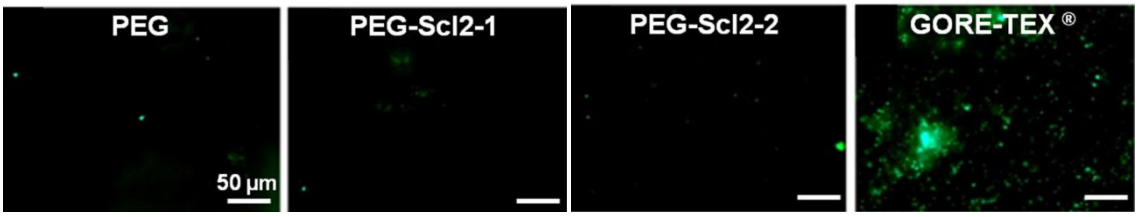

Figure 2.5. Platelet adhesion after 6 hours of whole blood flow through multilayer grafts in a pulsatile flow bioreactor. All grafts with luminal hydrogel layers remained patent during the testing time, while the ePTFE (GORE-TEX®) vascular graft occluded within one hour. Hydrogel samples had lower levels of platelet adhesion, spreading, and aggregation relative to ePTFE. Platelets were fluorescently labeled with mepacrine and imaged by fluorescent microscopy.

2.3.4.2 In Vitro Platelet Activation Circulating platelets activated at injury sites can promote thrombosis and coagulation. Specifically, activated platelets can initiate an

acute inflammatory response through the induction of P-selectin expression in ECs, which in turn stimulates leukocyte activity and coagulation.[189-190] Excessive platelet activation resulting in thrombotic emboli and neurologic complications has been observed after coronary artery bypass surgeries.[190] Therefore, minimizing activation of surrounding platelets in vascular grafts is critical to their long-term success. To establish hemocompatibility of PEG-Scl2-2 hydrogels, it is important to analyze their potential effects on surrounding, non-adherent platelets. Platelet activation in whole blood in contact with PEG-Scl2 hydrogels for 2 hours was assessed using flow cytometry to determine levels of P-selectin (CD62P) surface expression and PAC-1 binding. The former is selectively expressed on activated platelets, and the latter measures the active conformation of platelet integrin αIIbβ3, which is critical for platelet aggregation. Furthermore, Factor Xa generation in plasma after incubation with PEG-Scl2 hydrogels was measured.

Relative to the baseline, none of the hydrogel samples induced significant levels of PAC-1 binding or P-selectin expression in exposed blood samples, **Figure 2.6A-B**. In addition, no significant levels of Factor Xa generation were measured in the plasma from any hydrogel samples relative to baseline, **Figure 2.6C**. However, blood samples stimulated with 10 μM ADP displayed levels of non-adherent platelet activation significantly greater than the baseline. P-selectin is expressed only on the surface of activated cells, and its presence has been linked to development of atherosclerosis.[191] The PAC-1 antibody selectively binds to the activated form of the platelet glycoprotein (gp) IIb/IIIa complex and serves as a competitive binding inhibitor to fibrinogen. Since

fibrinogen binding to the activated gp IIb/IIIa complex is required for platelet aggregation, levels of PAC-1 binding can be correlated to numbers of activated platelets and indicates their potential for aggregation.[192] Similarly, Factor Xa plays several key roles in coagulation.[193] It is the primary component of the prothrombinase complex, which converts large amounts of prothrombin to thrombin. The burst of thrombin generation from Factor Xa is responsible for polymerizing fibrin into a thrombus.[193] Therefore, the PAC-1, P-selectin, and Factor Xa results indicate that the luminal PEG-Scl2-2 layer of these vascular grafts will have minimal effects on surrounding, non-adherent platelets. When these results are combined with those from the platelet adhesion studies, it can be concluded that PEG-Scl2-2 hydrogels provide a hemocompatible surface that minimizes platelet adhesion, activation, and thrombus formation.

2.3.4.3 In Vivo Acute Thromboresistance Multilayer grafts were able to hold sutures and retained blood flow without rupture. This indicates that their biomechanical properties are suitable for *in vivo* use. Acute (5 h) assessment with intravital imaging (carotid digital subtraction angiography) indicated excellent patency with no changes in arterial flow or narrowing of the artery. No platelet aggregates were evident in gross examination, **Figure 2.7**. Thus, multilayer grafts based on PEG-Scl2-2 hydrogels are resistant to acute *in vivo* thrombosis, and the initial *in vivo* characterization corroborates the *in vitro* thromboresistance study results.

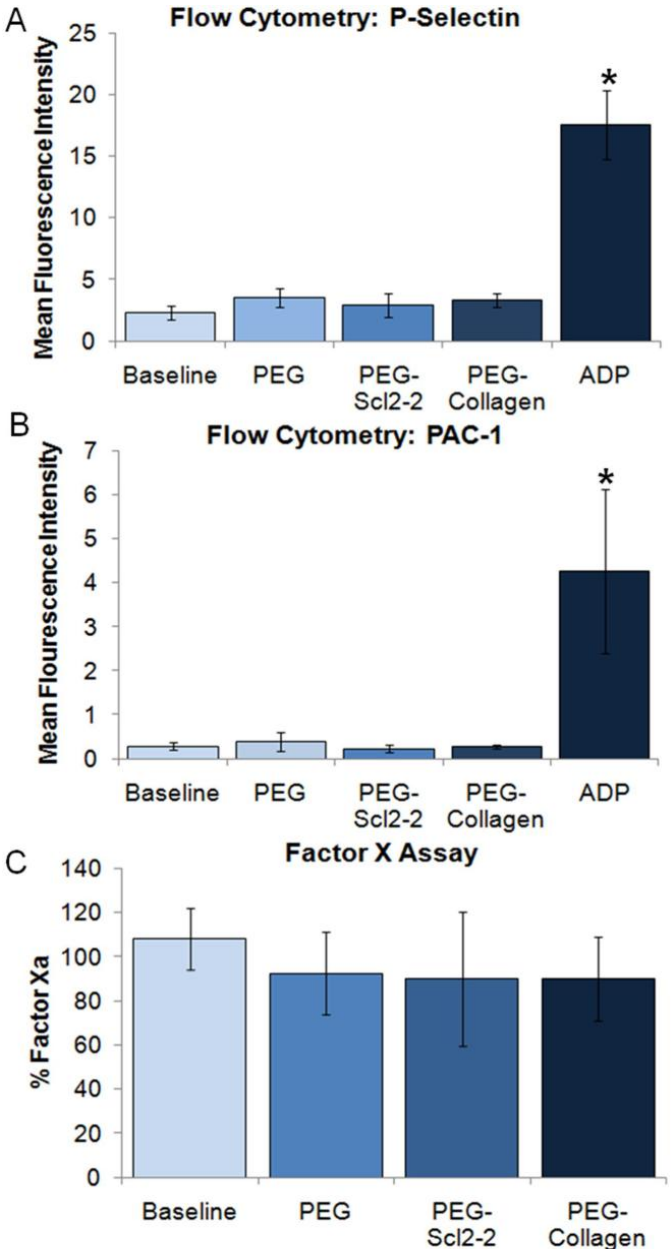

Figure 2.6. Activation of human platelets after 2 hour incubation with PEG-Scl2 hydrogels. Mean fluorescence intensity of (A) P-Selectin expression and (B) bound PAC-1. No significant increases in platelet activation relative to baseline were measured with either antibody for any hydrogel sample. (C) Factor Xa activity. No significant differences observed between baseline and samples. n=5; mean ± standard deviation displayed; *$p<0.05$ relative to baseline.

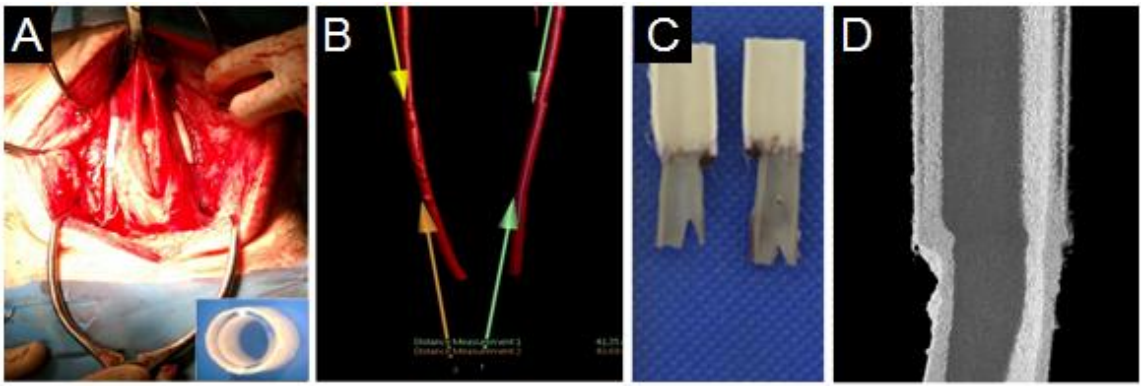

Figure 2.7. Multilayer vascular graft implantation. (A) Implantation into porcine carotid artery. In vivo acute thromboresistance was established via (B) angiography, (C) gross pathology, and (D) micro tomography.

2.4 Conclusions

In these studies, multilayered hydrogel-electrospun mesh scaffolds were fabricated in which a thromboresistant PEG-Scl2-2 hydrogel layer provides a local microenvironment that can be designed to induce rapid endothelialization and an electrospun polyurethane mesh provides bulk strength, compliance matching, and suture retention. These studies demonstrated that the intimal PEG-Scl2-2 hydrogel does not promote platelet adhesion, aggregation, or activation, and thus appears to provide a thromboresistant intimal layer. The biomechanical properties of the multilayer graft were modulated by varying fabrication parameters of the electrospun polyurethane mesh to attain values comparable to saphenous vein autografts. Finally, the bioactivity and biomechanical properties of these multilayer grafts remained unchanged after vacuum drying and sterilization which shows promise for off-the-shelf applications.

While these studies provide a broad, initial overview of the potential of these multilayer grafts to improve upon current synthetic options, extensive work remains to

be completed prior to their use as off-the-shelf vascular grafts. As these grafts are intended for long-term implantation, the chemistry of the PEG-based hydrogel must be altered to increase biostability, and the long-term biostability of the two layers will be evaluated. The potential for rapid endothelialization will be optimized to obtain EC adhesion levels more similar to PEG-collagen hydrogels, and alterations in bioactivity of PEG-Scl2-2 hydrogels over time will be determined prior to long-term *in vivo* analysis of endothelialization in a porcine animal model.

CHAPTER III

DEVELOPMENT OF A BIOSTABLE REPLACEMENT FOR PEGDA HYDROGELS*

3.1 Introduction

The overall goal for this work is to develop a vascular graft that is suitable for long-term implantation. Thus, the inner hydrogel layer must have long-term biostability. Although poly(ethylene glycol) diacrylate (PEGDA) hydrogels are often used as non-degradable controls in short-term, *in vitro* studies, it is widely acknowledged that the ester linkages introduced upon acrylation of PEG diol are susceptible to slow hydrolytic degradation *in vivo*, on the order of months to years.[194-199] Few reports provide quantification of the long-term hydrolytic degradation profile of PEGDA hydrogels, and most citations refer to a study with tri(ethylene glycol) diacrylate (TEGDA).[200] The majority of PEGDA hydrogels used in biomedical applications are fabricated with pre-polymers of molecular weight between 2,000 and 10,000 Da.[201-202] Relative to these formulations, low molecular weight (258 Da) TEGDA has a significantly increased ratio of ester linkages to backbone ether groups and reduced hydrophilicity. Therefore, it is likely that the degradation profiles of TEGDA and PEGDA hydrogels are not comparable. Despite their extensive use and characterization, a full investigation of PEGDA hydrogel degradation is not readily available in current literature.

---

*Reprinted with permission from "Development of a Biostable Replacement for PEGDA Hydrogels," by MB Browning and E Cosgriff-Hernandez, Biomacromolecules 2012, 13 (3), 779-786. Copyright (2012) American Chemical Society.

Although the exact degradation rate of PEGDA hydrogels is not known, it is generally accepted that slow hydrolytic cleavage of the end group ester linkages renders it unsuitable for long-term implants. Despite their desirable biocompatibility, tunable properties, and unique "non-fouling" surface features, increases in swelling and decreases in modulus that occur with degradation would ultimately cause failure of a gel-based device.[203-204] In our vascular graft design, a swelling increase would reduce the lumen diameter, and the resulting obstruction in blood flow could initiate thrombosis.[205-206] In another example, degradation of a non-fouling hydrogel coating on a glucose sensor could initiate a delayed host response to the sensor that would negatively affect *in vivo* sensitivity over time.[207] A PEG-based hydrogel system with improved biostability that maintains the desirable properties of PEGDA hydrogels would be valuable in preventing degradation-related failures of gel-based devices. Previously, Elbert and Hubbell synthesized PEG diacrylamide (PEGDAA) to improve the stability of conjugate addition reaction bonds between bioactive peptides and PEG hydrogels by replacing the hydrolytically-labile esters of PEGDA with more stable amide groups.[208] We propose that PEGDAA could be utilized as a biostable replacement for PEGDA.

Although hydrolysis of the labile esters has widely been suggested as the mechanism PEGDA biodegradation, an alternate or possible secondary mechanism of degradation includes oxidation of the ether backbone.[196-197,209-210] Despite their bioinert properties, PEG based devices are susceptible to a degree of non-specific protein adsorption after implantation, followed by macrophage recruitment, attachment, and activation at the implant site.[20,197] Activated macrophages secrete cytokines, growth

factors, reactive oxygen species, matrix metalloproteinases, and chemotactic factors that propagate the foreign body reaction and cause both oxidative and hydrolytic degradation of biomaterials.[20,22,211] Thus, the observed *in vivo* degradation of PEGDA hydrogels could be a result of oxidation, hydrolysis, or some combination of the two. While PEGDAA hydrogels do not provide increased resistance to oxidative degradation, they can serve as a hydrolytically stable control for *in vivo* degradation studies with PEGDA hydrogels. This provides information about the relative extents of hydrolytic and oxidative degradation of PEGDA and serves as a valuable tool in gaining a further understanding of the *in vivo* degradation mechanism of PEGDA hydrogels.

In the present study, PEGDAA was synthesized from PEG diamine as a biostable replacement for PEGDA. The ability to tune modulus and swelling with alterations in macromer molecular weight and concentration was compared between the two hydrogel systems. PEGDAA and PEGDA hydrogel cytocompatibility were also compared to evaluate their suitability for use in biomedical applications. Additionally, the innate resistance to cell adhesion and the ability to incorporate bioactivity into PEGDAA hydrogels was assessed. Finally, degradation of the candidate gels was analyzed *in vitro* under normal and accelerated conditions to confirm the relative biostability of PEGDAA to PEGDA and *in vivo* to determine the mechanism for PEGDA biodegradation. These studies serve to fill a gap in the characterization of a widely utilized biomaterial system and assess the potential of a novel PEG-based hydrogel system as a biostable replacement for PEGDA hydrogels in long-term, *in vivo* applications.

3.2 Materials and Methods

3.2.1 Materials All chemicals were purchased from Sigma Aldrich (St. Louis, MO) and used as received unless otherwise noted.

3.2.2 Polymer Synthesis PEGDA was synthesized according to a method adapted from Hahn, et al., **Figure 3.1A**.[172] Briefly, acryloyl chloride (4 molar equivalents) was added dropwise to a solution of PEG diol (3.4kDa or 10kDa; 1 molar equivalent) and triethylamine (TEA, 2 molar equivalents) in anhydrous dichloromethane (DCM) under nitrogen. The reaction was stirred for 24 hours, and the resulting solution was washed with 2M potassium bicarbonate (8 molar equivalents). After drying with anhydrous sodium sulfate, the product was precipitated in cold diethyl ether, filtered, and dried under vacuum. PEGDAA was prepared using a similar method to PEGDA, **Figure 3.1B**. Briefly, acryloyl chloride was added to a solution of PEG diamine (3.4kDa or 10kDa) and TEA in anhydrous DCM under nitrogen. The molar equivalent of PEG diamine, TEA, and acryloyl chloride was kept at 1:2:4. After reacting for 24 hours, the solution was washed with 8 molar equivalents of 2M potassium bicarbonate and dried with anhydrous sodium sulfate. The product was precipitated in cold diethyl ether, filtered, and dried under vacuum to obtain the final product.

Fourier transform infrared (FTIR) spectroscopy and proton nuclear magnetic resonance (^{1}H-NMR) spectroscopy were used to confirm functionalization of PEGDA and PEGDAA. Control and acrylated polymers were solution cast directly onto KBr pellets to acquire transmission FTIR spectra using a Bruker TENSOR 27 spectrometer. Successful acrylation of PEG diol was indicated by an ester peak at 1730 cm^{-1} in the

spectra. The presence of amide peaks at 1640 cm^{-1} and 1675 cm^{-1} signified successful acrylamidation of PEG diamine. Proton NMR spectra of control and functionalized polymers were recorded on Mercury 300 MHz spectrometer using a TMS/solvent signal as an internal reference. PEGDA: ^{1}H-NMR ($CDCl_3$): 3.6 ppm (m, -OC*H*$_2$C*H*$_2$-), 4.3 ppm (t, -C*H*$_2$OCO-), 6.1 ppm (dd, -C*H*=CH_2), 5.8 and 6.4 ppm (dd, -CH=C*H*$_2$). PEGDAA: ^{1}H-NMR ($CDCl_3$): 3.6 ppm (m, -OC*H*$_2$C*H*$_2$-); 6.5 ppm (s, -CH_2-N*H*-); 6.4 ppm (m, -C*H*=CH_2); 5.6 and 6.1 ppm (m, -CH=C*H*$_2$).

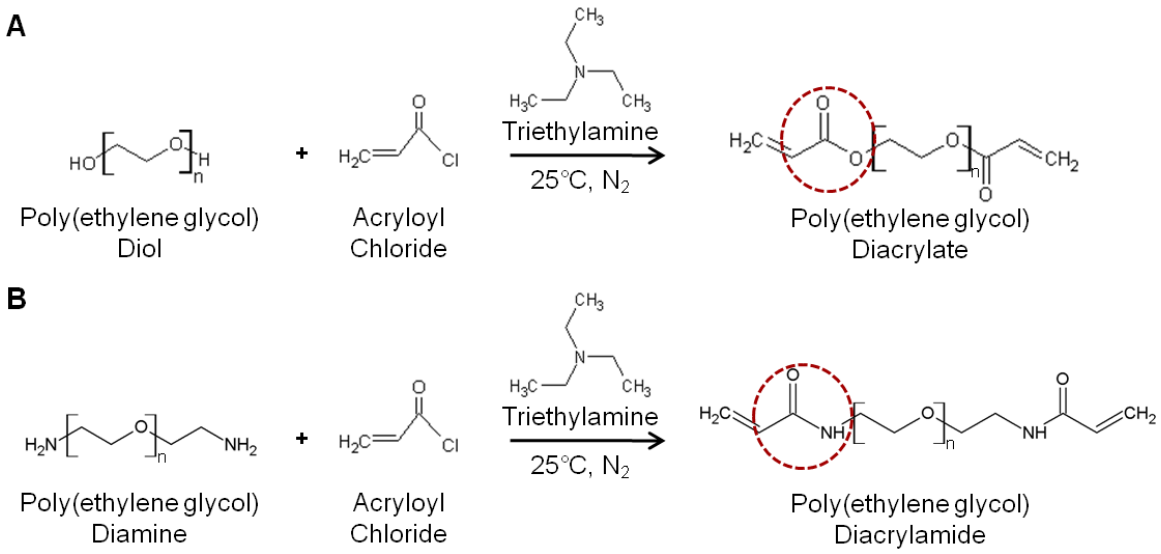

Figure 3.1. PEGDA and PEGDAA synthesis routes. Synthesis of (A) PEGDA and (B) PEGDAA with an amide group in place of the ester linkage in PEGDA.

3.2.3 Hydrogel Characterization

3.2.3.1 Hydrogel Preparation Hydrogels were prepared by dissolving PEGDA or PEGDAA in deionized water. A photointiator solution (1 mg Irgacure 2959 per 0.01 ml 70% ethanol) was added at 1 vol% of precursor solution. Solutions were pipetted

between 1.5 mm spaced plates and crosslinked by 6 min exposure to long wave UV light (Intelli Ray Shuttered UV Flood Light, Integrated Dispensing Solutions, Inc., 365 nm, 4 mW/cm^2).

3.2.3.2 Hydrogel Modulus Hydrogels were swollen in deionized water for 24 hours prior to compressive modulus measurements. Six 8-mm diameter discs were punched from swollen hydrogel sheets and subjected to mechanical testing using a dynamic mechanical analyzer (RSAIII, TA Instruments) equipped with a parallel-plate compression clamp. Testing was performed under unconstrained compression at room temperature. Dynamic strain sweeps were used to determine the linear viscoelastic range for each hydrogel formulation. Then, a strain within the upper end of the linear viscoelastic range was used in a constant strain frequency sweep. Tests were conducted between 0.79 and 79 Hz, and the compressive storage modulus was taken at 1.25 Hz.

3.2.3.3 Hydrogel Swelling Ratio Six 8-mm diameter discs were punched from each sheet directly after polymerization and weighed (W_i). The hydrogel discs were swollen in deionized water for 24 hours and weighed to determine the equilibrium swelling mass (W_s). Then, samples were dried under vacuum for 24 hours and weighed to assess dry (polymer) mass (W_d). The equilibrium volumetric swelling ratio, Q, was calculated from the equilibrium mass swelling ratio:

$$Q = \frac{W_s}{W_d} \qquad [3.1]$$

3.2.4 Cell Studies

3.2.4.1 Cell Culture NIH/3T3 Swiss mouse fibroblasts (ATCC-CCL92) were used for cell culture. Cells were cultured *in vitro* at 37°C/5% CO_2 with Dulbecco's

Modified Eagle Medium (DMEM, high glucose GlutaMAX^{TM}) supplemented with 10% heat-inactivated fetal bovine serum (FBS) and 1% Penicillin-Strepotomycin solution (Gibco). Cells were used between passages 6 and 8 after 3 days of culture for all studies.

3.2.4.2 Cytocompatibility To evaluate hydrogel cytocompatibility, an indirect contact method was adapted from Trudel et al.[212] Briefly, hydrogel solutions (10 wt%, 10kDa) were first sterile filtered with cellulose acetate syringe filters (0.2 µm pore size, VWR), and then 75 µl was pipetted into Transwell© inserts (Costar Corporation, 6.5 mm, 3 µm pore size poly(carbonate) membrane filter) and crosslinked in a laminar flow hood as described in Section 2.3.1. Sterile phosphate buffered saline (PBS) was added to lower wells, and hydrogels were swollen in the plate overnight at 37°C/5% CO_2. Wells with empty inserts served as controls. After swelling, the PBS was removed, and fibroblasts were seeded with 235 µl of culture media in the lower tissue culture poly(styrene) (TCPS) wells at 5,000 cells cm^{-1} using the pipette tip access ports of the Transwell© plate. After 24 and 72 hours of incubation, cell viability was determined using a Live/Dead Viability/Cytotoxicity Kit (Molecular Probes). Stained samples were examined at 10X magnification via fluorescence microscopy (Nikon Eclipse TE2000-S) to visualize viable (fluorescein filter set) and non-viable (rhodamine filter set) cells. Five field views were randomly assessed per specimen, with 3 specimens per sample. Percent cell viability was reported as the ratio of live cells to total cells in each field view.

3.2.4.3 Cell Adhesion and Spreading To evaluate the ability to incorporate bioactivity into PEGDAA hydrogels, PEG-collagen gels were fabricated and seeded with cells. Rat tail collagen type I was functionalized with photoreactive crosslink sites

through the established NHS-lysine Ɛ-amino group reaction according to a protocol adapted from Sebra et al.[171] Briefly, the protein was reacted with acrylate-PEG-N-hydroxysuccinimide (Acr-PEG-NHS, MW 3500, Jenkem Technologies USA, Allen, TX) in 50 mM sodium bicarbonate buffer (pH 8.5). The molar ratio of Acr-PEG-NHS:NH_2 was 2:1, and the reaction was allowed to proceed with stirring for 24 hours at room temperature. Dialysis against 0.1M hydrochloric acid for 24 hours was used to neutralize the basic reaction solution, and excess Acr-PEG-NHS and other reaction byproducts were removed via dialysis against deionized water for 24 hours (Thermo-Fisher Scientific, Slide-A-Lyzer dialysis cassettes, 20,000 MWCO). Functionalization of the modified proteins was confirmed with FTIR spectroscopy. FTIR absorbance peaks assigned to the protein (C=O of amide) at 1650 cm^{-1} and to PEG (C-O-C of ether) at 1110 cm^{-1} were present in the purified product, indicating successful functionalization of collagen.

Functionalized collagen was dissolved at 3 mg protein ml^{-1} in 10 wt% PEGDA and PEGDAA (10kDa) solutions, and hydrogels were crosslinked between 0.75 mm spaced plates as described in Section 2.3.1. Control hydrogels were prepared without functionalized collagen. After swelling in sterile PBS overnight, four 12 mm diameter punches were taken from each hydrogel, and fibroblasts were seeded onto specimens at 5000 cell cm^{-1}. After a 4 hour incubation at 37°C/5% CO_2, cells were fixed with 3.7% glutaraldehyde (Invitrogen) and stained with rhodamine phalloidin (F-actin/cytoplasm, Invitrogen) and SYBRGreen (DNA/nucleus, Invitrogen). Representative images were obtained with a Nikon Eclipse TE2000-S with 5 field views per specimen and 3

specimens per hydrogel formulation. The number of cell nuclei per image was used as a quantitative assessment of cell adhesion on each test surface and was counted using the SYBRGreen stained images. Average cell spreading, or cell area, was quantified by applying the Photoshop "magic wand" tool to the image background of the rhodamine phalloidin stained images and adjusting the tool tolerance so that all extracellular regions were selected. The histogram function was then utilized to evaluate the extracellular pixels (P_{Ex}). The average pixels per cell (A_{cell}) for that image was then quantified as follows:

$$A_{cell} = \frac{P_T - P_{Ex}}{N} \qquad [3.2]$$

where P_T represents total image pixels and N is total cell nuclei. Pixels were then converted to microns using known objective scaling.

3.2.5 Hydrogel In Vitro Degradation To compare the degradation profile of PEGDAA to PEGDA, twelve 8 mm diameter punches were taken from each hydrogel formulation and incubated in either PBS (pH≈7.5), 0.1M sodium hydroxide (NaOH, pH≈13.0), or 20% hydrogen peroxide (H_2O_2) with 0.1M cobalt chloride ($CoCl_2$) with shaking at 37°C. For degradation analysis in PBS, masses of swollen hydrogel punches were measured weekly and solutions were changed twice a week for 6 weeks. Hydrogels were incubated in 0.1M NaOH to evaluate degradation under accelerated hydrolytic conditions. PEGDA hydrogel punches were weighed every 3 hours and the 0.1M NaOH solution was changed every 6 hours until total dissolution occurred. PEGDAA hydrogels were weighed daily for the first week with solution changes each day, then weighed weekly with bi-weekly solution changes for an additional 5 weeks. Accelerated

oxidative degradation was carried out in 20% H_2O_2 with 0.1M $CoCl_2$, during which samples were weighed daily until complete dissolution occurred. For all degradation studies, swelling ratio was calculated at each time point relative to initial dry (polymer) mass to evaluate decreases in crosslink density that occurred with degradation. Measurements were normalized to the swelling ratio at time 0.

3.2.6 Hydrogel In Vivo Degradation All procedures were approved by the Institutional Animal Care and Use Committee. Hydrogels (10%, 10 kDa) were crosslinked under sterile conditions between 1.5 mm spaced plates. Specimens (2 mm by 12 mm) were cut and enclosed in cylindrical stainless steel mesh cages (1.5 mm length, 3 mm diameter). Three month old female Sprague Dawley rats were anesthetized before and during the procedure with 2% isoflurane. Their sides were shaved, and incision sites were scrubbed with chlorhexidine. Incisions (approximate 1 cm long) were made on the side of the rats, and blunt dissection was used to prepare implant pockets (2 per side). Specimens were introduced through the incision and positioned within the pocket away from the incision site. The incisions were then closed with stainless steel surgical wound clips. Clips were removed 7 days post-implantation. After 28 days, rats were euthanized with carbon dioxide inhalation. A subsequent bilateral thoracotomy was performed to ensure death. Implants were removed, and hydrogel specimens were removed from the stainless steel cages. Swelling ratio and modulus of explants was measured as a determination of the extent of degradation.

3.2.7 Statistical Analysis All the data were expressed as the mean ± standard derivation of the mean. Statistical analysis was performed by one-way analysis of variance and Tukey's post hoc test. Statistical significance was accepted at $p<0.05$.

3.3 Results and Discussion

3.3.1 Polymer Synthesis and Gel Formation Similar acrylation procedures were employed to generate PEGDA from PEG diol and PEGDAA from PEG diamine. Following purification, polymer structures were confirmed with FTIR and ^{1}H NMR spectroscopy. The presence of ester peaks at 1730 cm^{-1} in the FTIR spectra of PEGDA indicated successful acrylation of PEG diol. Similarly, new amide peaks at 1640 cm^{-1} and 1675 cm^{-1} verified acrylamidation of PEG diamine, **Figure 3.2**. The absence of ester peaks in the PEGDAA spectra confirmed that there were no hydrolytically-labile esters in the amide-based formulations. The integration ratio of acryloyl protons to backbone methyl protons in the ^{1}H NMR spectra confirmed the structures of PEGDA and PEGDAA as polyethers with acrylate and acrylamide endgroups, respectively, **Figure 3.3**. Greater than 90% conversions of hydroxyl to acrylate endgroups and amine to acrylamide endgroups were observed for all candidate macromers. Following characterization, PEGDA and PEGDAA were crosslinked into a hydrogel network using the same photoinitiator type and concentration (0.1 wt% of Irgacure 2959) and UV light intensity and exposure time (6 min of 4 mW/cm^2). This indicates that PEGDAA hydrogels could potentially be polymerized *in situ* in direct contact with cells or as cell carriers in a similar manner to PEGDA hydrogels that are currently in use.[209,213-216]

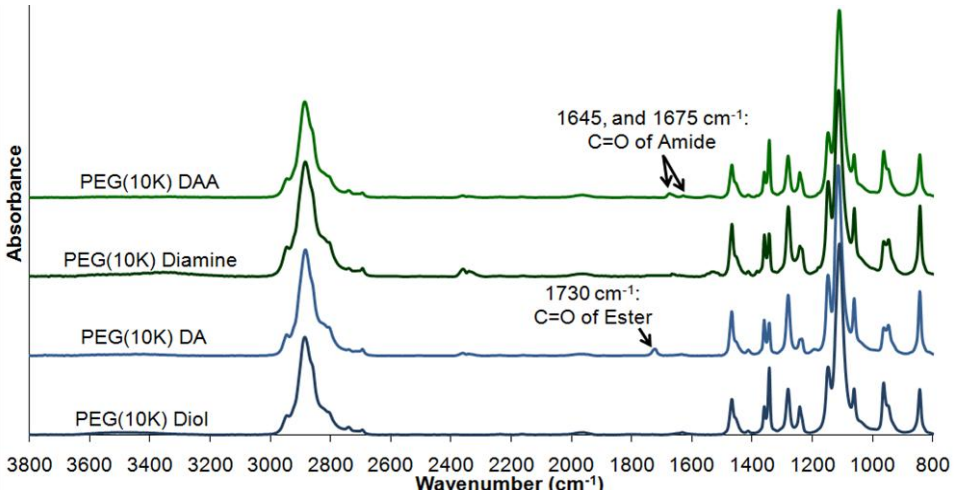

Figure 3.2. FTIR spectra of PEG(10K) DA synthesized from PEG(10K) diol and PEG(10K) DAA synthesized from PEG(10K) diamine.

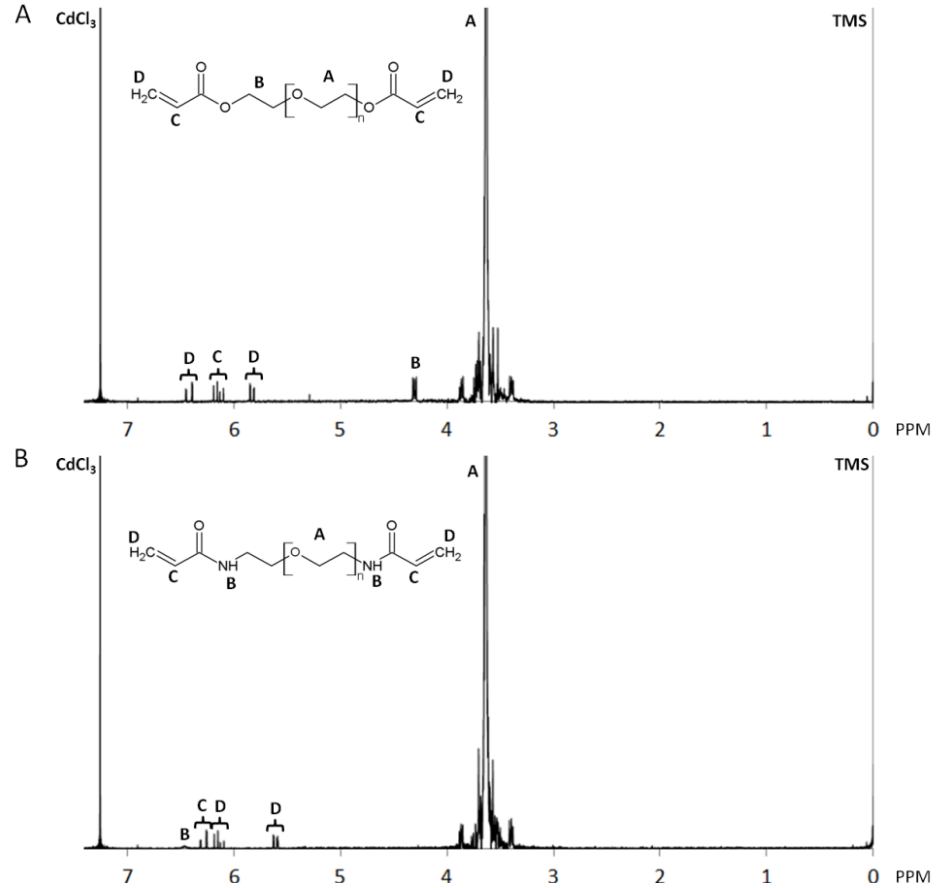

Figure 3.3. NMR spectra of (A) PEGDA and (B) PEGDAA.

3.3.2 Hydrogel Characterization Modulus and swelling ratios of PEGDAA and PEGDA hydrogels were measured for varied macromer molecular weights (3.4kDa and 10kDa) and concentrations (10 and 20 wt%) to evaluate the ability to tune scaffold properties. PEGDAA and PEGDA hydrogels exhibited similar changes in gel properties with compositional changes, **Figure 3.4**. Specifically, a decrease in molecular weight from 10kDa to 3.4kDa resulted in modulus increases for both PEGDAA and PEGDA gels (approximately 45% increases for 10% gels and 80% increases for 20% gels). An increase in polymer concentration from 10 to 20 wt%, resulted in a 65% increase in modulus of PEG(3.4k) hydrogels and 20% increase in modulus of PEG(10k) hydrogels. Hydrogel swelling ratios were also tuned over a wide range with changes in macromer molecular weight and concentration. PEGDAA and PEGDA hydrogels at 10% concentration exhibited swelling decreases of approximately 25% in response to a molecular weight decrease from 10 kDa to 3.4 kDa. Similarly, 20% PEGDAA and PEGDA hydrogels had roughly 30% decreases in swelling with decreased molecular weight. An increase in concentration from 10 to 20% caused a 20% decrease in swelling for both PEG(3.4k)DAA and PEG(3.4k)DA hydrogels and a 25% swelling decrease for PEG(10k)DAA and PEG(10k)DA hydrogels.

The tunability of PEG hydrogel modulus and swelling over a wide range with simple formulation changes is critical to their utility in a wide array of applications.[195,209,217-218] PEGDAA hydrogel properties can be tuned over a similar range and to comparable degrees as PEGDA hydrogels. This suggests the potential to rationally design PEGDAA hydrogels to meet specific application needs by utilizing the

properties of PEGDA hydrogel systems established in the literature.[166,219-220] Thus, translation from PEGDA to the more biostable PEGDAA hydrogel formulation can be carried out without the need for significant design changes.

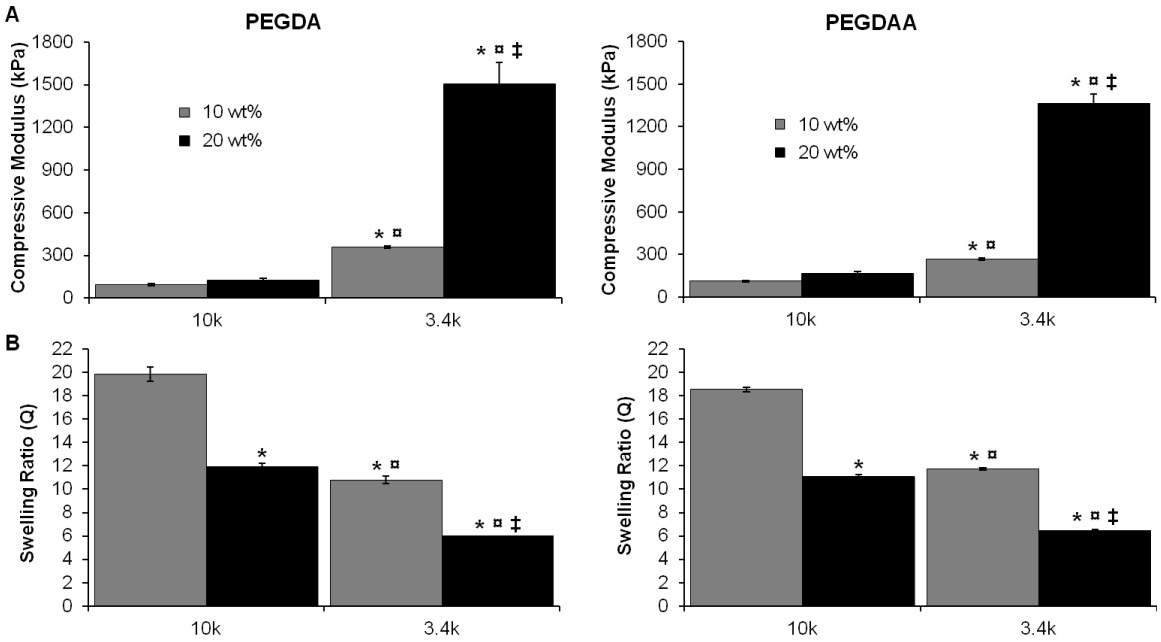

Figure 3.4. Characterization of hydrogel compressive modulus and swelling ratios. (A) Compressive modulus and (B) swelling ratio of PEGDA and PEGDAA hydrogels. Both modulus and swelling ratio of PEGDAA hydrogels can be tuned similarly to PEGDA hydrogels by altering macromer weight (3.4k or 10k) or concentration (10 wt% or 20 wt%). (n=6, mean ± standard deviation, *$p<0.05$ relative to 10% 10k gel, ¤$p<0.05$ relative to 20% 10k gel, ‡$p<0.05$ relative to 10% 3.4k gel)

3.3.3 Cell Studies The biocompatibility of PEGDA hydrogels is essential to their use in biomedical applications and any replacement system for PEGDA must retain a similar biocompatibility profile.[221-224] As a first measure, a Live/Dead Viability/Cytotoxicity assay was performed to confirm that PEGDAA retained the favorable cytocompatibility of PEGDA. The low levels of protein adsorption and cell

adhesion on unmodified PEG hydrogels make direct cytocompatibility studies difficult to perform. Therefore, a Transwell system was used to investigate viability of 3T3 mouse fibroblasts after indirect exposure to candidate hydrogels suspended in cell media. Both PEGDAA and PEGDA hydrogel systems had high levels of cell viability similar to the empty poly(carbonate) (PC) insert control after 24 and 72 hours (PEGDAA: 98 ± 3% and 97 ± 4%; PEGDA: 98 ± 5% and 97 ± 3%; PC: 99 ± 2% and 96 ± 4%, respectively), **Figure 3.5**. This serves as an initial measure of the suitability of PEGDAA hydrogel use in biomedical applications that currently employ PEGDA hydrogels.[207,225] Additionally, Constant et al. reported that PEGDAA-based implants induced less inflammation and reduced fibrous encapsulation after implantation in rabbits for 4 weeks compared to poly(ethylene) specimens.[226] Although these PEGDAA-based implants were prepared using a different method and formulation, the results from these studies further indicate the potential suitability of PEGDAA for *in vivo* applications.

Intrinsic resistance to protein adsorption and cell adhesion is a valuable aspect of PEG-based hydrogels. Not only does it provide a non-fouling surface *in vivo*, it also permits controlled introduction of bioactivity with the addition of peptides and proteins into the hydrogel network.[165,227] A biostable replacement for PEGDA hydrogels must provide a similarly bioinert surface that can be altered with the introduction of bioactive factors to allow for cell adhesion. To this end, fibroblasts were seeded on PEG hydrogels and on PEG-collagen hydrogels in the presence of serum proteins to assess cell adhesion and spreading, **Figure 3.6**.

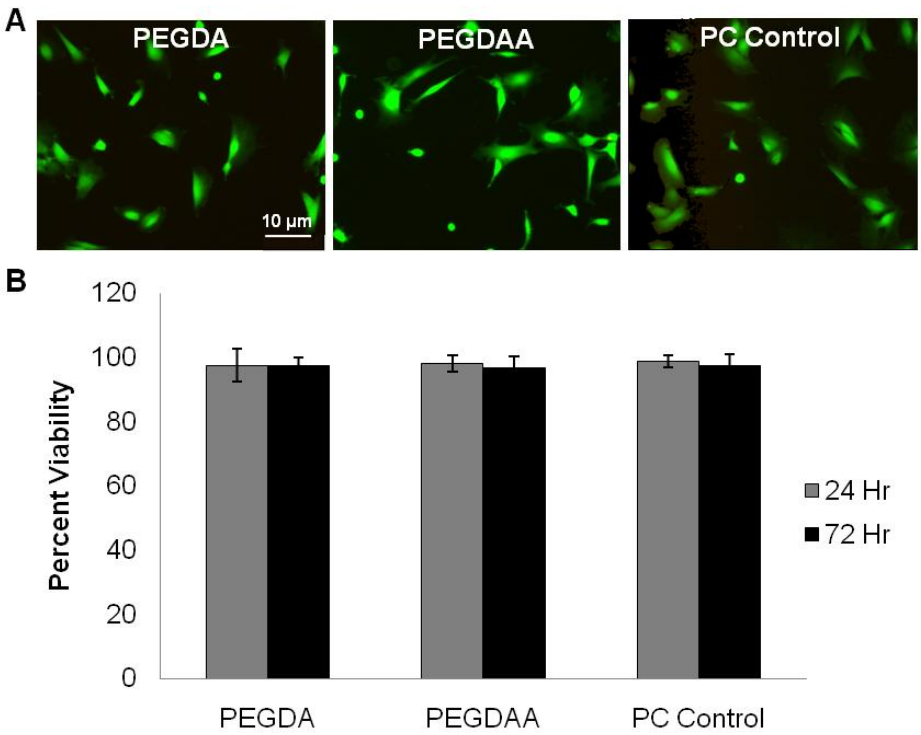

Figure 3.5. Hydrogel cytocompatibility. (A) Live/Dead staining of 3T3 fibroblasts adhered to TCPS after 24 hours of indirect contact with hydrogels. (B) PEGDA and PEGDAA samples displayed similarly high percent viability as compared to the poly(carbonate) (PC) control at both 24 and 72 hours. (n=3, mean ± standard deviation, $p>0.05$ for all samples at both time points)

PEGDAA hydrogels had low levels of cell adhesion and spreading comparable to PEGDA hydrogels, indicating that PEGDAA could be used as a non-fouling surface in place of PEGDA.[165,228-229] Acrylate-functionalized collagen was successfully crosslinked into PEGDAA hydrogels, resulting in a three-fold increase in cell adhesion and two-fold increase in spreading relative to pure PEGDAA hydrogels after three hours of culture. Similar increases in cell adhesion and spreading were observed on PEGDA-collagen hydrogels relative to PEGDA hydrogels. These studies demonstrate the ability to incorporate bioactivity into PEGDAA hydrogels as indicated by increased cell adhesion

and spreading with comparable results to those seen with PEGDA. This further validates the capacity to transition from PEGDA to PEGDAA with minimal changes in material design.[145,198,230-231]

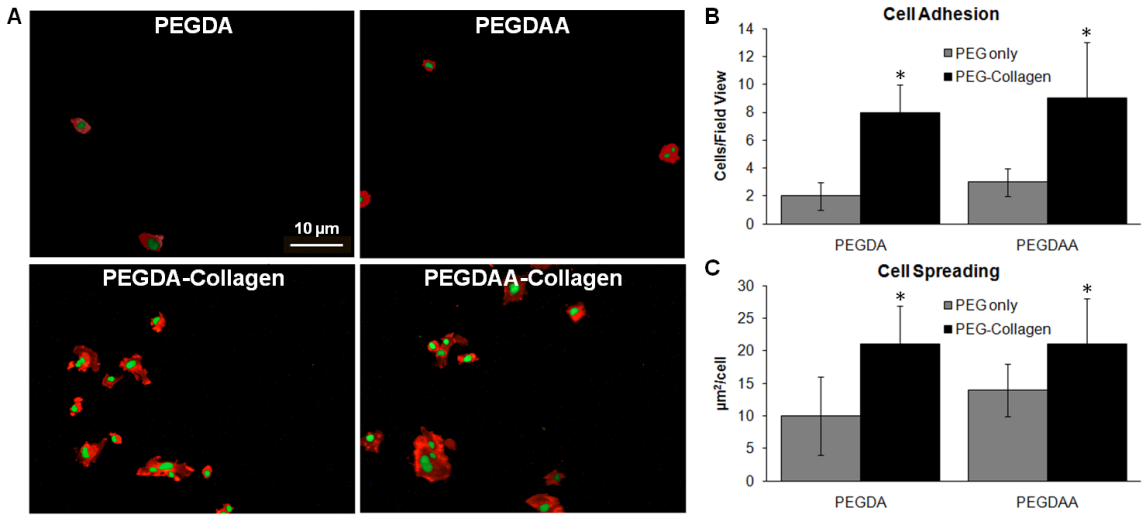

Figure 3.6. Cell adhesion to hydrogels. (A) Rhodamine phalloidin and SYBRGreen stained 3T3 fibroblast adhesion on hydrogels after a 3 hour incubation period. Increases in (B) adhesion and (C) spreading were seen in PEG-collagen hydrogels relative to controls, indicating that bioactivity can be incorporated into PEGDAA hydrogels similarly to PEGDA hydrogels. (n=3, mean ± standard deviation, *p<0.05 compared to PEGDA and PEGDAA)

3.3.4 Hydrogel In Vitro Degradation

3.3.4.1 Hydrolytic Degradation To verify the increased hydrolytic stability of PEGDAA relative to PEGDA, *in vitro* hydrolytic degradation was analyzed over a six week time frame. It was hypothesized that hydrolytic cleavage of ester linkages in PEGDA hydrogels results in decreased crosslink density, which can be monitored with corresponding increases in swelling ratio.[195] For degradation in PBS at 37°C, no

significant increases in swelling were observed in either hydrogel system (PEGDAA or PEGDA), **Figure 3.7A**.

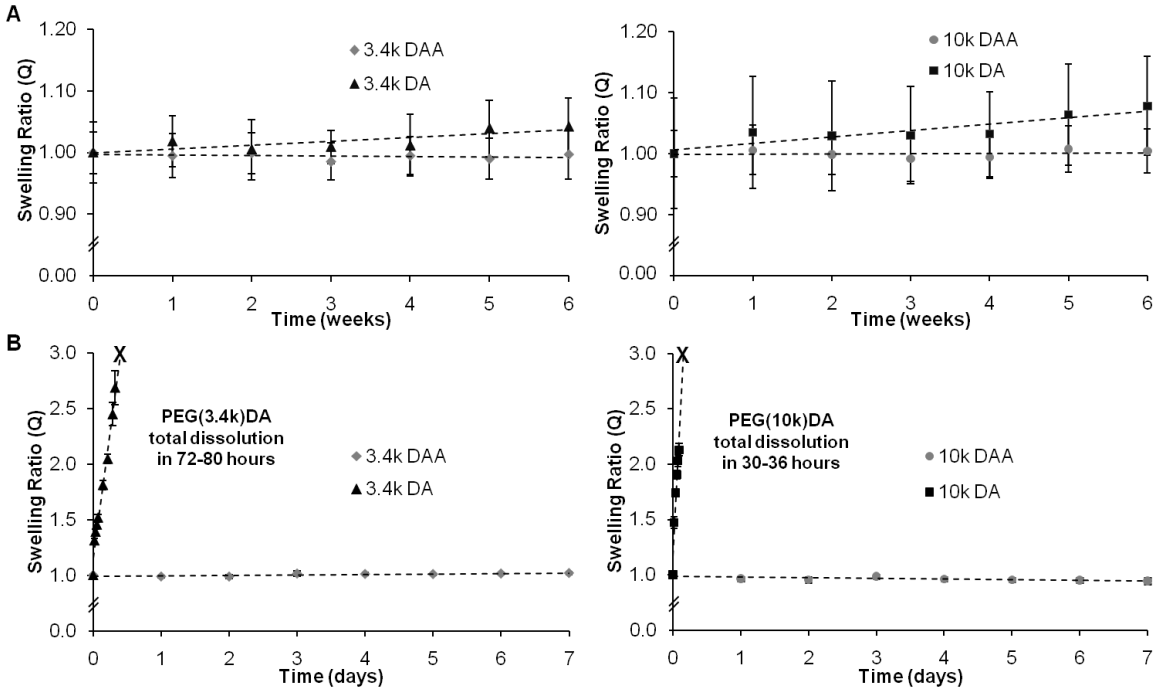

Figure 3.7. Hydrogel in vitro degradation in PBS and 0.1M NaOH. Changes in hydrogel swelling ratio as a function of incubation time in (A) PBS and (B) 0.1M NaOH at 37°C. No significant changes in swelling ratio were observed in PBS for the given time period ($p>0.05$ between all time points for each sample in PBS). In 0.1M NaOH, PEG(3.4k)DA hydrogels completely dissolved within 72 to 80 hours, and PEG(10k)DA hydrogels completely dissolved within 30 to 36 hours. PEGDAA hydrogels remained stable in 0.1M NaOH over 6 weeks (data beyond week 1 not shown) with minimal increases in swelling. ($n=6$, mean ± standard deviation, $p<0.05$ between all time points of PEGDA gels in 0.1M NaOH, $p>0.05$ between all time points shown of PEGDAA gels in 0.1M NaOH).

This was expected, based on previous *in vitro* degradation studies in which PEGDA hydrogels served as biostable controls.[201] Although the small increases in swelling that occurred in this study were not statistically significant, a linear regression

analysis of the measurements reveals a general increase in swelling over time for both PEGDA hydrogel formulations (0.38 mg and 0.78 mg increases in swollen mass per week for 3.4k and 10k hydrogels, respectively). In contrast, the same analysis of the PEGDAA measurements reveals minimal variations in swelling, equivalent to 0.00 mg and 0.03 mg respective increases in swollen mass of 3.4k and 10k hydrogels each week. These trends suggest that the PEGDA hydrogels were undergoing a slow rate of hydrolytic degradation during the time frame of the study whereas the PEGDAA hydrogels displayed no evidence of degradation.

An accelerated degradation study was carried out in 0.1M NaOH at 37°C to substantiate these results and predict longer implantation times, **Figure 3.7B**. Under accelerated hydrolytic conditions, PEG(3.4k)DA hydrogels experienced a loss in mechanical integrity in 50 to 56 hours and underwent complete dissolution in 72 to 80 hours. As expected, given the lower crosslink density, PEG(10k)DA hydrogels degraded at a faster rate with a loss in integrity in 15 to 18 hours and full dissolution in 30-36 hours. In contrast, both molecular weights of PEGDAA remained intact with no significant changes in swelling for one week. This confirms the significantly increased hydrolytic stability of PEGDAA relative to PEGDA due to elimination of ester linkages in the endgroups.[232] To further characterize the PEGDAA hydrogels, accelerated degradation was carried out to six weeks, during which they continued to remain stable with small increases in swelling. Thus, the amide-based PEGDAA hydrogels have significantly improved hydrolytic stability relative to PEGDA hydrogels.

3.3.4.2 Oxidative Degradation The utility of *in vitro* accelerated degradation testing to predict long-term *in vivo* behavior is contingent on identifying all potential mechanisms of biodegradation. Thus, accelerated oxidative degradation was carried out *in vitro* using a solution of 20% H_2O_2/0.1M $CoCl_2$ to compare susceptibility to oxidation of PEGDA and PEGDAA. Both systems had similar degradation profiles in the accelerated solution, indicating that PEGDAA undergoes oxidation similarly to PEGDA, **Figure 3.8**. This was expected, as oxidation affects the ether backbone of PEG, which is constant between the two systems. Additionally, the 3.4 kDa gels had higher oxidative stability relative to the 10 kDa gels, similarly to the PEGDA gels in the accelerated hydrolytic study.

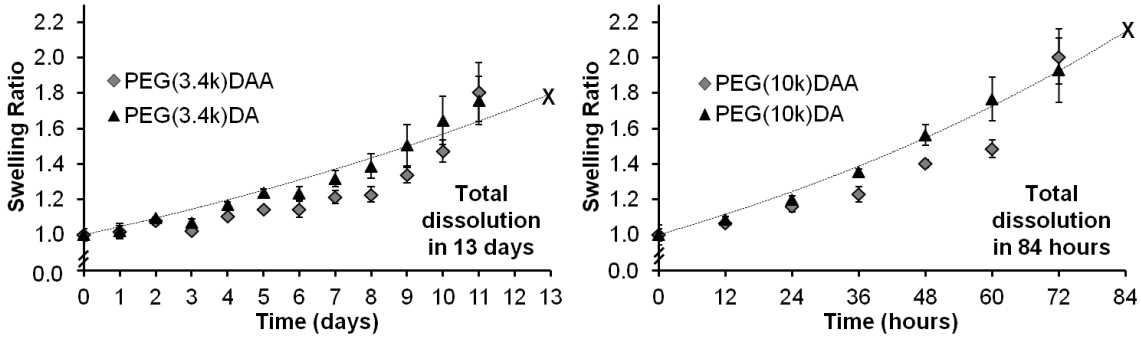

Figure 3.8. Accelerated oxidative degradation in 20% H_2O_2/0.1M $CoCl_2$ of 20% PEG(3.4k) and PEG(10k) DA and DAA gels at 37°C. PEG(3.4k) gels underwent complete dissolution within 13 days, while PEG(10k) gels underwent complete dissolution within 84 hours. (n=6, mean ± standard deviation, $p<0.05$ between all time points).

3.3.4.3 In Vivo Degradation Upon confirmation that PEGDAA gels have enhanced hydrolytic stability and similar susceptibility to oxidation as PEGDA gels, the two systems were utilized in an *in vivo* degradation study. After four weeks of

subcutaneous implantation enclosed in stainless steel mesh cages, samples were explanted. Swelling ratio and compressive modulus of explanted samples were measured and compared to their initial properties and to those of samples that had been incubated in PBS at 37°C for four weeks, **Figure 3.9**. PEGDA gels had significant increases in swelling and decreases in modulus after both *in vitro* and *in vivo* incubation, while PEGDAA gels had no changes in either swelling or modulus *in vitro* or *in vivo*. Slightly higher changes in PEGDA swelling and modulus indicated increased degradation *in vivo* and can be attributed to accelerated degradation that occurs with the *in vivo* host response. It has previously been shown that PEG hydrogels promote macrophage attachment and activation both *in vitro* and *in vivo*.[197] Upon activation, macrophages secrete degradative agents, including acids, cytokines, growth factors, reactive oxygen species, matrix metalloproteinases, and chemotactic factors.[20,22,211] The reactive oxygen species can accelerate oxidative degradation, whereas a reduced pH from lysosomal acids can accelerate hydrolytic degradation.[211] The results from this study serve as an initial indication that hydrolysis of endgroup esters has a greater effect on PEGDA hydrogel *in vivo* degradation than oxidation of backbone ethers, as the oxidatively-labile PEGDAA hydrogels remained stable. Future studies will evaluate these systems over 12 weeks to obtain a better indication of the relative extents of PEGDA hydrolytic and oxidative degradation *in vivo*. This work represents the first use of a suitable control for determination of the mechanism of PEGDA hydrogel degradation *in vivo* and the first indication of hydrolysis having a greater effect than oxidation in the short term.

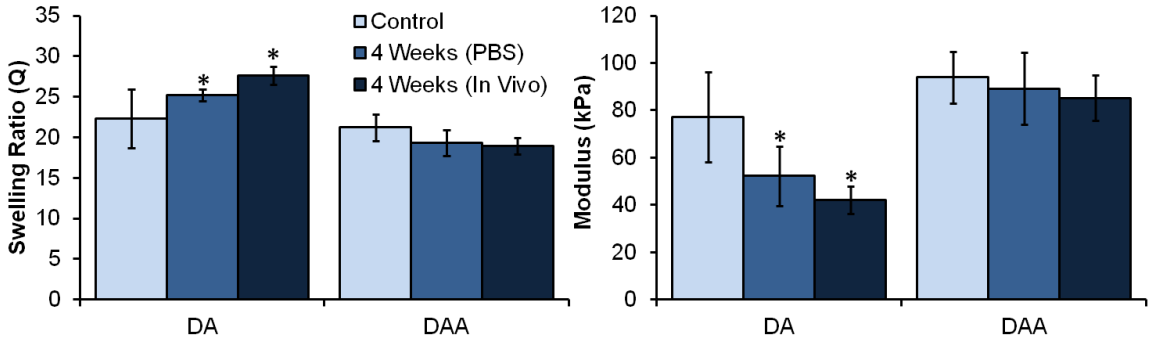

Figure 3.9. Hydrogel in vivo degradation. Swelling ratio and modulus measurements of 10% PEG(10k)DA and DAA gels after 4 weeks in PBS at 37°C and after 4 weeks *in vivo* enclosed in stainless steel mesh cages implanted subcutaneously into rats. PEGDA gels had significant increases in swelling and significant decreases in modulus over 4 weeks *in vitro* and *in vivo*. PEGDAA gels remained stable both *in vitro* and *in vivo* with no changes in modulus or swelling. (n=10, mean ± standard deviation, *$p<0.05$ relative to control).

3.4 Conclusions

The aim of this study was to develop a biostable replacement for traditional PEGDA hydrogels by synthesizing amide-based PEGDAA and to utilize PEGDAA to determine the relative extents of PEGDA hydrolytic and oxidative degradation *in vivo*. The range of PEGDAA hydrogel modulus and swelling that resulted from changes in macromer molecular weight or concentration was similar to that of PEGDA hydrogels. Therefore, the established properties of PEGDA hydrogel systems can be readily transferred to the design of replacement PEGDAA hydrogels. Results also indicated that PEGDAA hydrogels were cytocompatible and retained the low cell adhesion of PEGDA hydrogels. The ability to impart bioactivity as indicated by increased cell adhesion and spreading was demonstrated by conjugating collagen into the PEGDAA matrix. Accelerated hydrolytic degradation studies revealed significantly increased hydrolytic

stability of PEGDAA relative to PEGDA, and provided a well-defined *in vitro* degradation profile for PEGDA hydrogels. Accelerated oxidative degradation studies confirmed that the two systems have comparable susceptibility to oxidation, whereas *in vivo* degradation studies indicated that PEGDAA has increased biostability. Thus, it is likely that PEGDA hydrogels are more susceptible to hydrolytic degradation *in vivo*. These results indicate that PEGDAA could be used as a biostable replacement for PEGDA with minimal design changes to provide a gel-based device with similar properties and cell-material interactions. As such, PEGDAA has the potential to reduce degradation-related failure in long-term *in vivo* applications, such as is required for our vascular graft.

CHAPTER IV

MANIPULATION OF PROTEIN AND NETWORK VARIABLES TO ENHANCE INITIAL AND SUSTAINED EC ADHESION*

4.1 Introduction

Although PEG-Scl2-2 hydrogels appear to provide immediate thromboresistance, longer-term hemocompatibility will depend on the establishment of a confluent endothelial cell (EC) layer on the graft luminal surface. Many graft designs successfully grow confluent EC monolayers *in vitro*, but much of this layer can be lost upon exposure to physiological shear stresses.[127] Thus, the potential for a vascular graft to rapidly form a stable endothelium *in vivo* is important in preventing thrombosis and improving on current options. In short, PEG-Scl2-2 hydrogels must be able to promote EC adhesion, spreading, and migration. We have previously demonstrated the capability of PEG-Scl2-2 hydrogels to promote EC adhesion and spreading; however, PEG-collagen hydrogels consistently provide enhanced EC adhesion and spreading relative to PEG-Scl2-2 hydrogels.[164] Thus, the focus of this work is on utilizing the exceptional tunability of PEG-Scl2-2 hydrogels to further improve EC interactions through the use of the protein functionalization process.

While many methods exist for incorporation of bioactive agents into hydrogels,

---

*Reprinted with permission from "Bioactive hydrogels with enhanced initial and sustained cell interactions," by MB Browning, B Russell, J Rivera, M Höök, and E Cosgriff-Hernandez, Biomacromolecules. 2013, *Accepted*. Copyright (2013) American Chemical Society.

covalent attachment generally provides greater stability and control over biomolecule presentation and release.[233-234] Many growth factors and proteins contain lysines in their backbones that provide a primary amine for functionalization, including both collagen and Scl2-2. Thus, the NHS-lysine Ɛ-amino group reaction can be utilized to functionalize a wide range of bioactive agents with crosslinkable acrylate groups using Acr-PEG-NHS.[171,221,235] Following functionalization, Scl2-2 can be immobilized in PEG hydrogels during photopolymerization without detriment to bioactivity.[164] This method has been successfully utilized in a number of applications to provide scaffolds that deliver specific bioactive cues for tissue regeneration and healing.[164,231,236-237] Functionalization of therapeutic proteins with PEG linkers can also be used in drug delivery systems to increase circulation times.[238]

The PEG linkers on functionalized proteins serve to covalently stabilize them into synthetic networks; however, they can also introduce steric hindrance around integrin binding sites on proteins and interfere with cell-protein interactions, **Figure 4.1**.[239-240] In proteins and growth factors with multiple amine functionalization sites, the density of Acr-PEG-NHS can be easily varied in the traditional functionalization scheme to provide bioactive factors with a range of functionalization densities. A protein that is functionalized with fewer linkers could potentially have improved cell interactions through allowing increased access to integrin binding sites, **Figure 4.1**. However, Van Den Bulcke et al. demonstrated that gelatin hydrogels with lower functionalization levels had decreased moduli compared to those with higher functionalization levels. This indicates that a reduction in crosslinking occurs as protein functionalization density is

decreased due to reduced crosslinking sites on the protein.[241] From these findings, one can also assume that lowering the functionalization density would decrease initial incorporation and retention of proteins in a bioactive hydrogel network. Thus, there is an evident trade-off between reduced steric interactions that promote enhanced initial cell interactions and sufficient protein retention to support sustained cell interactions. These are both critical factors in the development of our vascular graft, as *in vivo* endothelialization can occur very slowly, and sustained bioactivity is desired throughout this process. However, the effect of functionalization density on both initial cell interactions and protein retention over time is poorly characterized in current literature.

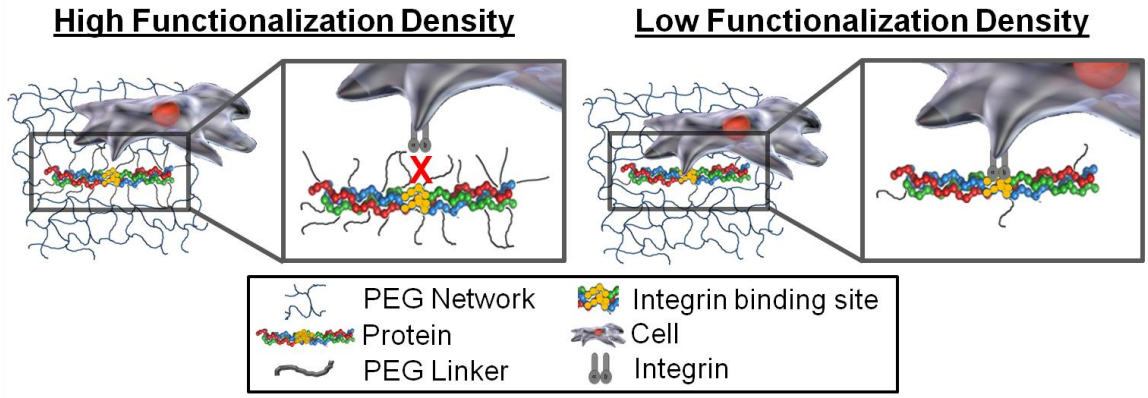

Figure 4.1. Schematic representation of hypothesized effects of protein functionalization density on integrin binding. A decreased number of PEG linkers on the protein backbone (low functionalization density) could reduce steric blocking and improve integrin binding to functionalized proteins.

In the present studies, we investigated the impact of reducing Acr-PEG-NHS functionalization density on EC adhesion and protein maintenance over time in both PEG-collagen and PEG-Scl2-2 hydrogel systems. Additionally, hydrolytic stability of

the PEG matrix and the protein linker was enhanced in an effort to improve protein retention, **Figure 4.2**. The resulting protein levels in the hydrogel matrix and the corollary effects on bioactivity were analyzed over a swelling time frame of 6 weeks to determine a functionalization scheme that increases initial and sustained cell-material interactions.[242]

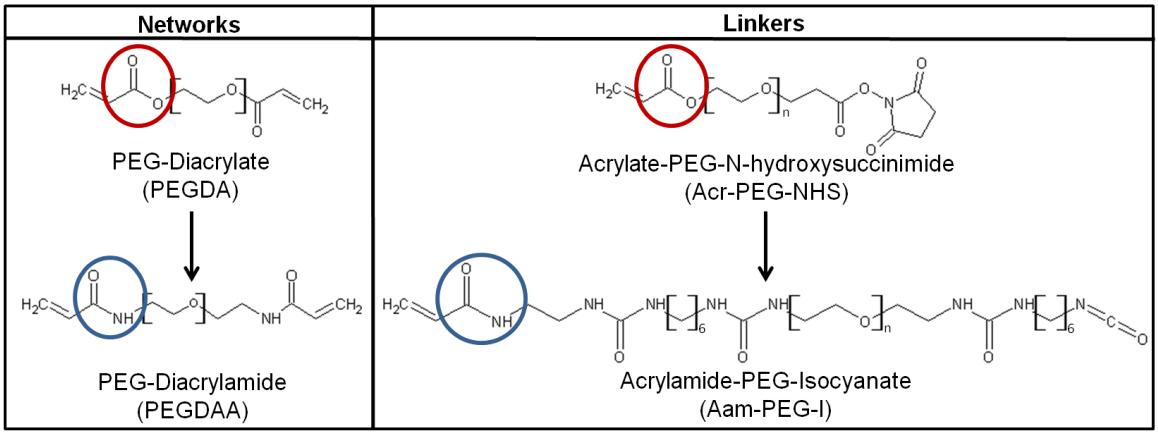

Figure 4.2. Comparison of network macromers and PEG functionalization linkers used to tune retention of collagen and Scl2-2. Ester linkages in PEGDA and Acr-PEG-NHS (red) were replaced with amides in PEGDAA and Aam-PEG-I (blue) to increase hydrolytic stability.

4.2 Materials and Methods

4.2.1 Materials All chemicals and materials were purchased from Sigma Aldrich (St. Louis, MO) and used as received unless otherwise noted. Acr-PEG-NHS (3.5 kDa) and PEG diamine (3.4 kDa) were purchased from Jenkem Technology USA (Allen, TX).

4.2.2 Synthesis of PEGDA and PEGDAA Poly(ethylene glycol) diacrylate (PEGDA) was synthesized as previously described.[172] Briefly, acryloyl chloride was added dropwise to a solution of PEG (3.4 kDa) diol and triethylamine (TEA) in

anhydrous dichloromethane (DCM) under nitrogen. The molar ratios of PEG diol, TEA, and acryloyl chloride were 1:2:4, respectively. After 24 hours of stirring, the reaction solution was washed with 8 molar equivalents of 2M potassium bicarbonate and dried with anhydrous sodium sulfate. The final product was precipitated in cold diethyl ether, filtered, and dried under vacuum.

PEG diacrylamide (PEGDAA) was prepared as previously described in a similar method to PEGDA.[242] Briefly, acryloyl chloride (4 molar equivalents) was added dropwise to a solution of PEG (3.4 kDa) diamine (1 molar equivalent) and TEA (2 molar equivalents) in anhydrous DCM under nitrogen. The reaction was allowed to proceed for 24 hours, and then it was washed with 2M potassium bicarbonate (8 molar equivalents). Following drying with anhydrous sodium sulfate, the product was precipitated in cold diethyl ether, filtered, and dried under vacuum.

Successful synthesis of PEGDA and PEGDAA was confirmed with Fourier transform infrared (FTIR) and proton nuclear magnetic resonance (^{1}H-NMR) spectroscopy. A Bruker TENSOR 27 spectrometer was used to obtain transmission FTIR spectra of control and functionalized polymers that were solution cast onto KBr pellets. Successful acrylation of PEG diol was indicated by the introduction of an ester peak at 1730 cm^{-1} and loss of the hydroxyl peak at 3300 cm^{-1}. The introduction of amide peaks at 1640 cm^{-1} and 1675 cm^{-1} indicated successful acrylamidation of PEG diamine. A Mercury 300 MHz spectrometer with a TMS/solvent signal as an internal reference was utilized to obtain ^{1}H-NMR spectra of control and functionalized polymers. Greater than 90% conversions of hydroxyl to acrylate endgroups and amine to acrylamide endgroups

were observed for all candidate macromers. PEGDA: ^{1}H-NMR ($CDCl_3$): 3.6 ppm (m, -OCH_2CH_2-), 4.3 ppm (t, -CH_2OCO-), 6.1 ppm (dd, -CH=CH_2), 5.8 and 6.4 ppm (dd, -CH=CH_2). PEGDAA: ^{1}H-NMR ($CDCl_3$): 3.6 ppm (m, -OCH_2CH_2-); 6.5 ppm (s, -CH_2-NH-); 6.4 ppm (m, -CH=CH_2); 5.6 and 6.1 ppm (m, -CH=CH_2).

4.2.3 Protein Functionalization with Acrylate-PEG-N-Hydroxysuccinimide The Scl2.28 sequence was amplified and purified as previously described.[161] Scl2-2 was modified from Scl2-1 through the introduction of the GFPGER sequence during site directed mutagenesis as previously described.[161] Scl2-2 and non-gelling rat tail collagen type I were functionalized with photoreactive crosslink sites according to a previously described protocol.[171] The backbones of both Scl2-2 and collagen type I contain ~33 lysines that can be utilized in the established NHS-lysine Ɛ-amino group reaction to allow for bioconjugation. The proteins were reacted with Acr-PEG-NHS (MW 3500) in 50 mM sodium bicarbonate buffer (pH 8.5) for 24 hours at room temperature. The molar ratio of Acr-PEG-NHS:NH_2 was varied from 0.1:1 to 1:1 to provide proteins with varied functionalization densities (0.1X, 0.5X, and 1X). Dialysis against 0.1M hydrochloric acid was carried out for 24 hours to remove basic byproducts, and additional purification was completed by dialysis against reverse osmosis (RO) water for 24 hours (MWCO = 20,000 Da). Following lyophilization of purified products, FTIR spectroscopy was utilized as described above to confirm functionalization of modified proteins with varied PEG-linker densities.

4.2.4 Synthesis of Acrylamide-PEG-Isocyanate Linker A solution of PEG (3.4 kDa) diamine in anhydrous DCM was added dropwise to hexane diisocyanate under

nitrogen at a 1:2 molar equivalent to synthesize PEG diisocyanate (PEGDI). The reaction was allowed to proceed with stirring for 2 hours. Upon completion of the PEGDI synthesis, a solution with 1 molar equivalent of aminoethyl acrylamide (Enamine, Kiev, Ukraine) in dimethyl sulfoxide was added dropwise to the reaction solution while stirring under nitrogen. After 2 hours, the final product was precipitated in cold diethyl ether, filtered, and dried under vacuum. Successful synthesis of PEGDI and Aam-PEG-I was confirmed with FTIR spectroscopy in a method like that described above. Aam-PEG-I structure was confirmed with ^{1}H-NMR spectroscopy as described above. Aam-PEG-I: ^{1}H-NMR ($CDCl_3$): 3.6 ppm (m, -OCH_2CH_2-), 3.3 ppm (m, -NHCH_2CH_2NH-), 1.4 and 3.1 ppm (m, -NH[CH_2]$_6$N-), 5.1-5.4 and 7.3 ppm (s, -N*H*-), 6.1 ppm (dd, -C*H*=CH_2), 5.8 and 6.2 ppm (dd, -CH=CH_2).

4.2.5 Protein Functionalization with Acrylamide-PEG-Isocyanate Scl2-2 and rat tail collagen type I were functionalized with Aam-PEG-I in a method that was modified from that described above. Briefly, Aam-PEG-I was dissolved in anhydrous dimethylformamide and added dropwise to protein solutions in phosphate buffered saline (PBS) at room temperature. The molar ratio of Aam-PEG-I:NH_2 was either 0.1:1 or 1:1 to provide proteins with low and high functionalization densities, respectively. After 2 hours of stirring, dialysis against RO water for 24 hours (MWCO = 20,000 Da) was used to purify functionalized proteins. FTIR spectroscopy confirmed functionalization of proteins with low and high Aam-PEG-I densities.

4.2.6 Preparation and Characterization of Bioactive PEG Hydrogels PEG, PEG-Scl2-2, and PEG-collagen hydrogels were prepared by dissolving PEG (3.4 kDa)

DA or PEG (3.4 kDa) DAA (10 wt%) and functionalized Scl2-2 or collagen (4 mg ml^{-1}) in 20 mM acetic acid. A photoinitiator solution (1 mg Irgacure 2959 per 0.01 ml 70% ethanol) was added at 1 vol% of precursor solution. Solutions were pipetted between 0.5-1.5 mm spaced plates or into microcentrifuge tubes and crosslinked by 6 min exposure to long wave UV light (Intelli Ray Shuttered UV Flood Light, Integrated Dispensing Solutions, Inc., 365 nm, 4 mW/cm^2).

To measure compressive modulus, six 8-mm diameter discs were punched from hydrogel sheets (1.5 mm thick) and swollen in RO water overnight. Samples were subjected to mechanical testing using a dynamic mechanical analyzer (RSAIII, TA Instruments) equipped with a parallel-plate compression clamp. Testing was performed under unconstrained compression at room temperature. Dynamic strain sweeps were used to determine the linear viscoelastic range for each hydrogel formulation. A strain within the upper region of the linear viscoelastic range was used in a constant strain frequency sweep. Tests were conducted between 0.79 and 79 Hz, and the compressive storage modulus was taken at 1.25 Hz.

For swelling assessments, six 8-mm diameter discs were punched from hydrogel sheets (1.5 mm thick) directly after polymerization. The hydrogel discs were swollen in RO water overnight and weighed to determine the equilibrium swelling mass (W_s). Then, samples were dried under vacuum overnight and weighed to assess dry (polymer) mass (W_d). The equilibrium volumetric swelling ratio, Q, was calculated from the equilibrium mass swelling ratio:

$$Q = \frac{W_s}{W_d} \qquad [4.1]$$

4.2.7 Protein Retention in Bioactive PEGDA Hydrogels PEGDA-collagen and PEGDA-Scl2-2 gels were crosslinked directly into microcentrifuge tubes and swelled in phosphate buffered saline (PBS) at 37°C with weekly solution changes. After a swelling time period of 1 day to 6 weeks, gels were dried under vacuum then incubated in a specified volume of 0.5M sodium hydroxide (NaOH) at 37°C for approximately 3 hours, or until complete hydrolysis occurred. Protein concentration in the hydrolyzed gel solutions was determined with a 3-(4-carboxy-benzoyl)-2-quinoline-carboxaldehyde (CBQCA) protein quantification kit (Molecular Probes, Life Technologies, Grand Island, NY), as specified by the manufacturer. Briefly, 10 µl aliquots of each sample were diluted in 125 µl of 0.1M sodium borate buffer. Then, 5 µl of 5 mM potassium cyanide (KCN) were added to each sample, followed by an addition of 10 µl of 5 mM CBQCA (dissolved to 40 mM in DMSO, then diluted to 5 mM in 0.1M sodium borate buffer). Each sample was tested in triplicate and run against a standard of the same protein type and functionalization density to prevent any errors that could occur due to different numbers of free amines on the varied functionalization densities and/or on the two protein types. After 1 to 3 hours of incubation in a black 96 well plate at room temperature with shaking, fluorescence was read using an Infinite M200 Pro plate reader (Tecan Group, Inc.; emission = 550 nm, excitation = 465 nm). Standard curves of fluorescence versus protein concentration were generated for each protein formulation, and the protein concentration (C, mg/ml) in the hydrolyzed gels was determined by inserting the measured fluorescence into a best-fit linear equation for corresponding

standard curves. Protein retention in PEGDA gels at each time point (PR_{DA}, mg/ml) was then calculated to be:

$$PR_{DA} = C \times \frac{V_{NaOH}}{V_0} \qquad [4.2]$$

where V_{NaOH} is the volume of the hydrolysis solution and V_0 is the original gel volume in milliliters. Initial protein incorporation (I) was defined as the percentage of protein retained relative to the initial concentration (C_0) after 1 day of swelling in PBS:

$$I = \frac{PR_{DA}}{C_0} \times 100\% \qquad [4.3]$$

Percent protein retention over time (% PR) was measured as the percent difference between the protein retained at each time point (PR_n) relative to the initial protein incorporation concentration taken after 1 day of swelling in PBS (PR_1):

$$\%\ PR = \frac{PR_1 - PR_n}{PR_1} \times 100\% \qquad [4.4]$$

4.2.8 Protein Retention in Bioactive PEGDAA Hydrogels PEGDAA-collagen and PEGDAA-Scl2-2 gels were prepared similarly to PEGDA gels and swelled in PBS at 37°C for up to 6 weeks. Due to the hydrolytic stability of PEGDAA gels, protein loss was measured to determine protein retention. It was confirmed that the two methods provided similar initial protein incorporation measurements (less than 10% difference) in PEGDA gels. Briefly, swelling solutions were retained throughout the specified time period, frozen at -80°C, and lyophilized to obtain the gel leachables. The lyophilized powders were dissolved in a known volume of PBS, and protein concentration of the resulting solution was determined with a CBQCA protein quantitation kit as described above. All samples were tested in triplicate against a standard of the same protein type

and functionalization density. The concentration of lost protein (C_L, mg/ml) in the hydrolyzed gels was determined by inserting the measured fluorescence into a best-fit linear equation for corresponding standard curves. Protein retention (PR_{DAA}, mg/ml) was then calculated as:

$$PR_{DAA} = \frac{C_0 \times V_0 - C_L \times V_{PBS}}{V_0} \quad [4.5]$$

where C_0 and V_0 are the original protein concentration (mg/ml) and gel volume (ml), respectively, and V_{PBS} is the volume of PBS used to dissolved the lyophilized leachables (ml). Initial protein incorporation (I) was measured from PR_{DAA} according to Equation 4.3, and percent protein retention was measured relative to the initial protein incorporation concentration according to Equation 4.4.

4.2.9 Endothelial Cell Adhesion and Spreading Bovine aortic endothelial cells (BAOECs) were used for all cell studies. Cells were cultured *in vitro* at 37°C/5% CO_2 with Dulbecco's Modified Eagle Medium (DMEM, high glucose GlutaMAX^{TM}, Invitrogen) supplemented with 10% heat-inactivated fetal bovine serum (FBS, Invitrogen) and 1% Penicillin-Strepotomycin solution (Gibco). Cells were used between passages 7 and 10 after 10-14 days of culture for all studies.

Bioactive hydrogels were crosslinked between 0.5 mm spaced plates as described above and swelled for 3 hours in 70% ethanol. Subsequently, gels were swelled in sterile PBS for approximately 6 hours with solution changes every 2 hours to remove residual ethanol. Then, 6 mm diameter punches were taken from each hydrogel formulation and discs were swelled in PBS at 37°C for a specified time period (1 day to 6 weeks) with regular solution changes. Only bioactive hydrogel formulations with greater than 10%

protein retention at 6 weeks were used in 6 week bioactivity retention studies. Following the desired time period, BAOECs were seeded onto specimens at 10,000 cells cm^{-1} for 3 hours at 37°C/5% CO_2. Cells were then fixed with 3.7% glutaraldehyde and stained with rhodamine phalloidin (F-actin/cytoplasm, Invitrogen) and SYBRGreen (DNA/nucleus, Invitrogen). Representative images were obtained with a Nikon Eclipse TE2000-S with 3 field views per specimen and 4 specimens per hydrogel formulation. The number of cell nuclei per image was used as a quantitative assessment of cell adhesion on each test surface and was counted using the SYBRGreen stained images. Average cell spreading, or cell area, was quantified by applying the Photoshop "magic wand" tool to the image background of the rhodamine phalloidin stained images and adjusting the tool tolerance so that all extracellular regions were selected. The histogram function was utilized to evaluate the extracellular pixels (P_{Ex}). The average pixels per cell (A_{cell}) for that image was quantified as:

$$A_{cell} = \frac{P_T \times P_{Ex}}{N} \qquad [4.6]$$

where P_T represents total image pixels and N is total number of cell nuclei. Pixels were then converted to microns using known objective scaling.

4.2.10 Statistical Analysis All modulus, swelling, and protein retention data were expressed as the mean ± standard derivation of the mean. All cell adhesion and spreading data were expressed as the mean ± standard error of the mean. Statistical analysis was performed by an unpaired two-tailed student's t-test. Statistical significance was accepted at $p<0.05$.

4.3 Results and Discussion

4.3.1 Protein Functionalization with Acr-PEG-NHS Fourier transform infrared (FTIR) spectroscopy was utilized to confirm functionalization of collagen and Scl2-2 with a range of Acr-PEG-NHS densities, **Figure 4.3**. IR absorbance peaks assigned to the amide of the protein (C=O) at 1650 cm^{-1} and the ether backbone of the Acr-PEG-NHS (C-O-C) at 1110 cm^{-1} were present in the purified products. As the reaction ratios of Acr-PEG-NHS-to-lysine were increased from 0.1:1 to 1:1, a corollary increase in the relative peak height ratios of ether-to-amide was also observed. This confirmed that proteins with a range of functionalization levels were synthesized. Additionally, relative peak ratios of different batches of functionalized proteins remained constant, indicating that similar functionalization levels were achieved between batches. For these studies, collagen and Scl2-2 were functionalized with 0.1:1, 0.5:1, and 1:1 molar ratios of Acr-PEG-NHS-to-lysine to yield 0.1X, 0.5X, and 1X functionalization densities, respectively.

4.3.2 Protein Functionalization with Acrylamide-PEG-Isocyanate Linker Acrylamide-PEG-isocyanate (Aam-PEG-I) was synthesized in which the hydrolyzable acrylate group of Acr-PEG-NHS was replaced with a biostable acrylamide group, **Figure 4.1**. FTIR spectroscopy was used to confirm key structural features during the two-step reaction of Aam-PEG-I, **Figure 4.4A**. First, isocyanate endcapping of PEG diamine was indicated by the introduction of an isocyanate peak at 2250 cm^{-1} and urea peaks at 1560 and 1650 cm^{-1}. In the second step, relative decreases in the isocyanate peak and increases in the urea peaks confirmed successful formation of the Aam-PEG-I

linker. The integration ratio of acryloyl protons to backbone methyl protons and presence of HDI methyl protons in the ^{1}H NMR spectra confirmed the structure and final average molecular weight of Aam-PEG-I, **Figure 4.4B**. Endgroup conversion ratios of greater than 80% and final molecular weights between 3800 and 4200 Da were observed for all candidate linkers, indicating that minimal coupling occurred during the synthesis.

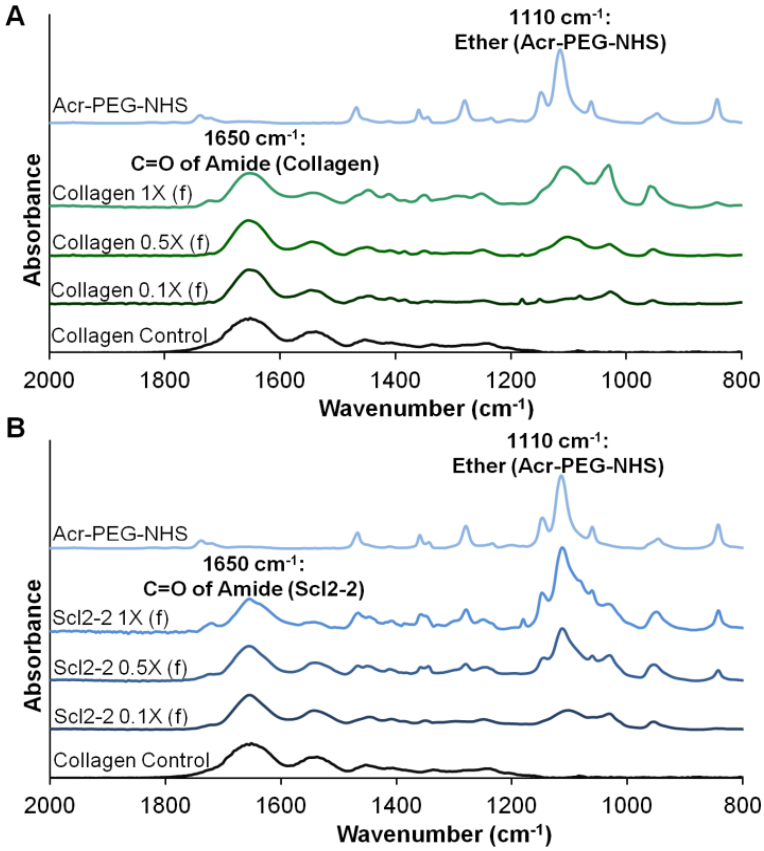

Figure 4.3. Transmission FTIR spectra of functionalized proteins. (A) Collagen and (B) Scl2-2. Ratio of 1110 cm^{-1} (ether of PEG) to 1650 cm^{-1} (amide of protein) peaks decreases with decreasing functionalization density.

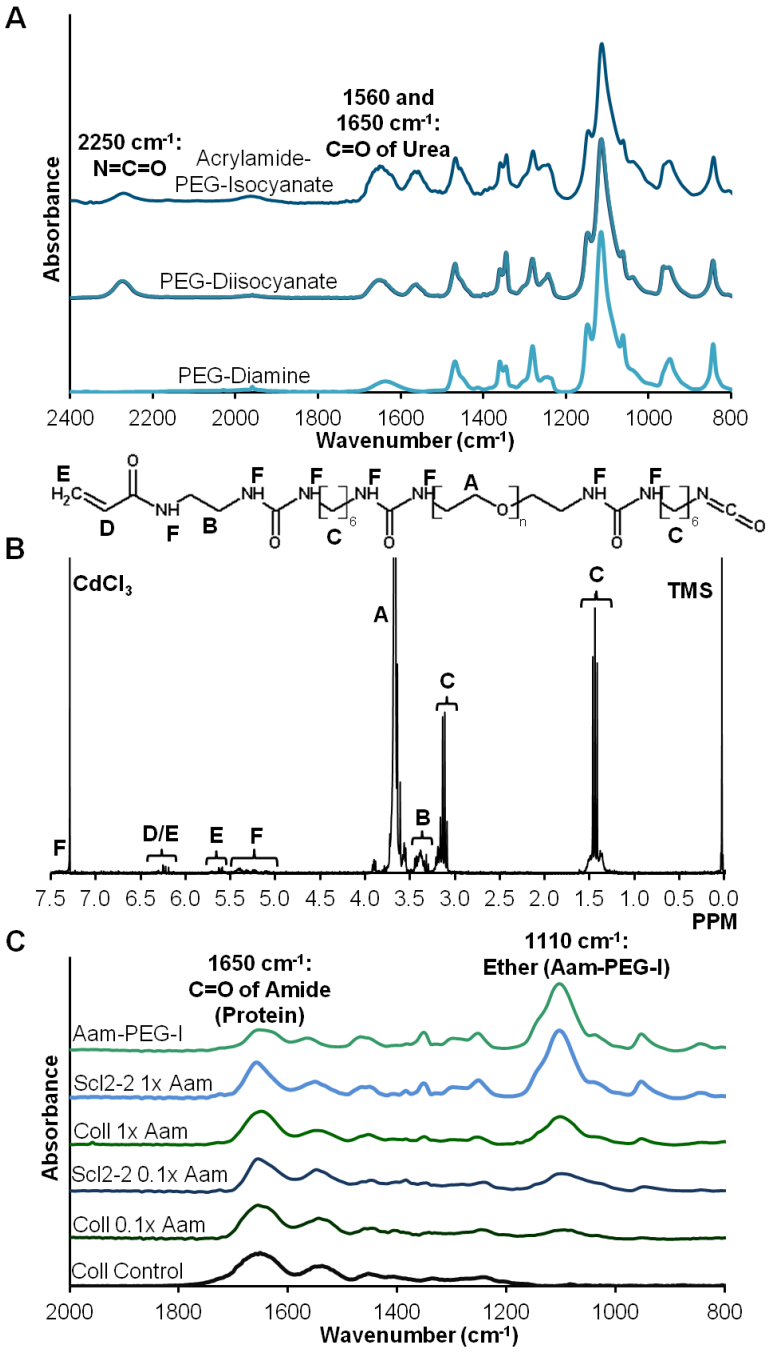

Figure 4.4. Confirmation of acrylamide-PEG-isocyanate synthesis and functionalization. (A) Transmission FTIR spectra of PEG (3.4 kDa) diisocyanate (PEGDI) synthesized from PEG (3.4 kDa) diamine and acrylamide-PEG (3.4 kDa)-isocyanate (Aam-PEG-I) synthesized from the resulting PEGDI. (B) ^{1}H NMR spectra of Aam-PEG-I. (C) Transmission FTIR spectra of Aam-PEG-I-functionalized collagen and Scl2-2. Ratio of 1110 cm^{-1} (ether) to 1650 cm^{-1} (amide) peaks decreases with decreasing functionalization density.

The final product was utilized to functionalize collagen and Scl2-2 with low (0.1X) and high (1X) functionalization densities. IR absorbance peak ratios of the ether of the Aam-PEG-I (1110 cm^{-1}) were decreased relative to the amide of the proteins (1650 cm^{-1}) as functionalization density was decreased, **Figure 4.4C**. Relative peak ratios were constant between different batches of Aam-PEG-I functionalized proteins, indicating that consistent levels of functionalization were achieved. This data confirmed that Aam-PEG-I can be used to functionalize proteins with varied functionalization densities similarly to the traditional Acr-PEG-NHS linker.

4.3.3 Bioactive Hydrogel Modulus and Swelling Ratio To confirm that protein functionalization density and linker type do not alter bulk network properties, 10% PEG (3.4 kDa) DAA gels were prepared with Acr-PEG-NHS- and Aam-PEG-I-functionalized collagen at high (1X) and low (0.1X) functionalization densities, and compressive modulus and swelling ratio were measured relative to 10% PEG (3.4 kDa) DAA gel controls. No significant differences in modulus or swelling were observed for any of the tested formulations, **Figure 4.5**. This was expected, as the protein component comprises less than 1% of the network, and properties should be dominated by the synthetic PEG matrix. Our previous studies have demonstrated similarly negligible effects from adding functionalized Scl2-2 into PEG-based hydrogel scaffolds.[164]

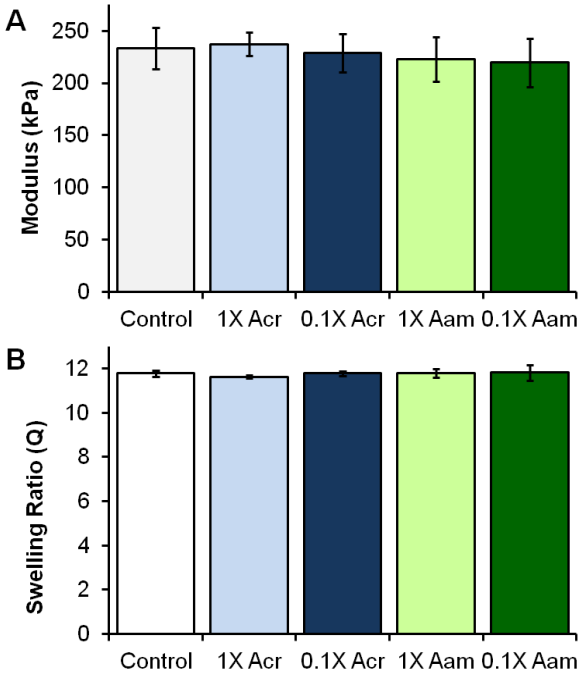

Figure 4.5. Bioactive hydrogel compressive modulus and swelling ratio. 10% PEG (3.4 kDa) DAA gels with no protein (Control), Acr-PEG-NHS-functionalized collagen at high (1X Acr) and low (0.1X Acr) functionalization densities, and Aam-PEG-I-functionalized collagen at high (1X Aam) and low (0.1X Aam) functionalization densities. No significant differences in either modulus or swelling ratio were measured between any of the tested groups ($p>0.05$). n=6.

4.3.4 Initial Protein Incorporation and Bioactivity PEGDA was crosslinked with each of the Acr-PEG-NHS-functionalized collagen and Scl2-2 proteins at an initial concentration of 4 mg protein ml^{-1}. After swelling the gels in PBS for 24 hours to remove uncrosslinked proteins, they were hydrolyzed in 0.5M NaOH. CBQCA was run on the resulting solutions relative to non-swollen controls to quantify the concentration of proteins remaining in the gels and determine the initial protein incorporation during crosslinking for each functionalization density, **Figure 4.6A**. As functionalization density is decreased, the initial incorporation of both collagen and Scl2-2 was reduced from ~80% to ~60%. This was expected given that the lower functionalization density

proteins have fewer available crosslinking sites. Despite having a reduced protein concentration after 1 day of swelling, gels with lower functionalization density proteins demonstrated significantly increased levels of BAOEC adhesion after 3 hours of incubation, **Figure 4.6B and C**. While spreading on PEG-Collagen gels was not significantly affected by functionalization density, spreading on PEG-Scl2-2 gels was significantly increased ($p<0.05$) by reducing functionalization from 1X to 0.1X (from 643 ± 285 to 1088 ± 332 mm^2/cell). Given that cell interactions with the bioactive PEG hydrogel are limited to the functionalized proteins, these results suggest that the PEG linkers could block integrin binding to functionalized proteins and reduce bioactivity. While similar effects have been observed with PEGylated drugs, this has not been documented with bioactive hydrogels.[240] Monfardini et al. reported that branched PEG linkers reduce bioactivity relative to linear linkers.[243] While linear PEG was used here, subsequent crosslinking into a PEG network may provide a similar effect. It can be concluded from these findings that reducing protein functionalization density is a facile method for improving cell-material interactions with bioactive hydrogels by reducing the steric hindrance around integrin binding sites.

It should be noted that BAOEC interactions with PEG-Scl2-2 hydrogels were consistently lower than those on PEG-Collagen hydrogels. This is to be expected, as collagen contains three $\alpha_1\beta_1$ and $\alpha_2\beta_1$ integrin binding sites whereas Scl2-2 only contains one.[3] However, reducing Scl2-2 functionalization density to 0.1X provided comparable EC adhesion and spreading to PEG-Collagen 1X and 0.5X gels. While similar effects could likely be achieved by increasing Scl2-2 concentration, the use of larger amounts of

protein increases scaffold cost.[227,231,244] Additionally, concentration increases can be limited by solubility of large molecules such as growth factors and proteins.[245] Thus, reducing functionalization density provides an alternate route for increasing cell interactions that is facile, adaptable, and cost effective.

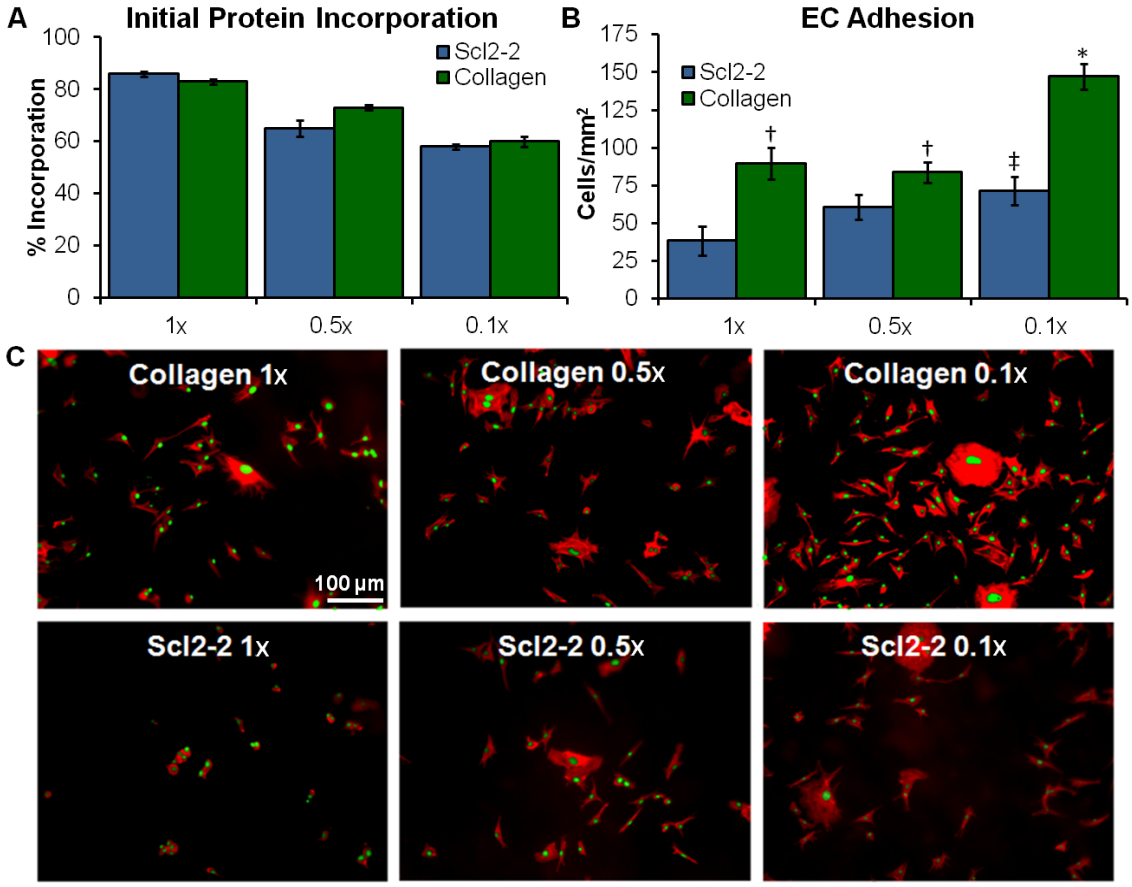

Figure 4.6. Initial protein incorporation and bioactivity of PEG-collagen and PEG-Scl2-2 hydrogels in response to functionalization density. (A) Initial protein incorporation in PEGDA-Scl2-2 and PEGDA-collagen hydrogels after 1 day of swelling in PBS at 37°C decreases with decreasing functionalization density. n=3; mean ± standard deviation; $p<0.05$ for each decrease in functionalization density. (B) General increases in BAOEC adhesion were seen with decreases in protein functionalization density. n=4 samples, 3 images per sample for a total of 12 images; mean ± standard error; *$p<0.05$ vs. all samples, †$p<0.05$ vs. Scl2-2 0.5X and Scl2-2 1X, ‡$p<0.05$ vs. Scl2-2 1X. (C) Rhodamine phalloidin and SYBR Green stained BAOECs adhered to PEG-collagen and PEG-Scl2-2 hydrogels after a 3 hour incubation period. Scale bar applies to all images.

4.3.5 Protein and Bioactivity Retention: Acr-PEG-NHS Although reduced functionalization density enhanced cell interactions, it was hypothesized that it may also reduce protein retention within the hydrogel over time. Indeed, following 6 weeks of swelling in PBS at 37°C, both collagen and Scl2-2 levels in PEGDA hydrogels were reduced by 91 to 100%, **Figure 4.7A**. These large protein losses were attributed to hydrolysis of the PEGDA network. While PEGDA hydrogels are typically considered biostable, the acrylate esters are susceptible to hydrolytic degradation that results in alterations of both scaffold properties and protein levels over time.[194-197] PEGDA is suitable for relatively long-term bioactive factor delivery applications on the order of months, but it cannot be used in applications that require several years of bioactivity. To address this, PEG diacrylamide (PEGDAA), a PEG-based hydrogel system that is comparable to traditional PEGDA hydrogels but with improved hydrolytic stability was utilized, **Figure 4.1**.[242] PEGDAA was previously employed by Elbert et al. to improve conjugate addition reaction bond stability between bioactive peptides and PEG hydrogels.[208] In the current study, increasing network stability with PEGDAA hydrogels resulted in significantly increased protein retention compared to PEGDA hydrogels (from 0-9% to 14-67%) after 6 weeks of swelling in PBS at 37°C, **Figure 4.7B**. Thus, PEGDAA enhanced sustained network protein levels and may provide a tool for better controlling long-term delivery of drugs and presentation of bioactive agents. It should be noted that the ether linkages in PEG hydrogels are also susceptible to oxidative degradation, which has been proposed as an alternate *in vivo* degradation mechanism.[197] It is likely that *in vivo* degradation of PEGDA hydrogels is due to some combination of

both hydrolytic and oxidative degradation; therefore, PEGDAA should enhance overall *in vivo* stability compared to PEGDA even if oxidation does occur.[196,200,242]

The effect of the observed protein loss over time on cell adhesion and spreading was investigated on bioactive hydrogel formulations that retained at least 10% of their protein at 6 weeks. Thus, none of the PEGDA-Acr-PEG-NHS systems were tested in bioactivity retention studies. Analysis of 3 hour BAOEC adhesion and spreading on PEGDAA hydrogels with Acr-PEG-NHS-functionalized collagen and Scl2-2 after swelling in PBS at 37°C for up to 6 weeks revealed that comparable adhesion and spreading levels were maintained for high functionalization density proteins (1X), **Figure 4.7C**. However, gels with low functionalization density proteins (collagen 0.1X; Scl2-2 0.5X and 0.1X) had significantly reduced BAOEC adhesion and spreading relative to controls (swollen in PBS at 37°C for 1 day). This corresponded to the large decreases in protein concentrations in low functionalization density gels, and could be expected due to decreased cell adhesion that typically occurs with decreased bioactive factor concentration.[198,227,244]

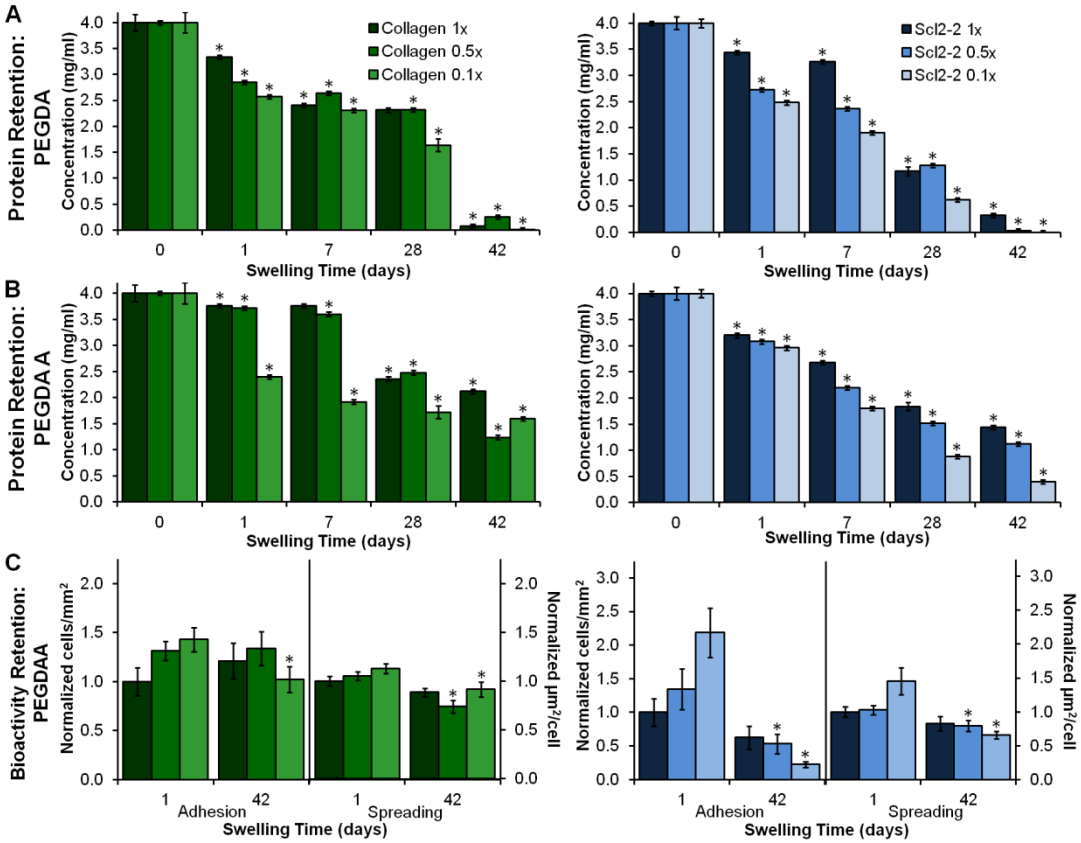

Figure 4.7. Protein and bioactivity retention over 6 weeks in PEGDA and PEGDAA gels. Protein retention in (A) PEGDA and (B) PEGDAA hydrogels over 6 weeks of swelling in PBS at 37°C. n=3; mean ± standard deviation; *p<0.05 relative to previous time point. (C) BAOEC adhesion and spreading on bioactive PEGDAA hydrogels after 6 weeks of swelling in PBS at 37°C. Measurements normalized to 1X samples at 1 day of swelling. n=4 samples, 3 images per sample for a total of 12 images; mean ± standard error; *p<0.05 relative to 1 day sample.

4.3.6 Protein and Bioactivity Retention: Aam-PEG-I Although the PEGDAA network provided increased stability that enhanced protein retention, there was still a significant reduction in protein concentration over time that corresponded with loss of bioactivity, especially at low functionalization densities. It was hypothesized that hydrolysis of the acrylate esters of the Acr-PEG-NHS linkers could also contribute to the observed protein losses. To test this hypothesis, Aam-PEG-I, a PEG linker with

improved hydrolytic stability, was utilized to investigate the effects of linker stability on long-term protein and bioactivity retention in bioactive PEG hydrogels, **Figure 4.1**. It was found that increasing linker stability with Aam-PEG-I resulted in significantly improved protein retention in both PEGDA and PEGDAA gels over 6 weeks of swelling compared with Acr-PEG-NHS functionalized proteins, **Figure 4.8A**. Thus, increasing functionalization linker stability with Aam-PEG-I appears to have an even greater effect on long-term protein retention than increasing network stability with PEGDAA when compared with the traditional Acr-PEG-NHS/PEGDA system. The functionalization linker developed here demonstrates strong potential for use as a protein, drug, or peptide functionalization linker in a wide range of systems to provide a sustained presence of bioactive factors.

BAOEC adhesion and spreading on PEGDAA hydrogels with collagen- and Scl2-2-Aam at 3 hours revealed that reducing the functionalization density with Aam-PEG-I produces similar increases in initial cell-material interactions as the traditional Acr-PEG-NHS system for both collagen and Scl2-2. Both protein systems had significant increases in BAOEC adhesion and spreading (40-70% and 10-40%, respectively) with reduction of functionalization density from 1X to 0.1X, and all analogous gel systems had statistically similar BAOEC interactions for the two linker types. Upon confirmation of similar initial bioactivity with the two linker systems, PEGDA and PEGDAA gels with collagen- and Scl2-2-Aam were swollen in PBS for 6 weeks at 37°C to evaluate bioactivity retention in the new system.

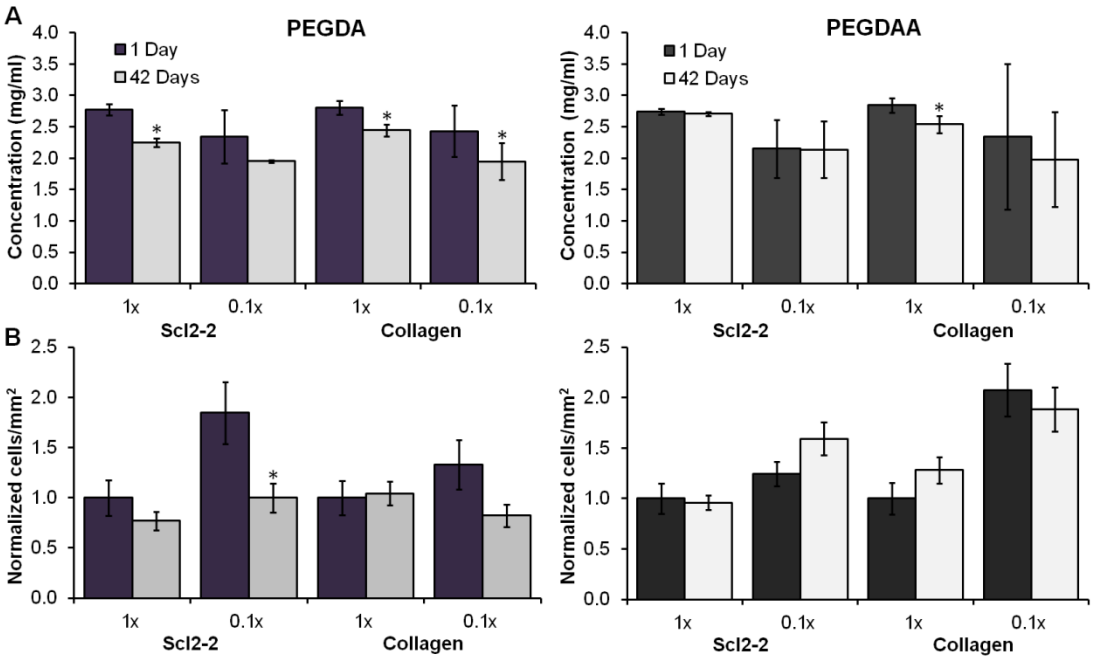

Figure 4.8. Aam-PEG-I functionalized collagen and Scl2-2 protein retention and bioactivity retention. (A) Aam-PEG-I-functionalized protein retention in PEGDA and PEGDAA hydrogels after 6 weeks of swelling in PBS at 37°C. n=6; mean ± standard deviation; *p<0.05 relative to 1 day time point. (B) 3 hour BAOEC adhesion on bioactive PEG hydrogels with Aam-PEG-I-functionalized proteins after swelling gels in PBS for 6 weeks at 37°C. Measurements normalized to 1X samples at 1 day of swelling. n=4 samples, 3 images per sample for a total of 12 images; mean ± standard error; *p<0.05 relative to 1 day time point.

In all PEGDAA gels with Aam-PEG-I, no significant alterations in BAOEC adhesion were measured after swelling gels for 6 weeks at 37°C, and gels with low functionalization density proteins maintained their enhanced BAOEC adhesion compared to high functionalization density protein gels, **Figure 4.8B**. Thus, the use of Aam-PEG-I allows for reduced functionalization density to increase bioactivity without losses over time. Similarly, bioactivity of PEGDA gels with Aam-PEG-I-functionalized proteins at low functionalization densities was similarly or better retained than analogous PEGDAA gels with Acr-PEG-NHS-functionalized proteins. No significant changes in

BAOEC spreading were measured for any of the Aam-PEG-I systems after 6 weeks of swelling. These results indicate that the use of a biostable linker and network significantly increases protein and bioactivity retention compared to the traditional PEGDA/Acr-PEG-NHS system. Additionally, the significant improvements in both protein and bioactivity retention with Aam-PEG-I-functionalized proteins in PEGDA hydrogels indicate that this linker could be utilized in degradable matrices to provide control over bioactive factor delivery independently of linker hydrolysis.

Aam-PEG-I allows for use of low functionalization densities for enhanced initial cell interactions while maintaining long term protein levels within the gel to sustain desired cell interactions. This linker in combination with a PEGDAA network would be valuable in long-term implantable devices in which prolonged cell-material interactions are desired, such as our off-the-shelf vascular graft. As *in vivo* endothelialization that occurs via migration from the anastomoses can be a slow process (on the order of 0.2 mm per day), retention of bioactive factors over longer time frames is required, and alterations in swelling or modulus and/or physical breakage that occur with gel degradation could disrupt this process.[203,206] Additionally, the combination of linkers, networks, and functionalization schemes presented here provides the means to tune protein and drug delivery with enhanced precision. For example, a drug delivery device could be designed to address the different stages of wound healing with temporally-controlled release of multiple bioactive agents by functionalization with linkers of varied biostability.[246] A similarly designed scaffold could be used to regulate stem cell differentiation *in vitro* or *in vivo* with controlled release of multiple cues.[247]

4.4 Conclusions

The ability to tune the mechanical, chemical, and biological properties of PEG-based hydrogels is highly valuable in the development of improved biomaterials for regenerative medicine and drug delivery. Functionalization of bioactive factors and subsequent incorporation into PEG hydrogels provides controllable bioactivity; however, PEG linkers used to functionalize proteins can also sterically hinder integrin binding sites and impair cell-material interactions. Reducing the density of PEG linkers during functionalization provides a facile method to significantly improve initial cell adhesion and spreading with many advantages over altering bioactive factor concentration, but this also reduces protein retention over time as a result of network and/or PEG linker hydrolysis. These studies demonstrate that this protein loss is substantial with almost total loss of protein observed after 6 weeks in low functionalization density systems. The novel Aam-PEG-I linker synthesized here presents a PEG linker option with significantly enhanced hydrolytic stability relative to the traditional Acr-PEG-NHS linker. When used at a low functionalization density in combination with PEGDAA, this system provides a hydrogel with significantly improved initial bioactivity that can be sustained over long swelling times. This will allow for a controlled investigation of longer-term cell interactions in future studies without concerns over effects of protein loss over time. Although these findings were focused on the characterization of bioactive hydrogels for use in a vascular graft, the common use of PEGylation to enhance circulation time of bioactive factors makes these findings highly relevant in drug delivery as well.

CHAPTER V

EFFECTS OF SUBSTRATE MODULUS AND PROTEIN CONCENTRATION ON EC INTERACTIONS

5.1 Introduction

Utilization of a synthetic hydrogel matrix in the fabrication of the intimal layer of our vascular graft not only provides a material with thromboresistance and controlled introduction of bioactivity, it also allows for independent exploration of effects of protein and matrix variables on cell-material interactions. It is extensively acknowledged in current literature that increasing bioactive factor concentration provides a means to increase cell adhesion and spreading.[227,231,244] This presents an additional variable for alteration of endothelial cell (EC) interactions with PEG-Scl2-2 hydrogels to achieve a vascular graft material that is capable of endothelialization. While protein parameters can be valuable in altering cell-material interactions, PEG hydrogels in particular provide matrix variables as well.

One of the most widely utilized properties of PEG hydrogels is the ability to alter their swelling and mechanical properties over wide ranges with simple changes in PEG molecular weight and/or concentration.[248] Multiple reports have demonstrated that substrate modulus affects cell-material interactions with various cell types.[151,167-168,249-252] Previous work with ECs has demonstrated that shear stresses on their apical side caused by hemodynamic forces affect cell function and structure and induce changes throughout the cell interior.[253] More recently, studies have focused on evaluating the interactions

between the extracellular matrix and the basal EC side for promotion of angiogenesis. In general, stiffer collagen and fibrin gels reduce vascular network formation.[254-255] However, ECs have been found to have increased spreading on stiffer gels due to the ability of the cells to generate traction forces on their matrix.[256] These spreading increases may be more valuable in generation of an off-the-shelf vascular graft than findings concerning angiogenesis. Previous studies have primarily been performed using natural polymer hydrogels, wherein substrate modulus can only be altered by changing overall protein concentration. Thus, little information is available on the effects of synthetic hydrogel matrix variables on EC interactions or on the effects of substrate modulus independent of protein concentration. PEG-Scl2-2 hydrogels provide a means to vary substrate modulus independently of bioactive factor concentration to evaluate its effects on EC adhesion and spreading.

Here, a full study of the effects of protein concentration with varied functionalization densities on EC adhesion and spreading over one week was performed to determine effects of Scl2-2 concentrations on initial and prolonged cell interactions. Additionally, two compositions of PEG-Scl2-2 and PEG-collagen gels (1X functionalization density, 1 mg protein/ml; 0.1X functionalization density, 8 mg protein/ml) were fabricated with two different substrate moduli by increasing PEG molecular weight from 3.4 kDa to 10 kDa to investigate effects of substrate modulus on the high and low end of bioactivity levels in our hydrogel formulations. Finally, EC migration was measured as a function of protein concentration to determine the ability to

tune migration rates on PEG-Scl2-2 hydrogels and as an initial evaluation of their potential for *in situ* endothelialization from the vascular graft anastomoses.

5.2 Materials and Methods

5.2.1 Materials All chemicals and materials were purchased from Sigma Aldrich (St. Louis, MO) and used as received unless otherwise noted. Acr-PEG-NHS (3.5 kDa) and PEG diamine (3.4 kDa) were purchased from Jenkem Technology USA (Allen, TX).

5.2.2 Synthesis of PEGDA and PEGDAA Poly(ethylene glycol) diacrylate (PEGDA) was synthesized as previously described.[172] Briefly, 4 molar equivalents of acryloyl chloride were added dropwise to a solution of PEG (3.4 kDa or 10 kDa) diol and 2 molar equivalents of triethylamine (TEA) in anhydrous dichloromethane (DCM) under nitrogen and allowed to react for 24 hours. Then, the reaction solution was washed with 8 molar equivalents of 2M potassium bicarbonate and dried with anhydrous sodium sulfate. The final product was precipitated in cold diethyl ether, filtered, and dried under vacuum.

PEG diacrylamide (PEGDAA) was prepared as previously described in a similar method to PEGDA.[242] Briefly, acryloyl chloride (4 molar equivalents) was added dropwise to a solution of PEG (3.4 kDa) diamine (1 molar equivalent) and TEA (2 molar equivalents) in anhydrous DCM under nitrogen. The reaction was allowed to proceed for 24 hours prior to being washed with 2M potassium bicarbonate (8 molar equivalents). Following drying with anhydrous sodium sulfate, the product was precipitated in cold diethyl ether, filtered, and dried under vacuum.

Successful synthesis of PEGDA and PEGDAA was confirmed with Fourier transform infrared (FTIR) and proton nuclear magnetic resonance (^{1}H-NMR) spectroscopy. Control and functionalized polymers were solution cast onto KBr pellets and FTIR spectra were obtained using a Bruker TENSOR 27 spectrometer. The introduction of an ester peak at 1730 cm^{-1} and loss of the hydroxyl peak at 3300 cm^{-1} indicated successful acrylation of PEG diol, and the introduction of amide peaks at 1640 cm^{-1} and 1675 cm^{-1} indicated successful acrylamidation of PEG diamine. A Mercury 300 MHz spectrometer with a TMS/solvent signal as an internal reference was utilized to obtain ^{1}H-NMR spectra of control and functionalized polymers. Greater than 90% conversions of hydroxyl to acrylate endgroups and amine to acrylamide endgroups were observed for all candidate macromers. PEGDA: ^{1}H-NMR ($CDCl_3$): 3.6 ppm (m, -OCH_2CH_2-), 4.3 ppm (t, -CH_2OCO-), 6.1 ppm (dd, -CH=CH_2), 5.8 and 6.4 ppm (dd, -CH=CH_2). PEGDAA: ^{1}H-NMR ($CDCl_3$): 3.6 ppm (m, -OCH_2CH_2-); 6.5 ppm (s, -CH_2-NH-); 6.4 ppm (m, -CH=CH_2); 5.6 and 6.1 ppm (m, -CH=CH_2).

5.2.3 Synthesis of Acrylamide-PEG-Isocyanate Linker One molar equivalent of PEG (3.4 kDa) diamine dissolved in anhydrous DCM was added dropwise to 2 molar equivalents of hexane diisocyanate under nitrogen to synthesize PEG diisocyanate (PEGDI). After 2 hours of stirring, a solution with 1 molar equivalent of aminoethyl acrylamide (Enamine, Kiev, Ukraine) in dimethyl sulfoxide was added dropwise to the reaction solution while stirring under nitrogen. The reaction was allowed to proceed for 2 hours, and then the final product was precipitated in cold diethyl ether, filtered, and dried under vacuum. Successful synthesis of PEGDI and Aam-PEG-I was confirmed

with FTIR spectroscopy in a method like that described above. The introduction of an isocyanate peak at 2250 cm^{-1} and urea peaks at 1560 and 1650 cm^{-1} confirmed isocyanate endcapping of PEG diamine, and relative decreases in the isocyanate peak and increases in the urea peaks confirmed successful formation of the Aam-PEG-I linker. Aam-PEG-I structure was confirmed with ^{1}H-NMR spectroscopy as described above. Aam-PEG-I: ^{1}H-NMR ($CDCl_3$): 3.6 ppm (m, -OCH_2CH_2-), 3.3 ppm (m, -NHCH_2CH_2NH-), 1.4 and 3.1 ppm (m, -NH[CH_2]$_6$N-), 5.1-5.4 and 7.3 ppm (s, -N*H*-), 6.1 ppm (dd, -C*H*=CH_2), 5.8 and 6.2 ppm (dd, -CH=CH_2).

5.2.4 Protein Functionalization The Scl2.28 sequence was amplified and purified as previously described.[161] Scl2-2 was modified from Scl2-1 through the introduction of the GFPGER sequence during site directed mutagenesis as previously described.[161] Scl2-2 and a rat tail collagen type I control were functionalized with Aam-PEG-I. Briefly, Aam-PEG-I was dissolved in anhydrous dimethylformamide and added dropwise to protein solutions in phosphate buffered saline (PBS) at room temperature. The molar ratio of Aam-PEG-I:NH_2 was 0.1:1, 0.5:1, or 1:1 to provide proteins with low, medium, and high functionalization densities, respectively. After 2 hours of stirring, functionalized proteins were purified using dialysis against reverse osmosis (RO) water for 24 hours (MWCO = 20,000 Da). FTIR spectroscopy confirmed functionalization of proteins with varied Aam-PEG-I densities. The presence of both ether peaks from the PEG linker at 1110 cm^{-1} and amide peaks from the proteins at 1560 cm^{-1} confirmed functionalization, and relative decreases in absorbance peak ratios of the ether of the Aam-PEG-I to the amide of the proteins confirmed variation in functionalization density.

5.2.5 Preparation and Characterization of Bioactive PEG Hydrogels PEG, PEG-Scl2-2, and PEG-collagen hydrogels were prepared by dissolving PEG (3.4 kDa) DA or PEG (3.4 kDa or 10 kDa) DAA (10 wt%) and functionalized Scl2-2 or collagen (1, 4, or 8 mg ml^{-1}) in 20 mM acetic acid. A photoinitiator solution (1 mg Irgacure 2959 per 0.01 ml 70% ethanol) was added at 1 vol% of precursor solution. Solutions were pipetted between 0.5-1.5 mm spaced plates or into microcentrifuge tubes and crosslinked by 6 min exposure to long wave UV light (Intelli Ray Shuttered UV Flood Light, Integrated Dispensing Solutions, Inc., 365 nm, 4 mW/cm^2).

To measure compressive modulus, six 8-mm diameter discs were punched from hydrogel sheets (1.5 mm thick) and swollen in RO water overnight. Samples were subjected to mechanical testing under unconstrained compression at room temperature using a dynamic mechanical analyzer (RSAIII, TA Instruments) equipped with a parallel-plate compression clamp. The linear viscoelastic range for each hydrogel formulation was determine using dynamic strain sweeps. A strain within the upper region of the linear viscoelastic range was used in a constant strain frequency sweep from 0.79 and 79 Hz. The compressive storage modulus was taken at 1.25 Hz.

For swelling assessments, six 8-mm diameter discs were punched from hydrogel sheets (1.5 mm thick) directly after polymerization. The hydrogel discs were swollen in RO water overnight and weighed to determine the equilibrium swelling mass (W_s). Then, samples were dried under vacuum overnight and weighed to assess dry (polymer) mass (W_d). The equilibrium volumetric swelling ratio, Q, was calculated from the equilibrium mass swelling ratio:

$$Q = \frac{W_s}{W_d} \qquad [5.1]$$

5.2.6 Initial Protein Incorporation PEGDAA-collagen and PEGDAA-Scl2-2 gels were crosslinked directly into microcentrifuge tubes and swelled in PBS at 37°C for 24 hours. The swelling solutions were then removed from the tubes, frozen at -80°C, and lyophilized to obtain the gel leachables. The lyophilized powders were dissolved in a known volume of phosphate buffered saline (PBS), and protein concentration of the resulting solution was determined with a 3-(4-carboxy-benzoyl)-2-quinoline-carboxaldehyde (CBQCA) protein quantification kit (Molecular Probes, Life Technologies, Grand Island, NY), as specified by the manufacturer. Briefly, 10 µl aliquots of each sample were diluted in 125 µl of 0.1M sodium borate buffer. Then, 5 µl of 5 mM potassium cyanide (KCN) were added to each sample, followed by an addition of 10 µl of 5 mM CBQCA (dissolved to 40 mM in DMSO, then diluted to 5 mM in 0.1M sodium borate buffer). Each sample was tested in triplicate and run against a standard of the same protein type and functionalization density. After 1 to 3 hours of incubation in a black 96 well plate at room temperature with shaking, fluorescence was read using an Infinite M200 Pro plate reader (Tecan Group, Inc.; emission = 550 nm, excitation = 465 nm). The concentration of lost protein (C_L, mg/ml) in the hydrolyzed gels was determined by inserting the measured fluorescence into a best-fit linear equation for corresponding standard curves. Protein retention at 24 hours (PR, mg/ml) was then calculated as:

$$PR = \frac{C_0 \times V_0 - C_L \times V_{PBS}}{V_0} \qquad [5.2]$$

where C_0 and V_0 are the original protein concentration (mg/ml) and gel volume (ml), respectively, and V_{PBS} is the volume of PBS used to dissolved the lyophilized leachables (ml). Initial protein incorporation (I) was measured from PR as:

$$I = \frac{PR_{DA}}{C_0} \times 100\% \qquad [5.3]$$

5.2.7 Endothelial Cell Adhesion and Spreading Bovine aortic endothelial cells (BAOECs) were used for all cell studies. *In vitro* culture was carried out at 37°C/5% CO_2 with Dulbecco's Modified Eagle Medium (DMEM, high glucose GlutaMAX™, Invitrogen) supplemented with 10% heat-inactivated fetal bovine serum (FBS, Invitrogen) and 1% Penicillin-Strepotomycin solution (Gibco). Cells were used between passages 2 and 5 after 7-10 days of culture for all studies.

Bioactive hydrogels were crosslinked between 0.5 mm spaced plates as described above and swelled for 3 hours in 70% ethanol. Subsequently, gels were taken through an ethanol swelling ramp (15 minutes each in 50%, 25%, and 0% ethanol in water) to remove residual ethanol. Then, 6 mm diameter punches were taken from each hydrogel formulation and swelled in PBS for 1-3 hours to ensure full hydration. BAOECs were seeded onto specimens at 10,000 cells cm^{-1} and cultured at 37°C/5% CO_2 for 3 hours, 72 hours, or 1 week. Media was changed at 3 hours and then every 48 hours. Following the desired culture time, cells were fixed with 3.7% glutaraldehyde and stained with rhodamine phalloidin (F-actin/cytoplasm, Invitrogen) and SYBRGreen (DNA/nucleus, Invitrogen). Representative images were obtained with a Nikon Eclipse TE2000-S with 3 field views per specimen and 4 specimens per hydrogel formulation. Fluorescent images (3 images per specimen, 4 specimens per sample) of SYBRGreen- and

rhodamine phalloidin-stained cells were utilized to quantify the extent of cell spreading. Average cell spreading, or cell area, was quantified by applying the Photoshop "magic wand" tool to the image background and adjusting the tool tolerance so that all extracellular regions were selected. The histogram function was then utilized to evaluate the extracellular pixels (P_{Ex}). The average pixels per cell (A_{cell}) for that image was then quantified as follows:

$$A_{cell} = \frac{P_T - P_{Ex}}{N} \qquad [5.4]$$

where P_T represents total image pixels and N is total number of cell nuclei. Pixels were then converted to microns using known objective scaling.

5.2.8 Endothelial Cell Migration For PEG-Scl2 hydrogels to support graft endothelialization, they must support both EC adhesion and migration. To analyze EC migration on PEG-Scl2 hydrogels, sterile filtered PEG-Scl2-2 (10 wt% PEG(3.4 kDa) DA, 6 or 12 mg protein/ml) and PEG-collagen (10 wt% PEG(3.4 kDa) DA, 2 or 4 mg protein/ml) hydrogels were prepared between glass plates separated by 0.5 mm spacers. The resulting hydrogels were immersed in PBS for 24 h, after which a set of 2.54 cm punches were collected from the swollen gels.

BAOECs were harvested and seeded onto the hydrogels at 10,000 cells cm^{-2}. Gels were cultured for 24 h at 37 °C/5% CO_2 to allow for cell adhesion and equilibrium cell spreading. EC migration was monitored for 1 h at 5 min intervals in at least three randomly selected locations of each hydrogel formulation using a Zeiss Axiovert microscope. For determination of single cell migration parameters, only cells that remained in isolation (>100 μm from other cells) were measured. Cell centroid position

at each 5 minute time increment was determined based on cell outlines using Photoshop. These centroids were then used to calculate the mean-square displacement (MSD, $<D^2>$) for a range of time intervals. In brief,

$$<D^2> = \frac{1}{N}\sum_{i=1}^{N} d_i \qquad [5.5]$$

where N is the total number of 5 minute time increments in the time interval under consideration, and d_i is the square of cell displacement during time increment i.[257] The speed, S, and direction persistence time (P) were determined by fitting the MSD ($<D^2>$) and the time interval, t, to the persistent random walk equation using nonlinear least squares regression analysis:[152]

$$\langle D^2\rangle = 2S^2P\left[t - P\left(1 - e^{-\left(\frac{t}{P}\right)}\right)\right] \qquad [5.6]$$

5.3 Results and Discussion

5.3.1 Effects of Protein Concentration on EC Adhesion and Spreading BAOEC adhesion and spreading on PEG-Scl2-2 and PEG-collagen gels over one week was analyzed as a function of protein concentration (1, 4, and 8 mg protein ml^{-1} hydrogel solution) with three different functionalization densities for each protein (1X, 0.5X, and 0.1X), **Figure 5.1.** In general, increases in protein concentration resulted in increases in EC adhesion at 3 hours for all functionalization densities of both protein types, and lower functionalization densities (0.1X) supported greater BAOEC adhesion than high functionalization densities (1X). The observed concentration effects were expected, based on the multitude of reports in literature demonstrating that increasing bioactive

factor concentration can be used to increase cell interactions.[198,227,244] Additionally, the effects of functionalization density correlate with our previous results.

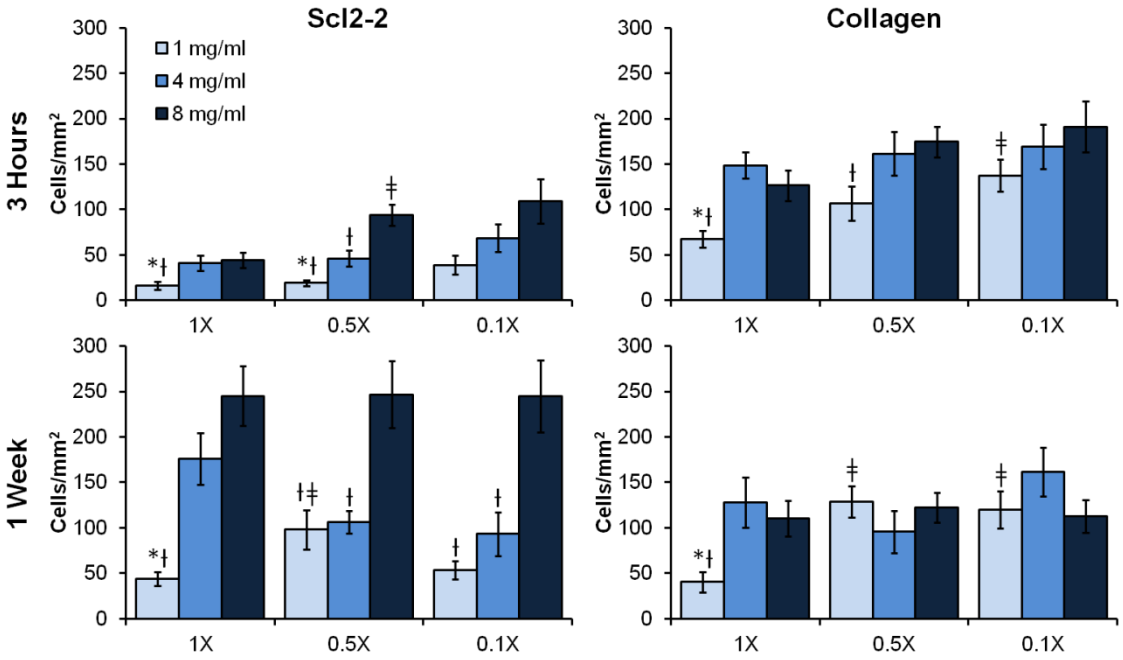

Figure 5.1. Effects of protein concentration on BAOEC adhesion over 1 week. All Scl2-2 samples had significant increases in adhesion from 3 hours to 1 week except for 0.1X 1 and 4 mg/ml samples, whereas no collagen samples exhibited significant increases in adhesion from 3 hours to 1 week. n=4 samples, 3 images per sample for a total of 12 images; mean ± standard error;*$p<0.05$ relative to corollary 4 mg/ml sample, ł$p<0.05$ relative to corollary 8 mg/ml sample, ǂ$p<0.05$ relative to corollary 1X sample.

PEG-Scl2-2 hydrogels exhibited BAOEC proliferation between 3 hours and 1 week to provide significant increases in EC adhesion for all samples except for the 1 and 4 mg/ml samples for the 0.1X functionalization density. This is the first time that we have confirmed the ability of Scl2-2 to support significant BAOEC proliferation. Although PEG-collagen hydrogels had greater initial adhesion than corollary Scl2-2 samples, no significant increases in EC adhesion occurred between 3 hours and 1 week.

This resulted in greater BAOEC adhesion on PEG-Scl2-2 gels at 1 week than on PEG-collagen gels, especially with higher concentration samples. It has previously been shown that $\alpha_1\beta_1$ is the only collagen receptor that can activate the Shc-mediated growth pathway.[258] Shc-linked integrin mediated adhesion promotes cell survival and progression through the Gap 1 phase of the cell cycle in which eukaryotic cell division takes place, whereas adhesion mediated by other types of integrins can cause exit from the cell cycle and, in some cases, cell death.[259-260] Thus, it is possible that the controlled presence of only $\alpha_1\beta_1$ and $\alpha_2\beta_1$ integrin binding sites in Scl2-2 provides more direct cell signaling to promote EC proliferation, whereas the multitude of integrin binding sites in collagen results in contradictory signaling that reduces proliferation.

It can be seen that for the most part, concentration effects on BAOEC adhesion to PEG-Scl2-2 hydrogels are enhanced over one week, while functionalization density effects are reduced. It was hypothesized that this could be due to the reduced initial protein incorporation that occurs with reducing functionalization density, as the effects of decreased concentration and increased access to integrin binding sites are conflicting. Although we have shown that this does not affect initial adhesion levels, it is possible that the concentration differences between high and low functionalization densities have a greater effect over time. Initial protein incorporation for each of these gel systems was measured to obtain an indication of these potential effects, **Table 5.1**. As expected, lower functionalization densities had reduced initial incorporations than higher functionalization densities. Thus, it is possible that normalizing initial concentrations for

each functionalization density would provide enhanced functionalization density effects in the long term similarly to short term effects.

Table 5.1. Initial protein incorporation of Aam-PEG-I-functionalized collagen and Scl2-2 in PEGDAA hydrogels.

Sample		Initial Incorporation (%)	% Difference from 1X
Scl2-2	1X	60 ± 1	--
	0.5X	47 ± 1	22%
	0.1X	41 ± 1	32%
Collagen	1X	59 ± 1	--
	0.5X	56 ± 4	5%
	0.1X	53 ± 2	10%

5.3.2 Effects of Protein Concentration on EC Migration EC migration from the anastomoses will be a significant mechanism in the endothelialization of the multilayer grafts. Thus, as an initial evaluation of the potential for rapid endothelialization, BAOEC migration on PEG-Scl2-2 hydrogels (1X functionalization density) with varied concentrations (6 and 12 mg protein/ml) was tracked over 1 hour and compared to that on PEG-collagen hydrogels, **Figure 5.2.** BAOEC migration rates on the hydrogels were affected by both type and concentration of protein, **Figure 5.3**. Specifically, an increase in the concentration of Scl2-2 from 6 to 12 mg of protein ml^{-1} of hydrogel solution resulted in a 3 fold increase in BAOEC migration rates from 4.2 ± 2.2 μm min^{-1} to 13.2 ± 4.2 μm min^{-1}. A corresponding increase in collagen concentration (2 to 4 mg of protein per ml, based on an equivalent number of binding sites relative to 6 and 12 mg of Scl2-2 per mL), did not cause a significant increase in migration rates. Additionally, migration speeds on PEG-Scl2-2 hydrogels were increased relative to those on equivalent PEG-

collagen hydrogels. It has been previously shown that cell adhesion strength generally increases to a saturation point with an increase in ligand density and affinity, but cell migration rate responds in a biphasic manner to increases in these variables.[168] Specifically, there is a maximum ligand density/affinity to which migration is increased and beyond which migration speed is reduced due to the increased adhesion strength.[261] Thus, it is likely that the reduced migration speed on PEG-collagen hydrogels would correlate with increased adhesion strengths.

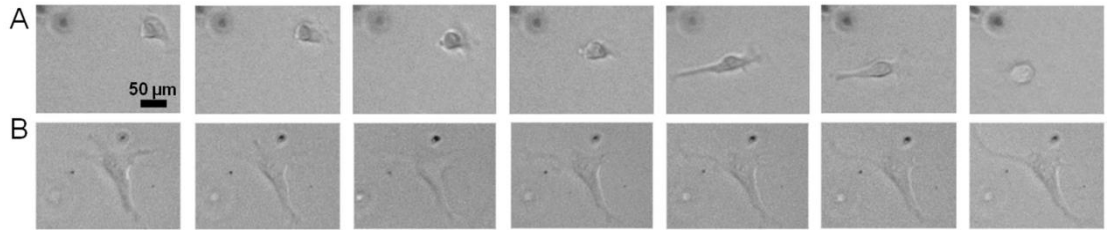

Figure 5.2. Micrographs used to track BAOEC centroid position to determine migration rates on (A) PEG-Scl2-2 hydrogels and (B) PEG-Collagen hydrogels. The scale bar applies to all images, and images are shown at 10 minute intervals.

These studies demonstrated that Scl2-2 concentration can be used to control EC migration rates, and PEG-Scl2-2 hydrogels have the potential to improve upon the rate of EC migration relative to collagen-based systems. Future studies will analyze EC migration rate and adhesion strength as a function of each of the protein and network variables tested in the 1 week adhesion studies. Elucidation of these interactions is essential in developing off-the-shelf grafts that promote rapid *in vivo* formation of the stable, endothelial linings.

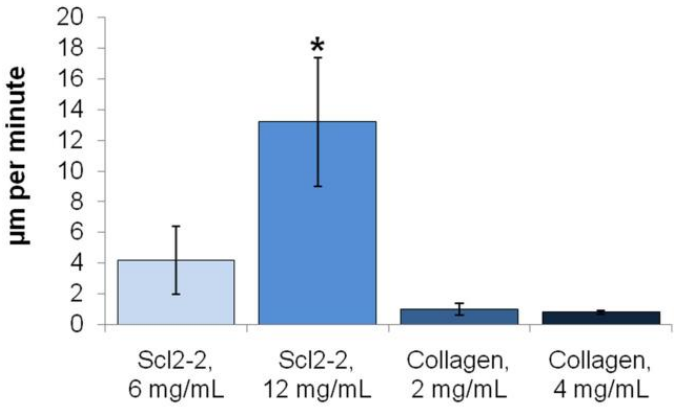

Figure 5.3. BAOEC migration. EC migration rates increased ~3 fold with increased concentration of Scl2-2, and average migration speeds on Scl2-2 gels were ~10 fold greater than those observed on equivalent PEG-collagen gels. n=6; mean ± standard error of mean displayed; *p>0.05 relative to lower concentration sample.

5.3.3 Effects of Substrate Modulus on EC Adhesion and Spreading The ability to tune PEG hydrogel properties over a wide range with simple alterations in molecular weight and concentration while maintaining a constant protein concentration enables facile investigation of the effects of scaffold properties on bioactivity. To evaluate this, Scl2-2 and collagen were crosslinked at either 1 mg/ml (1X functionalization density) or 8 mg/ml (0.1X functionalization density) into 10% PEG(3.4 kDa or 10 kDa) DAA solutions. The reduction of PEG molecular weight from 3.4 kDa to 10 kDa resulted in a modulus reduction and swelling ratio increase of approximately 60%, **Figure 5.4**. BAOEC adhesion and spreading was measured at 3 hours to obtain an initial indication of effects of substrate modulus, **Figure 5.5.** It was found that for all four formulations, there were decreases in BAOEC adhesion with reduced substrate modulus, with significant decreases for Scl2-2 samples. No significant trends in BAOEC spreading were measured in relation to substrate modulus. Although current literature does not

contain much information on the effects of substrate modulus on EC adhesion, these results do correlate with numerous reports that have shown that increasing substrate modulus increases cell adhesion.[167] Additionally, the decreases in spreading that have been shown with decreased natural polymer scaffold modulus were on scaffolds with much lower modulus values than the 10% PEG(10k) gels in this study.[256] Although protein concentrations are the same in the gel systems here, the 10% PEG(10k) gels have higher swelling ratios than the 10% PEG(3.4k) gels. Thus, it is possible that this increase in swelling results in larger distances between integrin binding sites in the gel, which would result in the reduced adhesion shown in these studies. In our previous work, we utilized a 4-arm PEG crosslinker to create local increases in crosslink density to increase modulus with minimal effects on mesh size.[248] In future investigations, compositions with similar swelling ratios and different modulus values could be utilized to decouple the effects of swelling from the effects of modulus on EC adhesion. This would provide definitive information on the effects of substrate modulus in our system; however, we have shown that modulus can be utilized as an additional tool to alter bioactivity of PEG-Scl2-2 hydrogels.

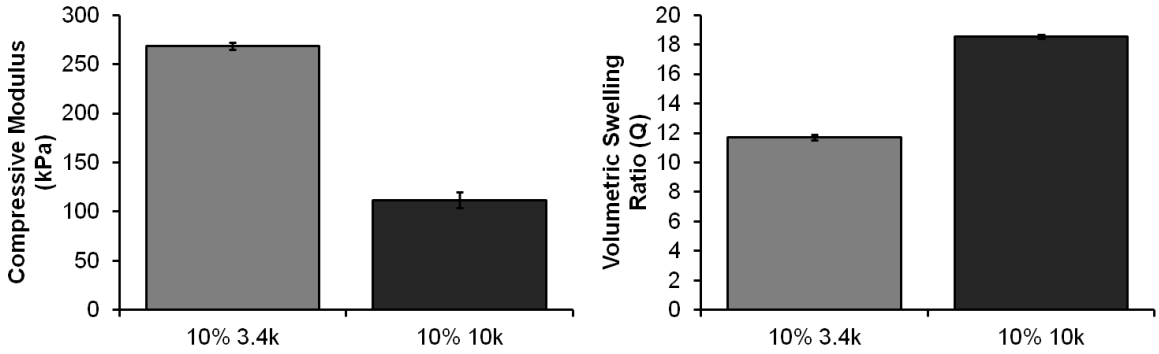

Figure 5.4. Effects of PEG molecular weight on compressive modulus and volumetric swelling ratio. Reducing molecular weight from 3.4 kDa to 10 kDa provided a reduction in modulus and increase in swelling of approximately 60%.

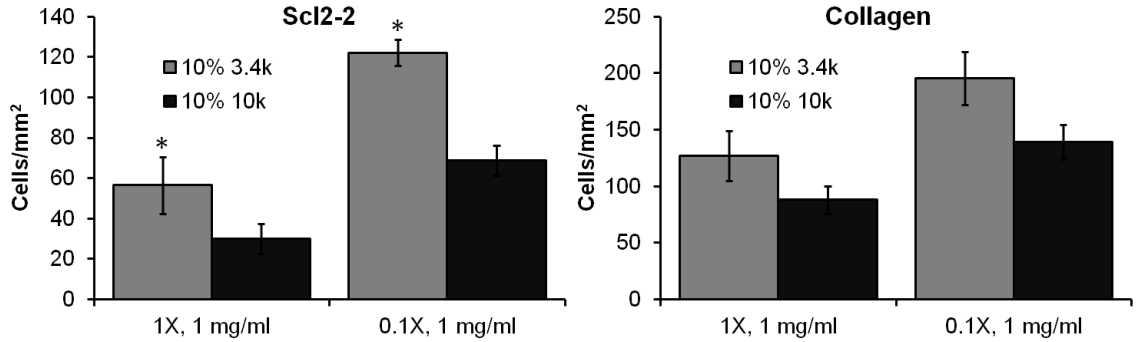

Figure 5.5. Effects of substrate modulus on 3 hour BAOEC adhesion. Significant increases in adhesion occurred with reducing functionalization density and increasing concentration. General decreases in adhesion occurred with reduced modulus. n=4 samples, 3 images per sample for a total of 12 images; mean ± standard error; *$p<0.05$ relative to corollary 10% 10k sample.

5.4 Conclusions

PEG-Scl2-2 hydrogels are an ideal system for the independent investigation of a wide range of protein and network variables on bioactivity. Here, we showed that increases in protein concentration can be used to increase both EC adhesion and migration. Additionally, PEG-Scl2-2 hydrogels promote significant EC proliferation over one week, resulting in adhesion levels that are greater than corollary PEG-collagen

gels. This is most likely due to the clarity in signaling that occurs with Scl2-2 relative to collagen, as it only contains integrin binding sites for $\alpha_1\beta_1$ and $\alpha_2\beta_1$ integrins whereas collagen contains numerous integrin binding sites. Substrate modulus can be easily decreased by reducing PEG molecular weight, which results in decreased EC adhesion. In future studies, the effects of each of these variables (functionalization density, protein concentration, and substrate modulus) on EC migration and adhesion strength will be evaluated. The formulation that promotes the highest EC migration rates under flow with adhesion strengths that are higher than of high shear thrombosis (70-100 dynes/cm^2) will be chosen for *in vivo* studies in our porcine carotid artery model to assess endothelialization and long-term (30 and 90 day) thromboresistance.

CHAPTER VI

CONCLUSIONS

6.1 Summary

In this work, multilayer vascular grafts were developed for use in small-diameter bypass applications. To progress beyond current clinically available synthetic options, cell-material interactions must be improved to provide both thromboresistance and potential for *in situ* endothelialization without the need for expensive cell harvesting or pre-culture. Additionally, compliance mismatch with native vasculature must be reduced while maintaining sufficient burst pressures to prevent flow alteration-induced intimal hyperplasia. PEG-Scl2-2 hydrogels proved to be thromboresistant in a series of whole blood studies in vitro as well as in a porcine carotid artery in vivo. Electrospun polyurethane mesh biomechanical properties were altered over a wide range with simple changes in mesh thickness to achieve comparable burst pressures and compliance values to autologous vascular grafts. Inter-layer integrity was confirmed following vacuum drying and re-swelling and after exposure to 4 weeks of pulsatile flow. PEGDAA hydrogels were fabricated and found to be similar to PEGDA hydrogels with enhanced biostability in vitro and in vivo. These studies indicate the potential of this design for long-term implantation with reduced risk of thrombosis and intimal hyperplasia.

To enhance EC adhesion to PEG-Scl2-2 hydrogels, protein functionalization density was reduced. With the use of acrylamide-PEG-isocyanate as a biostable functionalization linker, reduced functionalization densities were utilized that had

enhanced initial and sustained EC interactions, potentially suitable for long-term implantation and in situ endothelialization. EC adhesion was further increased by increasing Scl2-2 concentration and increasing substrate modulus. Initial studies show that EC migration speed can also be altered by increasing Scl2-2 concentration. Additionally, PEG-Scl2-2 hydrogels promoted significantly greater EC proliferation over one week than PEG-collagen hydrogels. In short, we have demonstrated the exceptional tunability of PEG-Scl2-2 hydrogels in efforts to determine a formulation that is capable of rapid endothelialization.

6.2 Significance of Work

Scl2 proteins are a valuable biomaterial system with many advantages over traditional proteins or peptides. However, prior to this work, the use of these proteins was severely limited due to their inability to form stable, 3D matrices. The methodology to functionalize Scl2 proteins with photocrosslinkable linkers without detriment to their other properties significantly broadens their potential for use. The Scl2 system could potentially be utilized to target a number of different integrins or enzyme-labile sites, and the use of them in this vascular graft design could serve as a catalyst to altering these strategies for a wide range of regenerative medicine applications. In general, these studies have given an initial indication of their great potential and served to characterize basic cell-material interactions with Scl2-based systems in response to a number of variables. This serves to provide a platform of information for use in future Scl2 protein-based applications.

In Chapter 3, we presented the first full characterization of PEGDA hydrogel degradation in current literature. Additionally, the use of PEGDAA provides a potential replacement for PEGDA hydrogels in long term in vivo applications with minimal design changes required for translation between systems. The ability to use PEGDAA in an in vivo degradation studies allows for controlled elucidation of the mechanisms of PEGDA hydrogel in vivo degradation for the first time. Both the in vitro and in vivo work serves to fill a gap in the understanding of this widely utilized biomaterial system.

In Chapter 4, the ability to use functionalization density as a means to control bioactivity was evaluated. This facile method allows for enhanced bioactivity to be achieved while potentially reducing the amount of protein needed and/or allowing use of different proteins, such as Scl2-2, that lower cell adhesion but have benefits over traditionally used proteins. Furthermore, the development of acrylamide-PEG-isocyanate (Aam-PEG-I) as a biostable functionalization linker has many potential uses beyond this work. It could be utilized in combination with degradable linkers in a number of applications that require temporally-controlled release of varied bioactive factors. The use of Aam-PEG-I and PEGDAA also allows for a controlled investigation of long-term cell-material interactions without concerns over effects of protein loss over time. Thus, this system has many potential wide-ranging uses in both regenerative medicine and drug delivery.

PEG-Scl2-2 hydrogels have many advantages over other systems that have been studied for use in vascular grafts. Notably, the thromboresistance provides a significant benefit over collagen, and the bioactivity capabilities are greater than those of peptides.

Scl2-2 allows for an in-depth investigation of how scaffold micro-environment affects EC adhesion through independent tuning of protein and network variables. The information gained in the presented studies can be used in future EC migration, adhesion strength, and phenotype evaluations to determine a formulation that has the best potential for in situ endothelialization and to gain a better understanding of EC interactions with their surroundings.

6.3 Challenges and Future Directions

Although this work presents many advances in the development of this vascular graft design, a significant amount of work is required prior to their successful employment. With the inner layer, a full study of EC static and dynamic migration, adhesion strength, and phenotype in response to the presented protein and matrix variables (functionalization density, protein concentration, substrate modulus) will be carried out. The final formulation must first provide adhesion strengths sufficient for high shear thrombosis (70-100 dynes/cm^2). From these, the formulations that promote EC proliferation and quiescent will be taken, and the one of these with the highest migration speed will be chosen for future studies. Upon determination of the PEG-Scl2-2 hydrogel with the most suitable EC interactions, thromboresistance will be confirmed in vitro after 6 hours of whole porcine blood flow with the bioreactor system presented in Chapter 2. In vivo host response will be evaluated in a rat model, and then this gel formulation will be incorporated into a multilayer graft and implanted into a porcine carotid artery model. In vivo thromboresistance and endothelialization will be evaluated at 30 and 90 days.

In previous in vivo studies, significant issues with suturing through the two layers have come about. Specifically, small pieces of hydrogel break off as the suture goes through the graft that can then travel downstream and cause occlusions in smaller vessels. This was a possible cause for seizures in a previous in vivo study and must be addressed prior to future in vivo work. One potential solution is to make the hydrogel layer thinner. This could be done by simply soaking or dipping the meshes in a hydrogel solution that is then crosslinked rather than crosslinking a full layer of gel between the mesh and a glass mandrel. This could also potentially reduce the overall host response to the vascular graft with the addition of a PEG coating on both the inside and outside surfaces. All previous in vivo studies were performed with 10% PEG(3.4 kDa) gels, which are relatively brittle. By increasing the molecular weight, hydrogel elasticity would be increased. These two methods would be easy to implement and could be used independently in combination with one another to improve graft suturability. Another option would be to alter the hydrogel network chemistry. Previously, researchers have developed hydrogels with very high toughness through the creation of semi-interpenetrating networks of covalently and physically crosslinked polymers.[262] In other work in our lab, PEG-based segmented polyureas have been synthesized. These could be used in the vascular graft project to form a physical network that could then be swelled in a PEGDAA solution that can be covalently crosslinked. This double network hydrogel should retain the favorable properties of PEG hydrogels, and could potentially have improved mechanical properties. Upon making any of these changes in formulation,

effects EC interactions and thrombogenicity would have to be assessed, but they could potentially improve the overall graft design and utility.

This design requires long-term biostability so that the vascular graft can remain in the patient throughout their lifetime. The electrospun mesh chemistry has already been altered to utilize a poly(carbonate urethane) that is resistant to both hydrolytic and oxidative degradation. While PEGDAA hydrogels have shown initially that they have improved biostability relative to PEGDA hydrogels, current in vivo studies are underway for 12 weeks to gain a better idea of the degradation profile of both systems. It is likely that PEGDA hydrogels are susceptible to some combination of both oxidative and hydrolytic degradation and that therefore PEGDAA hydrogels will degrade oxidatively over long time frames. While the inner layer of the vascular graft would likely be protected from the host response, degradative species could diffuse through the outer graft layer and cause degradation. If significant degradation is noted during the 12 week in vivo study, we could incorporate an antioxidant, such as retinol or ascorbic acid, into the electrospun mesh. Currently, we are investigating the use of a semi-interpenetrating network of the segmented polyurethane (physical network) and methacrylated poly(dimethyl sulfoxide) (covalent network). The hydroxyl groups on either of these antioxidants could be reacted with acryloyl chloride to create a photocrosslinkable acrylate group. This would allow for covalent incorporation of an antioxidant to prevent oxidation of the inner hydrogel layer over longer time frames.

Many design changes have been made in the hydrogel formulation since performing initial thrombosis studies, most notably the network and linker chemistries

presented in Chapter 4. While we do not expect thromboresistance to be affected by either change in chemistry, alternatives must be considered beforehand in the event that the new formulation has increased platelet interactions. The most likely cause would be the increased hydrophobicity introduced into the Aam-PEG-I linker with the use of hexane diisocyanate. Diisocyanobutane could be used instead with minimal protocol changes to produce a linker with fewer hydrophobic methanes. Another option would be to obtain custom synthesized acrylamide-PEG-NHS from the company that currently makes the Acr-PEG-NHS that we use (JenKem Technologies). If the acrylamide linkages in PEGDAA induce thrombosis, vinyl endgroups could be explored instead as an alternative photocrosslinkable system.

Although it has previously been demonstrated that Scl2-1 proteins are non-immunogenic, no in vivo studies have been performed to assess the host response to PEG-Scl2-2 hydrogels. PEG hydrogels have previously been shown to induce a minimal host response, but Scl2-2 is a bacterial protein that could potentially have an adverse response. To address this, current work in the Höök laboratory is focusing on replacing potentially immunogenic portions of Scl2 proteins with a "murinized" and "humanized" version of those amino acid sequences. It is expected that these alterations would minimize any potential concerns over the host response to PEG-Scl2-2 hydrogels.

While many steps are required between the current state of this work and implementation in the clinic, this design has the potential to present an off-the-shelf vascular graft that improves on current synthetic grafts. The future investigations on this project will allow for continued expansion on the knowledge of synthetic matrix

formation and characterization, endothelialization processes, and prevention of long-term implant degradation.

REFERENCES

(1) American Heart Association. Heart disease and stroke statistics--2010 update: A report from the American Heart Association. **2010**,

(2) Ross, R.; Glomset, J. A. Atherosclerosis and the arterial smooth muscle cell. *Science* **1973**, *180*, 1332-1339.

(3) Sweeney, S. M. *et al.* Angiogenesis in collagen I requires α2β1 ligation of a GFP*GER sequence and possibly p38 MAPK activation and focal adhesion disassembly. *Journal of Biological Chemistry* **2003**, *278*, 30516-30524.

(4) Kader, K. *et al.* eNOS-overexpressing endothelial cells inhibit platelet aggregation and smooth muscle cell proliferation in vitro. *Tissue Engineering* **2000**, *6*, 241-251.

(5) Rodgers, G. M. Hemostatic properties of normal and perturbed vascular cells. *The FASEB Journal* **1988**, *2*, 116-123.

(6) Abramson, D. L. *Blood Vessels and Lymphatics*. (Academic Press, New York, 1962).

(7) Boyle, E. M.; Pohlman, T. H.; Johnson, M. C.; Verrier, E. D. Endothelial cell injury in cardiovascular surgery: The systemic inflammatory response. *The Annals of Thoracic Surgery* **1997**, *63*, 277-284.

(8) Timpl, R. Macromolecular organization of basement membranes. *Current Opinion in Cell Biology* **1996**, *8*, 618-624.

(9) Newby, A.; Zaltsman, A. Molecular mechanisms in intimal hyperplasia. *Journal of Pathology* **2000**, *190*, 300-309.

(10) Schwartz, S. M.; deBlois, D.; O'Brien, E. R. M. The intima: Soil for atherosclerosis and restenosis. *Circulation Research* **1995**, *77*, 445-465.

(11) Savani, R. C. *et al.* Migration of bovine aortic smooth muscle cells after wounding injury: The role of hyaluronan and RHAMM. *Journal of Clinical Investigation* **1995**, *95*, 1158-1168.

(12) Fuchs, J. C.; Mitchener, J. S.; Hagen, P. O. Postoperative changes in autologous vein grafts. *Annals of Surgery* **1978**, *188*, 1-15.

(13) Salacinski, H.; Goldner, S.; Giudiceandrea, A.; Hamilton, G.; Seifalian, A. The mechanical behavior of vascular grafts: A review. *Journal of Biomaterials Applications* **2001**, *15*, 241-278.

(14) Darling, R. C.; Linton, R. R. Durability of femoropopliteal reconstructions: Endarterectomy versus vein bypass grafts *The American Journal of Surgery* **1972**, *123*, 472-479.

(15) Williams, S. Tissue engineered vascular grafts: From bench to clinical use. *The FASEB Journal* **2000**, *14*, 305.

(16) Bos, G.; Poot, A.; Beugeling, T.; van Aken, W.; Feijen, A. Small-diameter vascular graft prostheses: current status. *Archives of Physiology and Biochemistry* **1998**, *106*, 100-115.

(17) Hamlin, G. W.; Rajah, S. M.; Crow, M. J.; Kester, R. C. Evaluation of the thrombogenic potential of three types of arterial graft studied in an artificial circulation. *British Journal of Surgery* **1978**, *65*, 272-276.

(18) Edmondson, R. A.; Cohen, A. T.; Das, S. K.; Wagner, M. B.; Kakkar, V. V. Low-molecular weight heparin versus aspirin and dipyridamole after femoropopliteal bypass grafting. *The Lancet* **1994**, *344*, 914-918.

(19) Anderson, J. M. Chapter 4 Mechanisms of inflammation and infection with implanted devices. *Cardiovascular Pathology* **1993**, *2*, 33-41.

(20) Anderson, J. M.; Miller, K. M. Biomaterial biocompatibility and the macrophage. *Biomaterials* **1984**, *5*, 5-10.

(21) Mikos, A. G.; Temenoff, J. S. in *Biomaterials: The Intersection of Biology and Materials Science* Ch. 10, 371-386 (Pearson Education, Inc., Upper Saddle River, NJ, 2008).

(22) Anderson, J. M.; Rodriguez, A.; Chang, D. T. Foreign body reaction to biomaterials. *Seminars in Immunology* **2008**, *20*, 86-100.

(23) Jeffery, D. L.; Dressler, D. P.; Anderson, J. M.; Gallagher, M. J. Hemostatic and healing studies of sodium amylose succinate (IP760). *Journal of Biomedical Materials Research* **1982**, *16*, 51-61.

(24) Wildemann, B. *et al.* Local and controlled release of growth factors (combination of IGF-I and TGF-beta I, and BMP-2 alone) from a polylactide coating of titanium implants does not lead to ectopic bone formation in sheep muscle. *Journal of Controlled Release* **2004**, *95*, 249-256.

(25) Mikos, A. G.; Temenoff, J. S. in *Biomaterials: The Intersection of Biology and Materials Science* Ch. 11, 387-400 (Pearson Education, Inc., Upper Saddle River, NJ, 2008).

(26) Cadée, J. A. *et al.* In vivo biocompatibility of dextran-based hydrogels. *Journal of Biomedical Materials Research* **2000**, *50*, 397-404.

(27) Mikos, A. G.; Temenoff, J. S. in *Biomaterials: The Intersection of Biology and Materials Science* Ch. 13, 430-444 (Pearson Education, Inc., Upper Saddle River, NJ, 2008).

(28) Budd, J. S.; Allen, K. E.; Hartley, G.; Bell, P. R. F. The effect of preformed confluent endothelial cell monolayers on the patency and thrombogenicity of small calibre vascular grafts. *European Journal of Vascular Surgery* **1991**, *5*, 397-405.

(29) Antiplatelet Trialists' Collaboration. Collaborative overview of randomised trials of antiplatelet therapy - II: Maintenance of vascular graft or arterial patency by antiplatelet therapy. *BMJ* **1994**, *308*, 159-168.

(30) Jensen, N.; Lindblad, B.; Ljungberg, J.; Leide, S.; Bergqvist, D. Early attachment of leucocytes, platelets and fibrinogen in endothelial cell-seeded Dacron venous conduits. *British Journal of Surgery* **1997**, *84*, 52-57.

(31) Örtenwall, P.; Wadenvik, H.; Kutti, J.; Risberg, B. Reduction in deposition of indium 111—labeled platelets after autologous endothelial cell seeding of Dacron aortic bifurcation grafts in humans: A preliminary report. *Journal of Vascular Surgery* **1987**, *6*, 17-25.

(32) Esquivel, C. O. *et al.* Reduced thrombogenic characteristics of expanded polytetrafluoroethylene and polyurethane arterial grafts after heparin bonding. *Surgery* **1984**, *95*, 102-107.

(33) Hanson, S. R.; Harker, L. A.; Ratner, B. D.; Hoffman, A. S. In vivo evaluation of artificial surfaces with a nonhuman primate model of arterial thrombosis. *The Journal of Laboratory and Clinical Medicine* **1980**, *95*, 289-304.

(34) Dilley, R. J.; McGeachie, J. K.; Prendergast, F. J. A review of the histologic changes in vein-to-artery grafts, with particular reference to intimal hyperplasia. *Archives of Surgery* **1988**, *123*, 691-696.

(35) Spray, T. L.; Roberts, W. C. Morphologic observations in biologic conduits between aorta and coronary artery. *Cardiovascular Clinics* **1977**, *8*, 11-40.

(36) Bassiouny, H. S. *et al.* Anastomotic intimal hyperplasia: Mechanical injury or flow induced. *Journal of Vascular Surgery* **1992**, *15*, 708-717.

(37) Traub, O.; Berk, B. C. Laminar shear stress: Mechanisms by which endothelial cells transduce an atheroprotective force. *Arteriosclerosis, Thrombosis, and Vascular Biology* **1998**, *18*, 677-685.

(38) Keynton, R. S. *et al.* Intimal hyperplasia and wall shear in arterial bypass graft distal anastomoses: An in vivo model study. *Journal of Biomechanical Engineering* **2001**, *123*, 464-473.

(39) Asahara, T. *et al.* Local delivery of vascular endothelial growth factor accelerates reendothelialization and attenuates intimal hyperplasia in balloon-injured rat carotid artery. *Circulation* **1995**, *91*, 2793-2801.

(40) Shi, Q.; Bhattacharya, V.; Hong-De Wu, M.; Sauvage, L. R. Utilizing granulocyte colony-stimulating factor to enhance vascular graft endothelialization from circulating blood cells. *Annals of Vascular Surgery* **2002**, *16*, 314-320.

(41) Bhattacharya, V. *et al.* Administration of granulocyte colony-stimulating factor enhances endothelialization and microvessel formation in small-caliber synthetic vascular grafts. *Journal of Vascular Surgery* **2000**, *32*, 116-123.

(42) Conte, M. S. The ideal small arterial substitute: A search for the Holy Grail? *The FASEB Journal* **1998**, *12*, 43-45.

(43) Axthelm, S.; Porter, J.; Strickland, S.; Baur, G. Antigenicity of venous allografts. *Annals of Surgery* **1979**, *189*, 290-293.

(44) Weber, T. R. *et al.* Long-term patency of vein grafts preserved in liquid nitrogen in dimethyl sulfoxide. *Annals of Surgery* **1976**, *184*, 709-712.

(45) Carpenter, J.; Tomaszewski, J. Human saphenous vein allograft bypass grafts: Immune response. *Journal of Vascular Surgery* **1998**, *27*, 492-499.

(46) Iaffaldano, R. A.; Lewis, B. E.; Johnson, S. A.; Piffare, R.; McKieman, T. L. Patency of cryopreserved saphenous vein grafts as conduits for coronary artery bypass surgery. *CHEST* **1995**, *108*, 725-729.

(47) Lehalle, B.; Geschier, C.; Fiévé, G.; Stoltz, J. F. Early rupture and degeneration of cryopreserved arterial allografts. *Journal of Vascular Surgery* **1997**, *25*, 751-752.

(48) Sheil, A. G. R.; Stephen, M. S.; Boulas, J.; Johnson, D. S.; Loewenthal, J. Small arterial reconstruction using modified cadaveric saphenous veins. *The American Journal of Surgery* **1977**, *134*, 591-595.

(49) Ketchedjian, A. *et al.* Recellularization of decellularized allograft scaffolds in ovine great vessel reconstructions. *The Annals of Thoracic Surgery* **2005**, *79*, 888-896.

(50) Schaner, P. *et al.* Decellularized vein as a potential scaffold for vascular tissue engineering. *Journal of Vascular Surgery* **2004**, *40*, 146.

(51) Martin, N. D. *et al.* In vivo behavior of decellularized vein allograft. *Journal of Surgical Research* **2005**, *129*, 17-23.

(52) Numata, S. *et al.* Immunological and histological evaluation of decellularized allograft in a pig model: comparison with cryopreserved allograft. *The Journal of Heart Valve Disease* **2004**, *13*, 984-990.

(53) Wilson, G. J.; Courtman, D. W.; Klement, P.; Michael Lee, J.; Yeger, H. Acellular matrix: A biomaterials approach for coronary artery bypass and heart valve replacement. *The Annals of Thoracic Surgery* **1995**, *60, Supplement 2*, S353-S358.

(54) Heyligers, J. M. M.; Arts, C. H. P.; Verhagen, H. J. M.; de Groot, P. G.; Moll, F. L. Improving small-diameter vascular grafts: From the application of an endothelial cell lining to the construction of a tissue-engineered blood vessel. *Annals of Vascular Surgery* **2005**, *19*, 448-456.

(55) Lamm, P.; Juchem, G.; Milz, S.; Schuffenhauer, M.; Reichart, B. Autologous endothelialized vein allograft: A solution in the search for small-caliber grafts in coronary artery bypass graft operations. *Circulation* **2001**, *104*, I108-I114.

(56) Schmidt, C. E.; Baier, J. M. Acellular vascular tissues: Natural biomaterials for tissue repair and tissue engineering. *Biomaterials* **2000**, *21*, 2215-2231.

(57) Voytik-Harbin, S. L.; Brightman, A. O.; Kraine, M. R.; Waisner, B.; Badylak, S. F. Identification of extractable growth factors from small intestinal submucosa. *Journal of Cellular Biochemistry* **1997**, *67*, 478-491.

(58) Roeder, R. *et al.* Compliance, elastic modulus, and burst pressure of small-intestine submucosa (SIS), small-diameter vascular grafts. *Journal of Biomedical Materials Research* **1999**, *47*, 65-70.

(59) Badylak, S. F.; Lantz, G. C.; Coffey, A.; Geddes, L. A. Small intestinal submucosa as a large diameter vascular graft in the dog. *Journal of Surgical Research* **1989**, *47*, 74-80.

(60) Lantz, G. C.; Badylak, S. F.; Coffey, A. C.; Geddes, L. A.; Blevins, W. E. Small intestinal submucosa as a small-diameter arterial graft in the dog. *Journal of Investigative Surgery* **1990**, *3*, 217-227.

(61) Sandusky, G. E.; Lantz, G. C.; Badylak, S. F. Healing comparison of small intestine submucosa and ePTFE grafts in the canine carotid artery. *Journal of Surgical Research* **1995**, *58*, 415-420.

(62) Dixit, P.; Hern-Anderson, D.; Ranieri, J.; Schmidt, C. E. Vascular graft endothelialization: Comparative analysis of canine and human endothelial cell migration on natural biomaterials. *Journal of Biomedical Materials Research* **2001**, *56*, 545-555.

(63) Robotin-Johnson, M. C.; Swanson, P. E.; Johnson, D. C.; Schuessler, R. B.; Cox, J. L. An experimental model of small intestinal submucosa as a growing vascular graft. *The Journal of Thoracic and Cardiovascular Surgery* **1998**, *116*, 805-811.

(64) Lantz, G. C. *et al.* Small intestinal submucosa as a vascular graft: a review. *Journal of Investigative Surgery* **1993**, *6*, 297-310.

(65) Zheng, M. H. *et al.* Porcine small intestine submucosa (SIS) is not an acellular collagenous matrix and contains porcine DNA: Possible implications in human implantation. *Journal of Biomedical Materials Research Part B: Applied Biomaterials* **2005**, *73B*, 61-67.

(66) Kapadia, M. R.; Popowich, D. A.; Kibbe, M. R. Modified prosthetic vascular conduits. *Circulation* **2008**, *117*, 1873-1882.

(67) Ascer, E. *et al.* Complementary distal arteriovenous fistula and deep vein interposition: A five-year experience with a new technique to improve infrapopliteal prosthetic bypass patency. *Journal of Vascular Surgery* **1996**, *24*, 134-143.

(68) Batson, R. C.; Sottiurai, V. S.; Craighead, C. C. Linton patch angioplasty. *Annals of Surgery* **1984**, *199*, 684-693.

(69) Griffiths, G. D.; Nagy, J.; Black, D.; Stonebridge, P. A. Randomized clinical trial of distal anastomotic interposition vein cuff in infrainguinal polytetrafluoroethylene bypass grafting. *British Journal of Surgery* **2004**, *91*, 560-562.

(70) Syrek, J. R. *et al.* Do distal arteriovenous fistulae improve patency rates of prosthetic infrapopliteal arterial bypasses? *Annals of Vascular Surgery* **1998**, *12*, 148-152.

(71) Taylor, M. R. S.; Loh, A.; McFarland, R. J.; Cox, M.; Chester, J. F. Improved technique for polytetrafluoroethylene bypass grafting: Long-term results using anastomotic vein patches. *British Journal of Surgery* **1992**, *79*, 348-354.

(72) Karrer, L. *et al.* PPS-PEG surface coating to reduce thrombogenicity of small diameter ePTFE vascular grafts. *International Journal of Artificial Organs* **2005**, *28*, 993-1002.

(73) Jordan, S. W. *et al.* Fabrication of a phospholipid membrane-mimetic film on the luminal surface of an ePTFE vascular graft. *Biomaterials* **2006**, *27*, 3473-3481.

(74) San Román, J. *et al.* Experimental study of the antithrombogenic behavior of Dacron vascular grafts coated with hydrophilic acrylic copolymers bearing salicylic acid residues. *Journal of Biomedical Materials Research* **1996**, *32*, 19-27.

(75) Heise, M. *et al.* PEG-hirudin/iloprost coating of small diameter ePTFE grafts effectively prevents pseudointima and intimal hyperplasia development. *European Journal of Vascular and Endovascular Surgery* **2006**, *32*, 418-424.

(76) Greisler, H. *et al.* Enhanced endothelialization of expanded polytetrafluoroethylene grafts by fibroblast growth factor type 1 pretreatment. *Surgery* **1992**, *112*, 244-254.

(77) Laube, H. R.; Duwe, J.; Rutsch, W.; Konertz, W. Clinical experience with autologous endothelial cell-seeded polytetrafluoroethylene coronary artery bypass grafts. *Journal of Thoracic Cardiovascular Surgury* **2000**, *120*, 134-141.

(78) Fujita, Y. *et al.* Accelerated healing of dacron grafts seeded by preclotting with autologous bone marrow blood. *Annals of Vascular Surgery* **1999**, *13*, 402-412.

(79) Griese, D. P. *et al.* Isolation and transplantation of autologous circulating endothelial cells into denuded vessels and prosthetic grafts. *Circulation* **2003**, *108*, 2710-2715.

(80) Rotmans, J. I. *et al.* In vivo cell seeding with anti-CD34 antibodies successfully accelerates endothelialization but stimulates intimal hyperplasia in porcine arteriovenous expanded polytetrafluoroethylene grafts. *Circulation* **2005**, *112*, 12-18.

(81) Kibbe, M.; Billiar, T.; Tzeng, E. Inducible nitric oxide synthase and vascular injury. *Cardiovascular Research* **1999**, *43*, 650-657.

(82) Keefer, L. K. Nitric oxide (NO)- and nitroxyl (HNO)-generating diazeniumdiolates (NONOates): emerging commercial opportunities. *Current Topics In Medicinal Chemistry* **2005**, *5*, 625-636.

(83) Mowery, K. A.; H. Schoenfisch, M.; Saavedra, J. E.; Keefer, L. K.; Meyerhoff, M. E. Preparation and characterization of hydrophobic polymeric films that are thromboresistant via nitric oxide release. *Biomaterials* **2000**, *21*, 9-21.

(84) Pulfer, S. K.; Ott, D.; Smith, D. J. Incorporation of nitric oxide-releasing crosslinked polyethyleneimine microspheres into vascular grafts. *Journal of Biomedical Materials Research* **1997**, *37*, 182-189.

(85) Smith, D. J. *et al.* Nitric oxide-releasing polymers containing the [N(O)NO]-group. *Journal of Medicinal Chemistry* **1996**, *39*, 1148-1156.

(86) Batchelor, M. M. *et al.* More lipophilic dialkyldiamine-based diazeniumdiolates: Synthesis, characterization, and application in preparing thromboresistant nitric oxide release polymeric coatings. *Journal of Medicinal Chemistry* **2003**, *46*, 5153-5161.

(87) Jun, H.-W.; Taite, L. J.; West, J. L. Nitric oxide-producing polyurethanes. *Biomacromolecules* **2005**, *6*, 838-844.

(88) Reynolds, M. M. *et al.* Nitric oxide releasing polyurethanes with covalently linked diazeniumdiolated secondary amines. *Biomacromolecules* **2006**, *7*, 987-994.

(89) Jourd'heuil, D.; Hallén, K.; Feelisch, M.; Grisham, M. B. Dynamic state of S-nitrosothiols in human plasma and whole blood. *Free Radical Biology and Medicine* **2000**, *28*, 409-417.

(90) Bohl, K. S.; West, J. L. Nitric oxide-generating polymers reduce platelet adhesion and smooth muscle cell proliferation. *Biomaterials* **2000**, *21*, 2273-2278.

(91) Duan, X.; Lewis, R. S. Improved haemocompatibility of cysteine-modified polymers via endogenous nitric oxide. *Biomaterials* **2002**, *23*, 1197-1203.

(92) Nerem, R. M.; Seliktar, D. Vascular tissue engineering. *Annual Review of Biomedical Engineering* **2001**, *3*, 225-243.

(93) Chvapil, M.; Krajicek, M. Principle and construction of a highly porous collagen-fabric vascular graft. *Journal of Surgical Research* **1963**, *3*, 358-368.

(94) Weinberg, C. B.; Bell, E. A blood vessel model constructed from collagen and cultured vascular cells. *Science* **1986**, *231*, 397-400.

(95) He, W.; Ma, Z.; Yong, T.; Teo, W. E.; Ramakrishna, S. Fabrication of collagen-coated biodegradable polymer nanofiber mesh and its potential for endothelial cells growth. *Biomaterials* **2005**, *26*, 7606-7615.

(96) Hirai, J.; Kanda, K.; Oka, T.; Matsuda, T. Highly oriented, tubular hybrid vascular tissue for a low pressure circulatory system. *ASAIO Journal* **1994**, *40*, M383-M388.

(97) L'Heureux, N.; Germain, L.; Labbe, R.; Auger, F. In vitro construction of a human blood vessel from cultured vascular cells: a morphological study. *Journal of Vascular Surgery* **1993**, *17*, 499-509.

(98) Tranquillo, R. T.; Girton, T. S.; Bromberek, B. A.; Triebes, T. G.; Mooradian, D. L. Magnetically orientated tissue-equivalent tubes: application to a circumferentially orientated media-equivalent. *Biomaterials* **1996**, *17*, 349-357.

(99) Nemcova, S. *et al.* Evaluation of a xenogeneic acellular collagen matrix as a small-diameter vascular graft in dogs--preliminary observations. *Journal Of Investigative Surgery* **2001**, *14*, 321-330.

(100) Wissink, M. J. B. *et al.* Improved endothelialization of vascular grafts by local release of growth factor from heparinized collagen matrices. *Journal of Controlled Release* **2000**, *64*, 103-114.

(101) Wu, H.-C. *et al.* Coculture of endothelial and smooth muscle cells on a collagen membrane in the development of a small-diameter vascular graft. *Biomaterials* **2007**, *28*, 1385-1392.

(102) Wang, X.; Lin, P.; Yao, Q.; Chen, C. Development of small-diameter vascular grafts. *World Journal of Surgery* **2007**, *31*, 682-689.

(103) Mitchell, S.; Niklason, L. Requirements for growing tissue-engineered vascular grafts. *Cardiovascular Pathology* **2003**, *12*, 59-64.

(104) Koyama, H.; Raines, E. W.; Bornfeldt, K. E.; Roberts, J. M.; Ross, R. Fibrillar collagen inhibits arterial smooth muscle proliferation through regulation of Cdk2 inhibitors. *Cell* **1996**, *87*, 1069-1078.

(105) Li, D. Y. *et al.* Elastin is an essential determinant of arterial morphogenesis. *Nature* **1998**, *393*, 276-280.

(106) Matthews, J.; Wnek, G.; Simpson, D.; Bowlin, G. Electrospinning of collagen nanofibers. *Biomacromolecules* **2002**, *3*, 232-238.

(107) Boland, E. *et al.* Electrospinning collagen and elastin: preliminary vascular tissue engineering. *Frontiers in Bioscience* **2004**, *9*, 1422-1432.

(108) Buttafoco, L. *et al.* Electrospinning of collagen and elastin for tissue engineering applications. *Biomaterials* **2006**, *27*, 724-734.

(109) Stitzel, J. *et al.* Controlled fabrication of a biological vascular substitute. *Biomaterials* **2006**, *27*, 1088-1094.

(110) Wise, S. G. *et al.* A multilayered synthetic human elastin/polycaprolactone hybrid vascular graft with tailored mechanical properties. *Acta Biomaterialia* **2011**, *7*, 295-303.

(111) Stegemann, J. P.; Kaszuba, S. N.; Rowe, S. L. Review: Advances in vascular tissue engineering using protein-based biomaterials. *Tissue Engineering* **2007**, *13*,

(112) Grassl, E. D.; Oegema, T. R.; Tranquillo, R. T. A fibrin-based arterial media equivalent. *Journal of Biomedical Materials Research Part A* **2003**, *66A*, 550-561.

(113) Isenberg, B.; Williams, C.; Tranquillo, R. Small-diameter artificial arteries engineered in vitro. *Circulation Research* **2006**, *98*, 25-35.

(114) Swartz, D. D.; Russell, J. A.; Andreadis, S. T. Engineering of fibrin-based functional and implantable small-diameter blood vessels. *American Journal of Physiology - Heart and Circulatory Physiology* **2005**, *288*, H1451-H1460.

(115) Neidert, M. R.; Lee, E. S.; Oegema, T. R.; Tranquillo, R. T. Enhanced fibrin remodeling in vitro with TGF-β1, insulin and plasmin for improved tissue-equivalents. *Biomaterials* **2002**, *23*, 3717-3731.

(116) Cummings, C. L.; Gawlitta, D.; Nerem, R. M.; Stegemann, J. P. Properties of engineered vascular constructs made from collagen, fibrin, and collagen–fibrin mixtures. *Biomaterials* **2004**, *25*, 3699-3706.

(117) Rowe, S. L.; Stegemann, J. P. Interpenetrating collagen-fibrin composite matrices with varying protein contents and ratios. *Biomacromolecules* **2006**, *7*, 2942-2948.

(118) Aper, T.; Teebken, O. E.; Steinhoff, G.; Haverich, A. Use of a fibrin preparation in the engineering of a vascular graft model. *European Journal of Vascular and Endovascular Surgery* **2004**, *28*, 296-302.

(119) Grassl, E. D.; Oegema, T. R.; Tranquillo, R. T. Fibrin as an alternative biopolymer to type-I collagen for the fabrication of a media equivalent. *Journal of Biomedical Materials Research* **2002**, *60*, 607-612.

(120) Isenberg, B.; Williams, C.; Tranquillo, R. Endothelialization and flow conditioning of fibrin-based media-equivalents. *Annals of Biomedical Engineering* **2006**, *34*, 971-985.

(121) Leach, J.; Wolinsky, J.; Stone, P.; Wong, J. Crosslinked alpha-elastin biomaterials: towards a processable elastin mimetic scaffold. *Acta Biomaterialia* **2005**, *1*, 155-164.

(122) Long, J. L.; Tranquillo, R. T. Elastic fiber production in cardiovascular tissue-equivalents. *Matrix Biology* **2003**, *22*, 339-350.

(123) Patel, A.; Fine, B.; Sandig, M.; Mequanint, K. Elastin biosynthesis: The missing link in tissue-engineered blood vessels. *Cardiovascular Research* **2006**, *71*, 40-49.

(124) Rowe, S. L.; Lee, S.; Stegemann, J. P. Influence of thrombin concentration on the mechanical and morphological properties of cell-seeded fibrin hydrogels. *Acta Biomaterialia* **2007**, *3*, 59-67.

(125) Tschoeke, B. *et al.* Tissue-engineered small-caliber vascular graft based on a novel biodegradable composite fibrin-polylactide scaffold. *Tissue Engineering Part A* **2009**, *15*, 1909-1918.

(126) Baguneid, M. *et al.* Shear-stress preconditioning and tissue-engineering-based paradigms for generating arterial substitutes. *Biotechnology and Applied Biochemistry* **2004**, *39*, 151-157.

(127) Giudiceandrea, A.; Seifalian, A. M.; Krijgsman, B.; Hamilton, G. Effect of prolonged pulsatile shear stress in vitro on endothelial cell seeded PTFE and compliant polyurethane vascular grafts. *European Journal of Vascular and Endovascular Surgery* **1998**, *15*, 147-154.

(128) L'Heureux, N.; Paquet, S.; Labbe, R.; Germain, L.; Auger, F. A completely biological tissue-engineered human blood vessel. *The FASEB Journal* **1998**, *12*, 47-56.

(129) L'Heureux, N. *et al.* A human tissue-engineered vascular media: a new model for pharmacological studies of contractile responses. *The FASEB Journal* **2001**, *15*, 515-524.

(130) Niklason, L. E. *et al.* Functional arteries grown in vitro. *Science* **1999**, *284*,

(131) Solan, A.; Mitchell, S.; Moses, M.; Niklason, L. Effect of pulse rate on collagen deposition in the tissue-engineered blood vessel. *Tissue Engineering* **2003**, *9*, 579-586.

(132) Niklason, L. E. Replacement arteries made to order. *Science* **1999**, *286*, 1493-1494.

(133) McKee, J. A. *et al.* Human arteries engineered in vitro. *European Molecular Biology Organization Reports* **2003**, *4*, 633-638.

(134) Poh, M. *et al.* Blood vessels engineered from human cells. *The Lancet* **2005**, *365*, 2122-2124.

(135) Gong, Z.; Niklason, L. E. Small-diameter human vessel wall engineered from bone marrow-derived mesenchymal stem cells (hMSCs). *The FASEB Journal* **2008**, *22*, 1635-1648.

(136) L'Heureux, N. *et al.* Human tissue-engineered blood vessels for adult arterial revascularization. *Nature Medicine* **2006**, *12*, 361-365.

(137) Hubbell, J. A.; Massia, S. P.; Desai, N. P.; Drumheller, P. D. Endothelial cell-selective materials for tissue engineering in the vascular graft via a new receptor. *Nature Biotechnology* **1991**, *9*, 568-572.

(138) Lin, H.-B. *et al.* Endothelial cell adhesion on polyurethanes containing covalently attached RGD-peptides. *Biomaterials* **1992**, *13*, 905-914.

(139) Lin, Y.-S. *et al.* Growth of endothelial cells on different concentrations of Gly-Arg-Gly-Asp photochemically grafted in polyethylene glycol modified polyurethane. *Artificial Organs* **2001**, *25*, 617-621.

(140) Choi, W. *et al.* RGD peptide-immobilized electrospun matrix of polyurethane for enhanced endothelial cell affinity. *Biomedical Materials* **2008**, *3*, 1-8.

(141) Kim, T.; Park, T. Biomimicking extracellular matrix: cell adhesive RGD peptide modified electrospun poly(D,L-lactic-co-glycolic acid) nanofiber mesh. *Tissue Engineering* **2006**, *12*, 221-233.

(142) Shin, H.; Jo, S.; Mikos, A. G. Biomimetic materials for tissue engineering. *Biomaterials* **2003**, *24*, 4353-4364.

(143) Jun, H.-W.; West, J. Modification of polyurethaneurea with PEG and YIGSR peptide to enhance endothelialization without platelet adhesion. *Journal of Biomedical Materials Research* **2005**, *72B*, 131-139.

(144) Gobin, A. S.; West, J. L. Val-ala-pro-gly, an elastin-derived non-integrin ligand: Smooth muscle cell adhesion and specificity. *Journal of Biomedical Materials Research Part A* **2003**, *67A*, 255-259.

(145) Lee, H. J. *et al.* Collagen mimetic peptide-conjugated photopolymerizable PEG hydrogel. *Biomaterials* **2006**, *27*, 5268-5276.

(146) Sallach, R. E. *et al.* Elastin-mimetic protein polymers capable of physical and chemical crosslinking. *Biomaterials* **2009**, *30*, 409-422.

(147) Bella, J.; Berman, H. Integrin–collagen complex: a metal–glutamate handshake. *Structure* **2000**, *8*, R121-R126.

(148) Farndale, R. *et al.* Cell-collagen interactions: the use of peptide toolkits to investigate collagen-receptor interactions. *Biochemical Society Interactions* **2008**, *36*, 241-250.

(149) Knight, C. G. *et al.* The collagen-binding I-domains of integrins α1β1 and α2β1 recognize the same specific amino acid sequence, GFOGER, in native (triple-helical) collagens. *Journal of Biological Chemistry* **2000**, *275*, 35-40.

(150) Krijgsman, B. *et al.* An assessment of covalent grafting of RGD peptides to the surface of a compliant poly(carbonate-urea)urethane vascular conduit versus conventional biological coatings: Its role in enhancing cellular retention. *Tissue Engineering* **2002**, *8*, 673-680.

(151) Gray, D. S.; Tien, J.; Chen, C. S. Repositioning of cells by mechanotaxis on surfaces with micropatterned Young's modulus. *Journal of Biomedical Material Research* **2003**, *66A*, 605–614.

(152) Reinhart-King, C. A.; Dembo, M.; Hammer, D. A. Cell-cell mechanical communication through compliant substrates. *Biophysical Journal* **2008**, *95* 6044–6051.

(153) Detta, N. *et al.* Novel electrospun polyurethane/gelatin composite meshes for vascular grafts. *Journal of Materials Science: Materials in Medicine* **2010**, *21*, 1761-1769.

(154) Kidoaki, S.; Kwon, I.; Matsuda, T. Mesoscopic spatial designs of nano- and microfiber meshes for tissue-engineered matrix and scaffold based on newly devised multilayering and mixing electrospinning techniques. *Biomaterials* **2005**, *26*, 37-46.

(155) McMahon, R. E. *et al.* Hydrogel–electrospun mesh composites for coronary artery bypass grafts. *Tissue Engineering* **2011**, *17*, 1-11.

(156) Hahn, M. S.; McHale, M. K.; Wang, E.; Schmedlen, R. H.; West, J. L. Physiologic pulsatile flow bioreactor conditioning of poly(ethylene glycol)-based tissue engineered vascular grafts *Annals of Biomedical Engineering* **2007**, *35*, 190-200.

(157) Jeong, S. I. *et al.* Mechano-active tissue engineering of vascular smooth muscle using pulsatile perfusion bioreactors and elastic PLCL scaffolds. *Biomaterials* **2005**, *26*, 1405-1411.

(158) Burkel, W. E. The challenge of small diameter vascular grafts. *Medical Progress through Technology* **1989**, *14*, 165-175.

(159) Schmedlen, R. H.; Elbjeirami, W. M.; Gobin, A. S.; West, J. L. Tissue engineered small-diameter vascular grafts. *Clinics in Plastic Surgery* **2003**, *30*, 507-517.

(160) Brown, F. R.; Hopfinger, A. J.; Blout, E. R. The collagen-like triple helix to random-chain transition: Experiment and theory. *Journal of Molecular Biology* **1972**, *63*, 101-115.

(161) Xu, Y.; Keene, D. R.; Bujnicki, J. M.; Hook, M.; Lukomski, S. Streptococcal Scl1 and Scl2 proteins form collagen-like triple helices. *The Journal of Biological Chemistry* **2002**, *277*, 27312-27318.

(162) Han, R. *et al.* Assessment of collagen-like sequences derived from Scl1 and Scl2 proteins as a source of recombinant GXY polymers. *Applied Microbiology and Biotechnology* **2006**, *72*, 109-115.

(163) Senger, D. R. *et al.* The α1β1 and α2β1 integrins provide critical support for vascular endothelial growth factor signaling, endothelial cell migration, and tumor angiogenesis. *American Journal of Pathology* **2002**, *160*, 195-204.

(164) Cosgriff-Hernandez, E. *et al.* Bioactive hydrogels based on designer collagens. *Acta Biomaterialia* **2010**, *6*, 3969-3977.

(165) Gombotz, W. R.; Guanghui, W.; Horbett, T. A.; Hoffman, A. Protein adsorption to poly(ethylene oxide) surfaces. *Journal of Biomedical Materials Research* **1991**, *25*, 1547-1562.

(166) Anseth, K. S.; Bowman, C. N.; Brannon-Peppas, L. Mechanical properties of hydrogels and their experimental determination. *Biomaterials* **1996**, *17*, 1647-1657.

(167) Pelham Jr., R. J.; Wang, Y. Cell locomotion and focal adhesions are regulated by substrate flexibility. . *Proceedings of the National Academy of Science* **1997**, *94*, 13661–13665.

(168) Peyton, S.; Putnam, A. Extracellular matrix rigidity governs smooth muscle cell motility in a biphasic fashion. *Journal of Cell Physiology* **2005**, *204*, 198-209.

(169) Lamba, N. M. K.; Woodhouse, K. A.; Cooper, S. L. *Polyurethanes in Biomedical Applications*. (CRC Press LLC, Boca Raton, FL, 1998).

(170) Pham, Q. P.; Sharma, U.; Mikos, A. G. Electrospinning of polymeric nanofibers for tissue engineering applications: a review. *Tissue Engineering* **2006**, *12*, 1197-1211.

(171) Sebra, R.; Masters, K.; Bowman, C.; Anseth, K. Surface grafted antibodies: Controlled architecture permits enhanced antigen detection. *Langmuir* **2005**, *21*, 10907-10911.

(172) Hahn, M. S. *et al.* Photolithographic patterning of polyethylene glycol hydrogels. *Biomaterials* **2006**, *27*, 2519-2524.

(173) Bulick, A. S. *et al.* Impact of endothelial cells and mechanical conditioning on smooth muscle cell extracellular matrix production and differentiation. *Tissue Engineering* **2009**, *15*, 815-825.

(174) Johnson, C. P.; How, T.; Scraggs, M.; West, C. R.; Burns, J. A biomechanical study of the human vertebral artery with implications for fatal arterial injury. *Forensic Science International* **1999**, *109*, 169-182.

(175) ANSI/AAMI. Vol. ANSI/AAMI VP20 (Association for the Advancement of Medical Instrumentation, 1994).

(176) Sarkar, S.; Hillery, C.; Scifalian, A.; Hamilton, G. Critical parameter of burst pressure measurement in development of bypass grafts is highly dependent on methodology used. *Journal of Vascular Surgery* **2006**, *44*, 846-852.

(177) Stankus, J. *et al.* Fabrication of cell microintegrated blood vessel constructs through electrohydrodynamic atomization. *Biomaterials* **2007**, *28*, 2738-2746.

(178) Liu, V. A.; Bhatia, S. N. Three-dimensional photopatterning of hydrogels containing living cells. *Biomedical Microdevices* **2002**, *4*, 257-266.

(179) Lawrence, M.; McIntire, L.; Eskin, S. Effect of flow on polymorphonuclear leukocyte/endothelial cell adhesion. *Blood* **1987**, *70*, 1284-1290.

(180) Suggs, L. J.; West, J. L.; Mikos, A. G. Platelet adhesion on a bioresorbable poly(propylene fumarate-co-ethylene glycol) copolymer. *Biomaterials* **1999**, *20*, 683-690.

(181) Cholakis, C. H.; Zingg, W.; Sefton, M. V. Effect of heparin–PVA hydrogel on platelets in a chronic canine arterio-venous shunt. *Journal of Biomedical Materials Research* **1989**, *23*, 417-441.

(182) Michelson, A. D.; Barnard, M. R.; Krueger, L. A.; Frelinger, A. L.; Furman, M. I. Evaluation of platelet function by flow cytometry. *Methods* **2000**, *21*, 259-270.

(183) Schwartz, R. S.; Edelman, E. R. Preclinical evaluation of drug-eluting stents for peripheral applications. *Circulation* **2004**, *110*, 2498-2505.

(184) Heller, J.; Helwing, R. F.; Baker, R. W.; Tutte, M. E. Controlled release of water-soluble macromolecules from bioerodible hydrogels. *Biomaterials* **1983**, *4*, 262-266.

(185) Stewart, S. F. C.; Lyman, D. J. Effects of a vascular graft/natural artery compliance mismatch on pulsatile flow *Journal of Biomechanics* **1992**, *25*, 297-310.

(186) Walden, R.; L'Italien, G. J.; Megerman, J.; Abbott, W. M. Matched elastic properties and successful arterial grafting. *Archives of Surgery* **1980**, *115*, 1166-1169.

(187) Basmadjian, D.; Sefton, M. V.; Baldwin, S. A. Coagulation on biomaterials in flowing blood: Some theoretical considerations. *Biomaterials* **1997**, *18*, 1511-1522.

(188) Ratner, B. D. The catastrophe revisited: Blood compatibility in the 21st Century. *Biomaterials* **2007**, *28*, 5144-5147.

(189) Andre, P.; Hartwell, D.; Hrachovinova, I.; Saffaripour, S.; Wagner, D. D. Pro-coagulant state resulting from high levels of soluble P-selectin in blood. *Proceedings of the National Academy of Science* **2000**, *97*, 13835-13840.

(190) Dole, V. S.; Bergmeier, W.; Mitchell, H. A.; Eichenberger, S. C.; Wagner, D. D. Activated platelets induce Weibel-Palade–body secretion and leukocyte rolling in vivo: role of P-selectin *Blood* **2005**, *106*, 2334-2339.

(191) Burger, P. C.; Wagner, D. D. Platelet P-selectin faciliates atherosclerotic lesion development. *Blood* **2003**, *101*, 2661-2666.

(192) Shattil, S. J.; Hoxie, J. A.; Cunningham, M.; Brass, L. F. Changes in the platelet membrane glycoprotein IIb-IIIa complex during platelet activation. *The Journal of Biological Chemistry* **1985**, *260*, 11107-11114.

(193) Hoffman, M.; Monroe, D. M. Coagulation 2006: A modern view of hemostasis. *Hemotology/Oncology Clinics of North America* **2007**, *21*, 1-11.

(194) Benoit, D. S. W.; Durney, A. R.; Anseth, K. S. Manipulations in hydrogel degradation behavior enhance osteoblast function and mineralized tissue formation. *Tissue Engineering* **2006**, *12*, 1163-1673.

(195) Bryant, S. J.; Anseth, K. S. Hydrogel properties influence ECM production by chondrocytes photoencapsulated in poly(ethylene glycol) hydrogels. *Journal of Biomedical Materials Research* **2002**, *59*, 63-72.

(196) Bryant, S. J.; Anseth, K. S. Controlling the spatial distribution of ECM components in degradable PEG hydrogels for tissue engineering cartilage. *Journal of Biomedical Materials Research Part A* **2003**, *64A*, 70-79.

(197) Lynn, A. D.; Kyriakides, T. R.; Bryant, S. J. Characterization of the in vitro macrophage response and in vivo host response to poly(ethylene glycol)-based hydrogels. *Journal of Biomedical Materials Research Part A* **2009**, *93A*, 941-953.

(198) Mann, B.; Gobin, A.; Tsai, A.; Schmedlen, R.; West, J. Smooth muscle cell growth in photopolymerized hydrogels with cell adhesive and proteolytically degradable domains: synthetic ECM analogs for tissue engineering. *Biomaterials* **2001**, *22*, 3045-3051.

(199) Patel, P. N.; Gobin, A. S.; West, J. L.; Patrick, C. W. Poly(ethylene glycol) hydrogel system supports preadipocyte viability, adhesion, and proliferation. *Tissue Engineering* **2005**, *11*, 1498-1505.

(200) Larsen, I. B.; Munksgaard, E. C. Effect of human saliva on surface degradation of composite resins. *European Journal of Oral Sciences* **1991**, *99*, 254-261.

(201) Metters, A. T.; Anseth, K. S.; Bowman, C. N. Fundamental studies of a novel, biodegradable PEG-b-PLA hydrogel *Polymer* **2000**, *41*, 3993-4004.

(202) West, J. L.; Hubbell, J. A. Photopolymerized hydrogel materials for drug delivery applications. *Reactive Polymers* **1995**, *25*, 139-147.

(203) Deible, C. R. *et al.* Molecular barriers to biomaterial thrombosis by modification of surface proteins with polyethylene glycol. *Biomaterials* **1998**, *19*, 1885-1893.

(204) Hill-West, J.; Chowdhury, S.; Slepian, M.; Hubbell, J. Inhibition of thrombosis and intimal thickening by in situ photopolymerization of thin hydrogel barriers. *Proceedings of the National Academy of Science* **1994**, *91*, 5967-5971.

(205) Anseth, K. *et al.* In situ forming degradable networks and their application in tissue engineering and drug delivery. *Journal of Controlled Release* **2002**, *78*, 199-209.

(206) Clowes, A. W.; Gown, A. M.; Hanson, S. R.; Reidy, M. A. Mechanisms of arterial graft failure. 1. Role of cellular proliferation in early healing of PTFE prostheses. *American Journal of Pathology* **1985**, *118*, 43-54.

(207) Quinn, C. A. P.; Connor, R. E.; Heller, A. Biocompatible, glucose-permeable hydrogel for in situ coating of implantable biosensors. *Biomaterials* **1997**, *18*, 1665-1670.

(208) Elbert, D. L.; Hubbell, J. A. Conjugate addition reactions combined with free-radical cross-linking for the design of materials for tissue engineering. *Biomacromolecules* **2001**, *2*, 430-441.

(209) Bryant, S. J.; Bender, R. J.; Durand, K. L.; Anseth, K. S. Encapsulating chondrocytes in degrading PEG hydrogels with high modulus: engineering gel structural changes to facilitate cartilaginous tissue production. *Biotechnology and Bioengineering* **2004**, *86*, 747-755.

(210) Christenson, E. M.; Anderson, J. M.; Hiltner, A. Oxidative mechanisms of poly(carbonate urethane) and poly(ether urethane) biodegradation: *In vivo* and *in vitro* correlations. *Journal of Biomedical Materials Research Part A* **2004**, *70A*, 245-255.

(211) Labow, R.; Meek, E.; Santerre, J. Hydrolytic degradation of poly-(carbonate)-urethanes by monocyte-derived macrophages. *Biomaterials* **2001**, *22* 3025–3033.

(212) Trudel, J.; Massia, S. P. Assessment of the cytotoxicity of photocrosslinked dextran and hyaluronan-based hydrogels to vascular smooth muscle cells. *Biomaterials* **2002**, *23*, 3299-3307.

(213) Namba, R. M.; Cole, A. A.; Bjugstad, K. B.; Mahoney, M. J. Development of porous PEG hydrogels that enable efficient, uniform cell-seeding and permit early neural process extension. *Acta Biomaterialia* **2009**, *5*, 1884-1897.

(214) Nguyen, K. T.; West, J. L. Photopolymerizable hydrogels for tissue engineering applications. *Biomaterials* **2002**, *23*, 4307-4314.

(215) Qui, Y.; Park, K. Environment-sensitive hydrogels for drug delivery. *Advanced Drug Delivery Reviews* **2001**, *53*, 321-339.

(216) Weber, L. M.; He, J.; Bradley, B.; Haskins, K.; Anseth, K. S. PEG-based hydrogels as an in vitro encapsulation platform for testing controlled beta-cell microenvironments. *Acta Biomaterialia* **2006**, *2*, 1-8.

(217) Gunn, J.; Turner, S.; Mann, B. Adhesive and mechanical properties of hydrogels influence neurite extension. *Journal of Biomedical Materials Research* **2004**, *72A*, 91-97.

(218) Kraehenbuehl, T. P. *et al.* Three-dimensional extracellular matrix-directed cardioprogenitor differentiation: Systematic modulation of a synthetic cell-responsive PEG-hydrogel *Biomaterials* **2008**, *29*, 2757-2766.

(219) Bryant, S. J.; Chowdhury, T. T.; Lee, D. A.; Bader, D. L.; Anseth, K. S. Crosslinking density influences chondrocyte metabolism in dynamically loaded photocrosslinked poly(ethylene glycol) hydrogels. *Annals of Biomedical Engineering* **2003**, *32*, 407-417.

(220) Temenoff, J. S.; Athanasiou, K. A.; LeBaron, R. G.; Mikos, A. G. Effect of poly(ethylene glycol) molecular weight on tensile and swelling properties of oligo(poly(ethylene glycol) fumarate) hydrogels for cartilage tissue engineering. *Journal of Biomedical Materials Research* **2001**, *59*, 429-437.

(221) Burdick, J. A.; Anseth, K. S. Photoencapsulation of osteoblasts in injectable RGD-modified PEG hydrogels for bone tissue engineering. *Biomaterials* **2002**, *23*, 4315-4323.

(222) Nuttelman, C. R.; Benoit, D. S. W.; Tripodi, M. C.; Anseth, K. S. The effect of ethylene glycol methacrylate phosphate in PEG hydrogels on mineralization and viability of encapsulated hMSCs. *Biomaterials* **2006**, *27*, 1377-1386.

(223) Suggs, L. J.; Shive, M. S.; Garcia, C. A.; Anderson, J. M.; Mikos, A. G. In vitro cytotoxicity and in vivo biocompatibility of poly(propylene fumarate-co-ethylene glycol) hydrogels. *Journal of Biomedical Materials Research* **1999**, *46*, 22-32.

(224) Zustiak, S. P.; Leach, J. B. Hydrolytically degradable poly(ethylene glycol) hydrogel scaffolds with tunable degradation and mechanical properties. *Biomacromolecules* **2010**, *11*, 1348-1357.

(225) Elisseeff, J. *et al.* Transdermal photopolymerization of poly (ethylene oxide)-based injectable hydrogels for tissue-engineered cartilage. *Plastic & Reconstructive Surgery* **1999**, *104*, 1014-1022.

(226) Constant, M. J.; Keeley, E. M.; Cruise, G. M. Preparation, characterization, and evaluation of radiopaque hydrogel filaments for endovascular embolization.

Journal of Biomedical Materials Research Part B: Applied Biomaterials **2009**, *89*, 306-313.

(227) Hern, D. L.; Hubbell, J. A. Incorporation of adhesion peptides into nonadhesive hydrogels useful for tissue resurfacing. *Journal of Biomedical Materials Research* **1998**, *39*, 266-276.

(228) Elbert, D. L.; Hubbell, J. A. Surface treatment of polymers for biocompatibility. *Annual Review of Materials Science* **1996**, *26*, 365-294.

(229) Han, D. K. *et al.* Plasma protein adsorption to sulfonated poly(ethylene oxide)-grafted polyurethane surface. *Journal of Biomedical Material Research* **1996**, *30*, 23-30.

(230) Gonen-Wadmany, M.; Oss-Ronen, L.; Seliktar, D. Protein–polymer conjugates for forming photopolymerizable biomimetic hydrogels for tissue engineering. *Biomaterials* **2007**, *28*, 3876-3886.

(231) Mann, B.; Schmedlen, R.; West, J. Tethered-TGF-beta increases extracellular matrix production of vascular smooth muscle cells. *Biomaterials* **2001**, *22*, 439-444.

(232) Christenson, E. M.; Dadsetan, M.; Anderson, J. M.; Hiltner, A. Biostability and macrophage-mediated foreign body reaction of silicone-modified polyurethanes. *Journal of Biomedical Materials Research, Part A* **2005**, *74A*, 141-155.

(233) Hermanson, G. *Bioconjugate Techniques*. (Academic Press, San Diego, 1996).

(234) Zustiak, S. P.; Wei, Y.; Leach, J. B. Protein–hydrogel interactions in tissue engineering: Mechanisms and applications. *Tissue Engineering* **2013**, *19*, 160-171.

(235) Greenwald, R. B.; Choe, Y. H.; McGuire, J.; Conover, C. D. Effective drug delivery by PEGylated drug conjugates. *Advanced Drug Delivery Reviews* **2003**, *55*, 217-250.

(236) DeLong, S.; Moon, J.; West, J. Covalently immobilized gradients of bFGF on hydrodgel scaffolds for directed cell migration. *Biomaterials* **2005**, *26*, 3227-3234.

(237) Gobin, A. S.; West, J. L. Effects of epidermal growth factor on fibroblast migration through biomimetic hydrogels. *Biotechnology Progress* **2003**, *19*, 1781-1785.

(238) Abuchowski, A.; McCoy, J. R.; Palczuk, N. C.; van Es, T.; Davis, F. F. Effect of covalent attachment of polyethylene glycol on immunogenicity and circulating life of bovine liver catalase. *Journal of Biological Chemistry* **1977**, *252*, 3582-3586.

(239) Esposito, P. *et al.* PEGylation of growth hormone-releasing hormone (GRF) analogues. *Advanced Drug Delivery Reviews* **2003**, *55*, 1279-1291.

(240) Pasut, G.; Veronese, F. M. Polymer–drug conjugation, recent achievements and general strategies. *Progress in Polymer Science* **2007**, *32*, 933-961.

(241) Van Den Bulcke, A. I. *et al.* Structural and rheological properties of methacrylamide modified gelatin hydrogels. *Biomacromolecules* **2000**, *1*, 31-38.

(242) Browning, M. B.; Cosgriff-Hernandez, E. Development of a biostable replacement for PEGDA hydrogels. *Biomacromolecules* **2012**, *13*, 779-786.

(243) Monfardini, C. *et al.* A branched monomethoxypoly(ethylene glycol) for protein modification. *Bioconjugate Chemistry* **1995**, *6*, 62-69.

(244) Civerchia-Perez, L. *et al.* Use of collagen-hydroxyethylmethacrylate hydrogels for cell growth. *Proceedings of the National Academy of Science* **1980**, *77*, 2064-2068.

(245) Trevino, S. R.; Scholtz, J. M.; Pace, C. N. Measuring and increasing protein solubility. *Journal of Pharmaceutical Sciences* **2008**, *97*, 4155-4166.

(246) Chen, R. R.; Mooney, D. J. Polymeric growth factor delivery strategies for tissue engineering. *Pharmaceutical Research* **2003**, *20*, 1103-1112.

(247) Bae, S. E.; Choi, D. H.; Han, D. K.; Park, K. Effect of temporally controlled release of dexamethasone on in vivo chondrogenic differentiation of mesenchymal stromal cells. *Journal of Controlled Release* **2010**, *143*, 23-30.

(248) Browning, M.; Wilems, T.; Hahn, M.; Cosgriff-Hernandez, E. Compositional control of poly(ethylene glycol) hydrogel modulus independent of mesh size. *Journal of Biomedical Material Research Part A* **2011**, *98*, 268-273.

(249) Discher, D. E.; Janmey, P.; Wang, Y.-l. Tissue cells feel and respond to the stiffness of their substrate. *Science* **2005**, *310*, 1139-1143.

(250) Georges, P. C.; Janmey, P. A. Cell type-specific response to growth on soft materials. *Journal of Applied Physiology* **2005**, *98*, 1547-1553.

(251) Thompson, M. T.; Berg, M. C.; Tobias, I. S.; Rubner, M. F.; Van Vliet, K. J. Tuning compliance of nanoscale polyelectrolyte multilayers to modulate cell adhesion. *Biomaterials* **2005**, *26*, 6836-6845.

(252) Yeung, T. *et al.* Effects of substrate stiffness on cell morphology, cytoskeletal structure, and adhesion. *Cell Motility and the Cytoskeleton* **2005**, *60*, 24-34.

(253) Helmke, B. P.; Davies, P. F. The cytoskeleton under external fluid mechanical forces: Hemodynamic forces acting on the endothelium. *Annals of Biomedical Engineering* **2002**, *30*, 284-296.

(254) Vailhé, B.; Ronot, X.; Tracqui, P.; Usson, Y.; Tranqui, L. In vitro angiogenesis is modulated by the mechanical properties of fibrin gels and is related to αvβ3 integrin localization. *In Vitro Cellular & Developmental Biology - Animal* **1997**, *33*, 763-773.

(255) Vernon, R. B.; Angello, J. C.; Iruela-Arispe, M. L.; Lane, T. F.; Sage, E. H. Reorganization of basement membrane matrices by cellular traction promotes the formation of cellular networks in vitro. *Laboratory Investigation; a Journal of Technical Methods and Pathology* **1992**, *66*, 536-547.

(256) Sieminski, A. L.; Hebbel, R. P.; Gooch, K. J. The relative magnitudes of endothelial force generation and matrix stiffness modulate capillary morphogenesis in vitro. *Experimental Cell Research* **2004**, *297*, 574-584.

(257) Stokes, C. L.; Lauffenburger, S. K. W. Migration of individual microvessel endothelial cells: Stochastic model and parameter measurement. *Journal of Cell Science* **1991**, *99*, 419-430.

(258) Pozzi, A.; Wary, K. K.; Giancotti, F. G.; Gardner, H. A. Integrin α1β1 mediates a unique collagen-dependent proliferation pathway in vivo. *The Journal of Cell Biology* **1998**, *142*, 587-594.

(259) Mainiero, F. *et al.* The coupling of alpha6beta4 integrin to Ras–MAP kinase pathways mediated by Shc controls keratinocyte proliferation. *The EMBO Journal* **1997**, *16*, 2365-2375.

(260) Wary, K. K.; Mainiero, F.; Isakoff, S.; Marcantonio, E. E.; Giancotti, F. G. The adaptro protein Shc couples a class of integrins to the control of cell cycle progression. *Cell* **1996**, *87*, 733-743.

(261) Rasmussen, L.; Ledet, T. Aortic collagen alterations in human diabetes mellitus. Changes in basement membrane collagen content and in the susceptibility of total collagen to cyanogen bromide solubilisation. *Diabetologia* **1993**, *36*, 445-453.

(262) Sun, J.-Y. *et al.* Highly stretchable and tough hydrogels. *Nature* **2012**, *489*, 133-136.

(263) Griffith, L. G.; Naughton, G. Tissue engineering - current challenges and expanding opportunities. *Science* **2002**, *295*, 1009-1014.

(264) Hoffman, A. S. Hydrogels for biomedical applications. *Advanced Drug Delivery Reviews* **2002**, *43*, 3-12.

(265) Lee, K. Y.; Mooney, D. J. Hydrogels for tissue engineering. *Chemical Review* **2001**, *101*, 1869-1880.

(266) Rakovsky, A.; Marbach, D.; Lotan, N.; Lanir, Y. Poly(ethylene glycol)-based hydrogels as cartilage substitutes: synthesis and mechanical characteristics. *Journal of Applied Polymer Science* **2008**, *112*, 390-401.

(267) Martens, P.; Anseth, K. Characterization of hydrogels formed from acrylate modified poly(vinyl alcohol) macromers *Polymer* **2000**, *41*, 7715-7722.

(268) Elliott, J. E.; Anseth, J. W.; Bowman, C. N. Kinetic modeling of the effect of solvent concentration on primary cyclization during polymerization of multifunctional monomers. *Chemical Engineering Science* **2000**, *56*, 3173-3184.

(269) Munoz-Pinto, D. J.; Bulick, A. S.; Hahn, M. S. Uncoupled investigation of scaffold modulus and mesh size on smooth muscle cell behavior. *Journal of Biomedical Materials Research Part A* **2009**, *90*, 303-316.

(270) Bader, D. L.; Bryant, S. J.; Anseth, K. S.; David, L. A. Crosslinking density influences the morphology of chondrocytes photoencapsulated in PEG hydrogels during the application of compressive strain. *Journal of Orthopaedic Research* **2004**, *22*, 1143-1149.

(271) Peyton, S. R.; Raub, C. B.; Keschrumrus, V. P.; Putnam, A. J. The use of poly(ethylene glycol) hydrogels to investigate the impact of ECM chemistry and mechanics on smooth muscle cells. *Biomaterials* **2006**, *27*, 4881-4893.

(272) Stegemann, J. P.; Hong, H.; Nerem, R. M. Mechanical, biochemical, and extracellular matrix effects on vascular smooth muscle cell phenotype. *Journal of Applied Physiology* **2005**, *98*, 2321-2328.

(273) Hutmacher, D. W. Scaffold design and fabrication technologies for engineering tissues — state of the art and future perspectives. *Journal of Biomaterials Science and Polymer Education* **2000**, *12*, 107-124.

(274) Liao, H. *et al.* Influence of hydrogel mechanical properties and mesh size on vocal fold fibroblast extracellular matrix production and phenotype. *Acta Biomaterialia* **2008**, *4*, 1161-1171.

(275) Ford, M. C. *et al.* A macroporous hydrogel for the coculture of neural progenitor and endothelial cells to form functional vascular networks in vivo. *Proceedings of the National Academy of Science* **2006**, *103*, 2512-2517.

APPENDIX A

COMPOSITIONAL CONTROL OF PEG HYDROGEL MODULUS INDEPENDENT OF MESH SIZE*

A.1 Introduction

Poly(ethylene glycol) (PEG) hydrogels are currently being investigated in a wide range of tissue engineering applications due to their established biocompatibility, high permeability, and tunable properties.[137,214,263-266] Aqueous solutions of acrylate-derivatized PEG (PEGDA) can be rapidly crosslinked under mild conditions, permitting *in situ* polymerization in direct contact with cells and tissues.[214-215] This feature enables ready fabrication of cell-laden PEGDA scaffolds with complex geometries.[195,213,216] Perhaps the most widely studied aspect of these versatile hydrogels is the ability to spatially and systematically tune their biochemical and biomechanical properties by varying the properties and conditions of the polymerization process.[166,195,201,209,219,267] However, the interdependence of hydrogel modulus and mesh size hampers our ability to correlate specific cell responses to independent scaffold properties.[268-269] Given that both substrate modulus and mesh size are known to impact a wide range of cellular responses, the inability to independently tune these effects limits the rational selection of scaffold parameters to achieve desired cell behaviors.[209,219,269-272]

---

*Reprinted with permission from "Compositional Control of PEG Hydrogel Modulus Independent of Mesh Size," by MB Browning, T Wilems, M. Hahn, and E. Cosgriff-Hernandez, Journal of Biomedical Materials Research, Part A. 2011, 98 (2), 268-273.

The mechanical properties and network architecture of PEG hydrogels can be controlled by varying the compositional properties and polymerization conditions of the hydrogel.[166] Traditionally, the crosslink density of the polymer network has been modulated by altering the molecular weight and/or concentration of PEGDA to these purposes. For linear homopolymers, the molecular weight of the polymer is one of the most accessible compositional variables that can be used to control the properties of the hydrogel network.[220] Lower molecular weight PEG hydrogels have a decreased chain length between crosslinks, which translates to an increased crosslink density. An increase in crosslink density results in increases in modulus of these polymer networks. Thus, decreases in PEG molecular weight can be used to dramatically increase the modulus of hydrogels.[220] Modulation of PEGDA concentration is also used to control hydrogel properties. Bryant et. al. found that by doubling the concentration of PEG in hydrogels, the crosslink density was tripled due to an increase in the number of interchain reactions that occurred during polymerization.[219] This increase in crosslink density resulted in statistically significant increases in modulus.[219] However, increases in modulus that result from increased crosslink density are coupled with decreases in mesh size that can have undesirable effects on diffusivity and swelling of the network.[166] Thus, to increase the relatively low mechanical properties of PEG hydrogels, the mesh size must be reduced and hydrogel permeability sacrificed.[273]

We propose to develop a methodology that circumvents this limitation such that hydrogel modulus can be tuned independently of mesh size. Prior research has typically used linear PEGDA to form hydrogel networks. We hypothesize that adding a low

concentration of 4-arm PEG cross-linker will create local increases in crosslink density that substantially increase the modulus while minimally perturbing bulk average mesh size, **Figure A.1**. In addition to decoupling the mesh size and modulus, adding a 4-arm PEG cross-linker is expected to increase the range of mechanical properties achievable by PEG hydrogel systems and allow for finer tuning of the gel modulus.

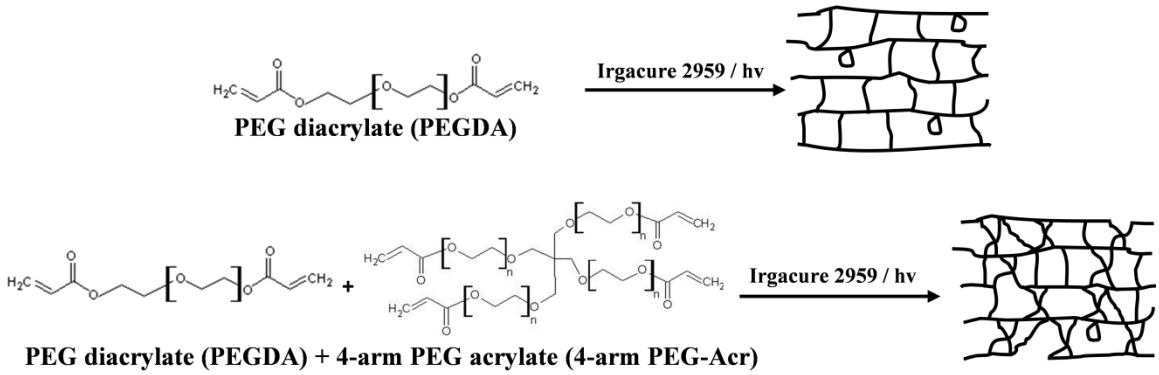

Figure A.1. Schematic representation of PEG hydrogel network formation with and without 4-arm PEG-acrylate illustrating the hypothesized local increase in cross-link density with minimal change in hydrogel mesh size.

A.2. Materials and Methods

A.2.1. Materials All chemicals were used as received. 4-arm poly(ethylene glycol) (2 kDa) (4-arm PEG) was purchased from JenKem Technology (Allen, Texas). All other chemicals were purchased from Sigma Aldrich (St. Louis, MO).

A.2.2. Polymer Synthesis PEGDA was synthesized according to a method adapted from Hahn, et al.[172] Briefly, acryloyl chloride was added dropwise to a solution of PEG (3.4, 6, or 10 kDa) and triethylamine in anhydrous dichloromethane (DCM) under nitrogen. The molar ratio of PEG, acryloyl chloride, and triethylamine was 1:2:4,

respectively. After the addition of acryloyl chloride, the reaction was stirred for an additional 24 hours at room temperature. The resulting solution was then washed with 8 molar equivalents of 2M potassium bicarbonate to remove acidic byproducts and dried with anhydrous sodium sulfate. The product was precipitated in cold diethyl ether, filtered, and dried under vacuum.

4-arm PEG-acrylate (4-arm PEG-Acr) was prepared using a method similar to PEGDA. Briefly, acryloyl chloride was added dropwise to a solution of 4-arm PEG and triethylamine in anhydrous DCM under nitrogen. The molar ratio of 4-arm PEG, acryloyl chloride, and triethylamine was 1:4:8, respectively, so that the ratios of the reactant and catalyst were kept constant relative to the hydroxyl end groups of the PEG. After the addition of acryloyl chloride, the reaction was stirred for an additional 24 hours. The resulting solution was then washed with 16 molar equivalents of 2 M potassium bicarbonate to remove acidic byproducts, washed with brine to remove residual water, and dried with anhydrous sodium sulfate. The organic solvents were then removed with rotary evaporation (Buchi, R-210) and the product was dried under vacuum.

Functionalization of linear PEG and 4-arm PEG was confirmed using Fourier transform infrared (FTIR) spectroscopy and proton nuclear magnetic resonance (^{1}H-NMR) spectroscopy. Transmission FTIR spectra of control and functionalized polymers were acquired on a Bruker TENSOR 27 spectrometer by solution casting directly onto KBr pellets. The presence of ester peaks at 1730 cm^{-1} and loss of hydroxyl peaks at 3300 cm^{-1} in the IR spectra indicated successful acrylation, **Figure A.2**. Proton NMR spectra

of control and functionalized polymers were recorded on a Mercury 300 MHz spectrometer using a TMS/solvent signal as an internal reference. Percent conversions of hydroxyl to acrylate endgroups of greater than 85% were observed for all candidate polymers. ^{1}H-NMR ($CDCl_3$): δ 3.6 ppm (m, -OCH_2CH_2-), 4.3 ppm (t, -CH_2OCO-) 5.8 ppm (dd, -CH=CH_2), 6.1 and 6.4 ppm (dd, -CH=CH_2).

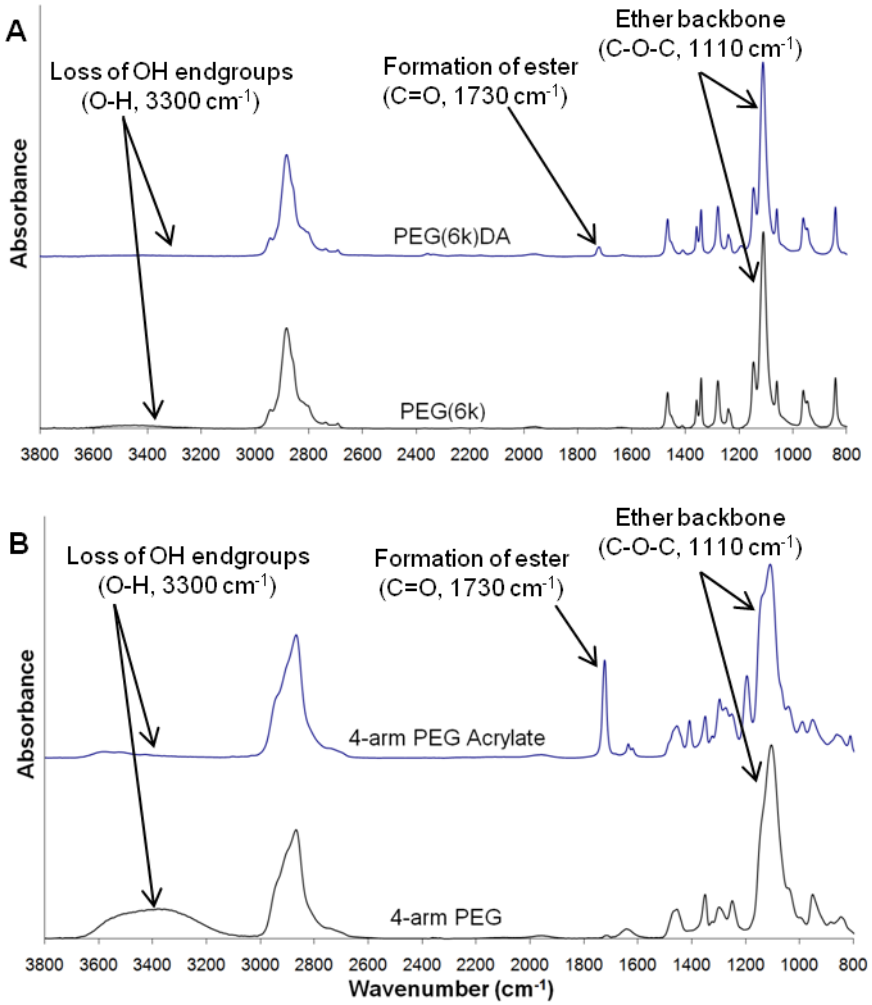

Figure A.2. Transmission FTIR spectra of PEGDA and 4-arm PEG acrylate. (A) PEG(6K)DA compared to PEG(6K); (B) 4-arm PEG acrylate relative to 4-arm PEG.

A.2.3. Hydrogel Preparation Variations of PEG molecular weight (3.4, 6, or 10 kDa), linear PEGDA concentration (10, 20, or 30 wt%), and 4-arm PEG-Acr concentration (0, 10, or 20 wt%) were combined to create 27 distinct hydrogel formulations to be characterized. Precursor solutions were prepared by dissolving PEGDA and 4-arm PEG-Acr in phosphate buffered saline (PBS). The solutions were mixed, and photointiator solution (1 mg Irgacure 2959 per 10 µl 70% ethanol) was added at 1% volume of precursor solution. Solutions were pipetted into an appropriate mold and polymerized by 10 min exposure to long wave UV light (Ultraviolet Products High Performance UV Transilluminator, 365 nm, 1 mW/cm^2).

A.2.4. Hydrogel Mechanical Properties To characterize hydrogel mechanical properties, both tensile and compressive tests were conducted on the selected PEGDA formulations. To avoid slippage artifacts associated with the tensile testing of rectangular hydrogel segments, tensile specimens were prepared by polymerizing hydrogel solutions in cylindrical molds (OD = 5 mm, ID = 3 mm) and swelling in PBS for 24 hours prior to mechanical testing. Six ring specimens (2-4 mm long) were cut from each tubular hydrogel and strained until fracture at a uniaxial strain rate of 6 mm/min using an Instron 3342. The secant modulus of elasticity was calculated from the resulting stress-strain data. The range of strains within 30% of blood pressure (approximately 9 to 17 kPa) and the corresponding stresses were used to determine the secant modulus in this study. Specimens for compressive modulus assessment were prepared by polymerizing hydrogel solutions into 1.5 mm sheets and swelling in PBS for 24 hours prior to testing. Six 8-mm discs were punched from each formulation and

subjected to mechanical testing under unconstrained compression at room temperature using a dynamic mechanical analyzer (RSAIII, TA Instruments) equipped with a parallel-plate compression clamp. Dynamic strain sweeps were performed to determine the linear viscoelastic range for each hydrogel formulation. Then, a strain within the upper end of the linear viscoelastic range was used in a constant strain frequency sweep. The test was conducted between 0.79 and 79 Hz, and the storage modulus of each hydrogel was taken at 1.25 Hz.

A.2.5. Hydrogel Swelling Ratios Hydrogels were polymerized in 0.75 mm thick sheets to assess the effects of compositional variables on swelling behavior. Eight 8-mm discs were punched from each sheet directly after polymerization and weighed (W_i). Each disc was swelled in deionized water for 24 hours and weighed to determine the equilibrium swelling mass (W_s). Then, the hydrogel discs were dried under vacuum for 24 hours and weighed to determine dry (polymer) mass (W_d). The equilibrium volumetric swelling ratio, Q, was calculated from the equilibrium mass swelling ratio:

$$Q = \frac{W_s}{W_d} \qquad [A.1]$$

A.2.6. Hydrogel Mesh Size Hydrogel mesh size was characterized using a series of Dextran diffusion experiments as described by Liao et al.[274] Briefly, hydrogels were polymerized into 0.75 mm thick sheets and swelled for 24 hours in PBS to constant dimensions. Discs 8-mm in diameter were punched from each hydrogel formulation. Fluorescently labeled dextrans (4, 20, 40 and 70 kDa) were dissolved at 0.05 mg ml^{-1} in PBS and added at 0.5 ml per hydrogel disc (four discs per dextran molecular weight). Dextran solutions were allowed to diffuse into the hydrogels for 24 hours, after which

each disc was dipped in PBS, gently blotted, and transferred to 0.5 ml of fresh PBS. Dextran that had diffused into the hydrogels was then allowed to diffuse out into the surrounding solution for 24 hours. Two 200 µl aliquots were taken from each PBS solution surrounding the discs, and their fluorescence was measured at ex/em 480/520. Standard curves of each dextran molecular weight were used to convert the fluorescence signals to concentrations.

For the 30% PEG(6 kDa) hydrogel formulation, the fluorescence readings fell to background levels for dextran molecular weight exceeding 20 kDa (data not shown). The hydrodynamic diameter of the 20 kDa dextran is approximately 6.5 nm, and the hydrodynamic diameter of the next largest dextran used in the investigation (40 kDa) is approximately 9.6 nm. Therefore, the mesh size of the 30% PEG(6 kDa) hydrogel was approximated to be the average of these two diameters, or 8.0 nm. Then, the mesh sizes of the remaining hydrogel formulations were calculated relative to that of the 30% PEG(6 kDa) hydrogel. For all hydrogel formulations, the measured concentrations for each dextran molecular weight were plotted versus the dextran hydrodynamic diameter. The area under the resulting curve was used as a quantitative indicator of hydrogel permissivity over the assigned range of hydrodynamic diameters. For a given hydrogel (x), the mesh size (ξ) was then calculated according to the following equation:

$$\xi_x \sim \frac{A_x}{A_{30\%\ 6\ \mathrm{kDa}}} \times 8\ \mathrm{nm} \qquad [A.2]$$

A.2.7. Statistical Analysis All of the data were expressed as the mean ± standard derivation of the mean. Statistical analysis was performed by an unpaired two-tailed student's t-test. Statistical significance was accepted at $p<0.05$

A.3. Results and Discussion

The ability to independently tune hydrogel modulus and mesh size is important in advancing our understanding of how scaffold properties impact cellular behavior. In this study, small amounts of 4-arm PEG-Acr were incorporated into PEGDA polymer networks to create local increases in crosslink density with minimal effects on gel mesh size. We hypothesized that this methodology would provide the means to decouple PEG hydrogel modulus and mesh size and provide finer control over cell-microenvironment interactions. To this end, we investigated the effect of each compositional variable (PEG molecular weight, PEGDA concentration, and 4-arm PEG-Acr concentration) on compressive modulus, tensile modulus, and gel mesh size.

A.3.1 Hydrogel Mechanical Properties Tensile testing was used to examine the effect of compositional variables on hydrogel mechanical properties, **Figure A.3A**. As expected, increases in hydrogel modulus were associated with decreased PEG molecular weight and increased PEGDA concentration. Statistically significant increases in secant modulus were also observed with increased 4-arm PEG-Acr concentrations. Without the addition of the 4-arm PEG cross-linker, a decrease in PEG molecular weight from 10k to 3.4k resulted in an average increase in secant modulus of 153%, and an increase in PEGDA concentration from 10% to 30% induced an average increase in secant modulus of 128%. The addition of the 4-arm PEG-Acr resulted in more moderate increases in secant modulus with a mean of 25%. Furthermore, the overall range of moduli was broadened by adding this third compositional variable. Relative to the 10% PEG hydrogels, the 30% PEG hydrogels with 20% 4-arm PEG-Acr were associated with

increases in moduli (e.g. PEG(10k) DA: 78 kPa versus 412 kPa) that were ~1.7X greater than the increases seen with only linear PEGDA (e.g. PEG(10k) DA: 78 kPa versus 257 kPa). Similarly, compression testing resulted in the expected trends, with higher storage moduli observed with decreasing PEG molecular weight and increasing PEGDA concentration, **Figure A.3B**. The addition of 4-arm PEG-Acr into the polymer networks also resulted in statistically significant increases in storage modulus for all hydrogel systems and a broader range of available moduli.

A.3.2 Hydrogel Mesh Size and Equilibrium Swelling It is difficult to visualize PEG hydrogel mesh size using traditional methods, such as standard scanning electron microscopy.[275] Thus, in this study, a series of dextran diffusion experiments were used to give a quantitative indicator of scaffold mesh size. The resulting mesh sizes relative to that of the 30% 6kDa hydrogels are shown in **Figure A.3C**. As expected, mesh size decreased with decreasing PEG molecular weight and increasing PEGDA concentration due to the corresponding increases in crosslink densities that occur with these changes in composition. Decreasing the molecular weight of PEG resulted in an average decrease in mesh size of 112%, and increasing the concentration of PEGDA reduced the mesh size by an average of 85%. In contrast, the addition of 4-arm PEG-Acr to the hydrogel networks induced a mean decrease in mesh size of only 9%. It was hypothesized that small concentrations of 4-arm PEG cross-linker would have local, limited effects on crosslink density and therefore would minimally disrupt bulk average mesh size. Although adding 4-arm PEG-Acr did result in decreased mesh size, contrary to hypothesis, these changes were moderate-to-minimal, and in many cases, below

statistical significance. Equilibrium swelling ratios, **Figure A.4**, supported these mesh size trends. Specifically, the addition of the 4-arm PEG-Acr resulted in more moderate decreases in swelling than a commensurate addition of linear PEGDA and, in several instances, was associated with no statistically significant change in swelling.

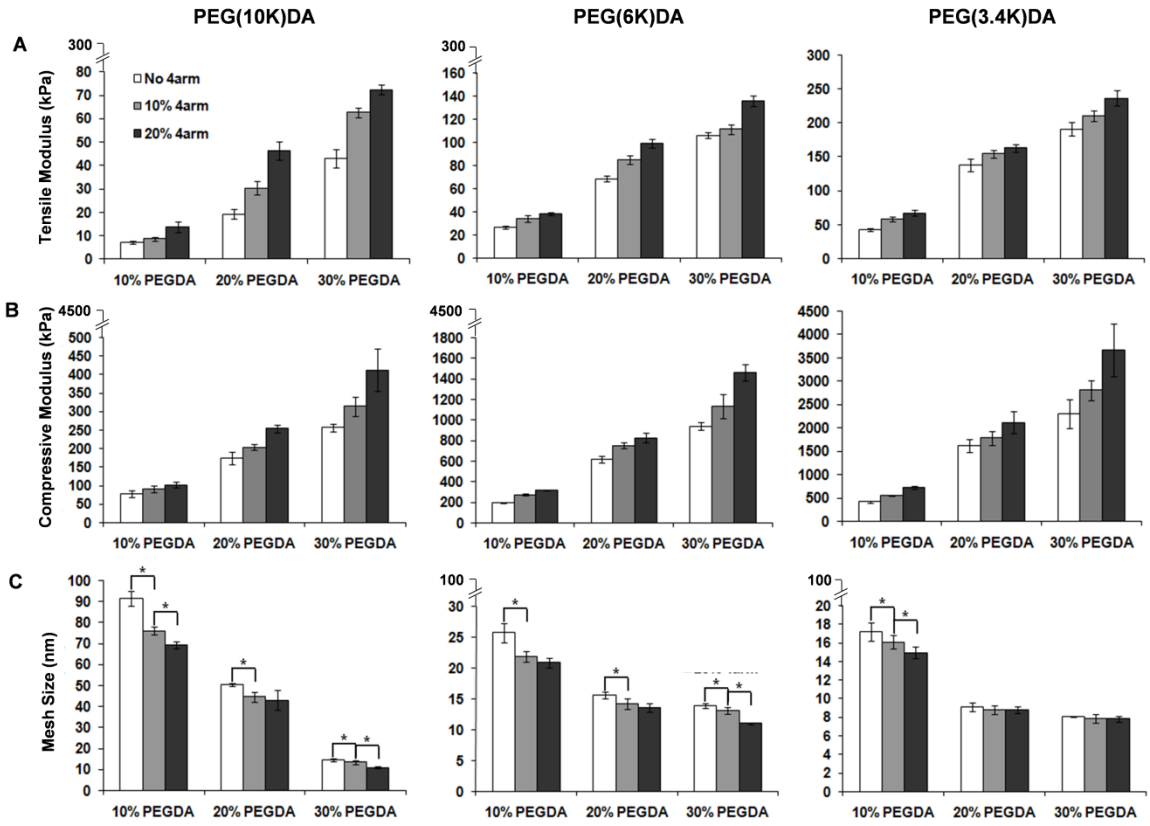

Figure A.3. Hydrogel material properties. (A) Tensile modulus of hydrogel ring specimens (n = 6; average ± standard deviation). Statistically significant increases in moduli were observed for all increases in 4-arm PEG-Acr concentration ($p<0.05$). (B) Compressive modulus of hydrogel disc specimens from constant viscoelastic strain at a frequency of 1.25 Hz (n = 6; average ± standard deviation). Statistically significant increases in modulus were observed for all increases in 4-arm PEG-Acr concentration ($p<0.05$). (C) Hydrogel mesh size (n=4; average ± standard deviation, * $p < 0.05$).

Cumulatively, these results demonstrate that substantial increases in modulus can be induced by the local alterations in hydrogel crosslink density introduced by 4-arm PEG-Acr and that hydrogel formulations can be identified in which these modifications in local crosslink density minimally disrupt bulk gel mesh size. Indeed, there are several sets of gels that can be chosen throughout the range of hydrogels that were tested that have either statistically indistinguishable bulk mesh sizes but distinct moduli or similar moduli and significantly different mesh sizes. **Figure A.5** displays a scatter plot of tensile modulus versus mesh size with regions circled that show the ability to tune these two properties independent of each other. Specific examples of this are highlighted in **Table A.1.** The present methodology represents a powerful tool in tissue engineering design by enabling the independent investigation of scaffold material properties on cell behavior and response. For example, desired modulus increases were typically obtained by decreasing PEGDA molecular weight or increasing PEGDA concentration. These changes resulted in a corollary decrease in mesh size. Nuttleman et. al. reported decreased diffusivity with decreased hydrogel mesh size which negatively affected cell viability.[222] Thus, researchers were challenged to obtain desired mechanical properties while maintaining mesh sizes that enabled prolonged viability of encapsulated cells. This study demonstrates compositional control of hydrogel properties with the potential ability to increase the modulus of relatively weak PEG hydrogels without adversely affecting cell viability by decreasing diffusivity.

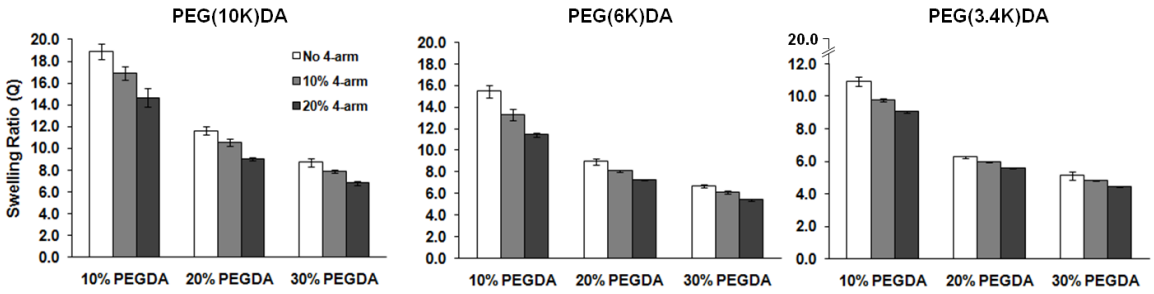

Figure A.4. Hydrogel equilibrium volumetric swelling ratio. Statistically significant decreases in swelling ratios were observed for all increases in 4-arm PEG-Acr concentration (n = 8; average ± standard deviation, $p < 0.05$).

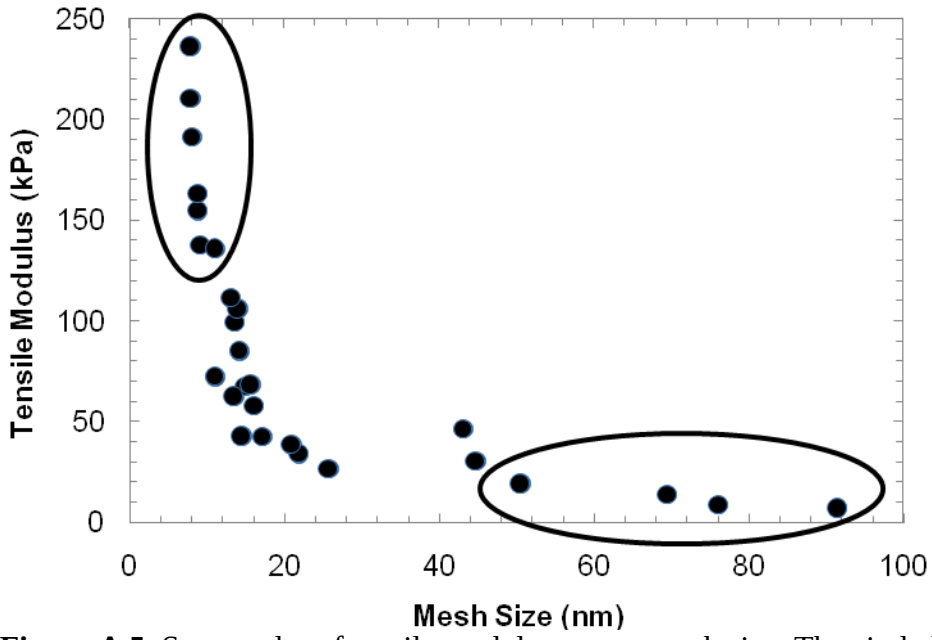

Figure A.5. Scatter plot of tensile modulus versus mesh size. The circled regions display the ability to use 4-arm PEG cross-linker to vary the modulus independent of mesh size (upper circle) or vary the mesh size independent of modulus (lower circle).

Table A.1. Demonstration of successful decoupling of PEG hydrogel modulus and mesh size. In the first group, tensile modulus is significantly different for the three hydrogels ($p < 0.05$) whereas mesh size is statistically the same ($p > 0.05$). In the second group, mesh size is significantly different for the three hydrogels ($p < 0.05$) while modulus is statistically the same ($p > 0.05$).

Variable	Compositional Variables			Hydrogel Properties	
	PEGDA MW	PEGDA Concentration	4-arm PEG-Acr Concentration	Secant Modulus (kPa)	Relative Mesh Size (nm)
Modulus Increases Independent of Mesh Size	10 kDa	30%	0%	44 ± 4	14.5 ± 0.7
	3.4 kDa	10%	20%	67 ± 4 (↑ **52%**)	15.0 ± 0.6
	6 kDa	20%	10%	85 ± 4 (↑ **93%**)	14.2 ± 0.9
Mesh Size Increases Independent of Modulus	10 kDa	30%	0%	43 ± 4	14.5 ± 0.7
	3.4 kDa	10%	0%	43 ± 2	17.2 ± 1.0 (↑ **19%**)
	10 kDa	20%	20%	46 ± 4	43.1 ± 4.6 (↑ **197%**)

A.4. Conclusions

The aim of this study was to develop a new approach for tuning PEG hydrogel modulus independent of mesh size such that the modulus of PEG hydrogels could be increased without adverse effects on gel mesh size. The incorporation of 4-arm PEG-Acr into PEG hydrogels resulted in significant increases in modulus with minimal effects on the mesh size. It also demonstrated the ability to alter mesh size while maintaining modulus. Furthermore, the 4-arm PEG cross-linker provides an additional compositional variable that can be modulated to broaden the range of available mechanical properties and more finely tune the modulus of PEG hydrogel systems. This new methodology expands the compositional control over these properties and provides new tools to probe the individual and combined effects of modulus and mesh size on cell behavior.